2012

INTERNAL FACIES ARCHITECTURE OF A REGRESSIVE TO TRANSGRESSIVE WAVE-DOMINATED DELTA IN THE UPPER CRETACEOUS EAGLE FORMATION, SOUTH-CENTRAL MONTANA

Eleanor Spangler
The University of Montana

INTERNAL FACIES ARCHITECTURE OF A REGRESSIVE TO TRANSGRESSIVE WAVE-DOMINATED DELTA IN THE UPPER CRETACEOUS EAGLE FORMATION, SOUTH-CENTRAL MONTANA

By

ELEANOR ROSE SPANGLER

B.S., Geology, California State University, Chico – Chico, California
2008

Thesis

Presented in partial fulfillment of the requirements
for the degree of

Master of Science
in Geosciences

The University of Montana
Missoula, MT

December 2012

Approved by:

Sandy Ross, Associate Dean of The Graduate School
Graduate School

James R. Staub, Committee Chair
Department of Geosciences

Marc S. Hendrix
Department of Geosciences

Holly A. Thompson
Department of Chemistry

Spangler, Eleanor, M.S., Fall, 2012 Geosciences

Internal Facies Architecture of a Regressive to Transgressive Wave-Dominated Delta in the Upper Cretaceous Eagle Formation, South-Central Montana

Chairperson: James R. Staub

The Santonian-Campanian Eagle Formation in south-central Montana was deposited along the western margin of the Cretaceous Western Interior Seaway and is composed of a series of well preserved regressive and transgressive deposits. This study documents the depositional evolution of the informal lower member of the Eagle Formation exposed near Billings, MT. Detailed mapping and characterization of the internal stratigraphy, facies architecture, and bounding surfaces of the lower Eagle provide the basis for reconstruction of a paleodelta system that serves as a valuable reservoir analog within the Cretaceous Seaway and elsewhere. This study demonstrates that the informal lower member of the Eagle Formation in south-central Montana was deposited in a regressive to transgressive wave-dominated deltaic system. Within this deltaic succession the identification of five facies and four bounding surface types are used to establish a two-phase depositional history: 1) a regressive phase characterized by prograding pro-delta to distal delta front deposits emplaced below fair weather wave base but above storm wave base; and 2) a transgressive phase characterized by landward dipping proximal to distal shoal overwash fan deposits derived from combined-flow storm-generated turbidity currents. A maximum regressive surface (MRS) separates underlying prograding deltaic deposits from downlapping shoal overwash fan deposits above. Shoal overwash fan packages dip and stack en-echelon towards the paleoshoreline indicating landward migration of the shoal during delta transgression. A time-transgressive ravinement surface (TRS) developed on the basinward side of the transgressive shoal and migrated landward with the shoreline, truncating of shoal overwash fan deposits.

TABLE OF CONTENTS

INTRODUCTION 1

PURPOSE 1
GEOLOGIC FRAMEWORK 4
REGIONAL BACKGROUND AND STUDY AREA 5
PREVIOUS WORK 7

METHODS 9

RESULTS 12

FACIES 12
PETROGRAPHIC DATA 17
STRATIGRAPHIC SURFACES 17

DEPOSITIONAL PROCESSES AND ENVIRONMENTS 21

DEPOSITIONAL PROCESSES 21
FACIES ARCHITECTURE 26
DEPOSITIONAL ENVIRONMENT AND EVOLUTION 29
IMPLICATIONS FOR RESERVOIR DEVELOPMENT 37

CONCLUSIONS 42

REFERENCES 44

FIGURES AND TABLES 64

APPENDICES 87

APPENDIX A: STRATIGRAPHIC SECTIONS 87
APPENDIX B: THREE-DIMENSIONAL DATA 108
TOTAL STATION DATA 108
GPS POINTS OF STRATIGRAPHIC SECTION LOCATIONS 118
APPENDIX C: DIP CORRECTION 119
APPENDIX D: PETROGRAPHIC DATA 122

LIST OF FIGURES AND TABLES

FIGURE 1: MAP OF STUDY AREA 64
FIGURE 2: DISTRIBUTION OF UPPER CRETACEOUS STRATA IN SOUTH-CENTRAL MONTANA 65
FIGURE 3: STRATIGRAPHIC SECTION AND GAMMA RAY PROFILE OF PACKAGES A AND Bb. 66
FIGURE 4: OUTCROP EXAMPLES OF FACIES 1, 2, AND 3 67
FIGURE 5: QFL DIAGRAM OF SAMPLES FROM THE LOWER MEMBER OF THE EAGLE FM. 68
FIGURE 6: OUTCROP EXAMPLES OF FACIES 4 69
FIGURE 7: OUTCROP EXAMPLES OF FACIES 5 70
FIGURE 8: PETROGRAPHIC IMAGES OF FACIES 2, 4, AND 5 71
FIGURE 9: OUTCROP EXAMPLES OF STRATIGRAPHIC SURFACES 72
FIGURE 10: PLAN-VIEW MAPS OF OUTCROP-SCALE SURFACES 73
FIGURE 11: ANNOTATED PHOTOMOSAICS OF THE E-W AND N-S CLIFFS 74
FIGURE 12: ANNOTATED PHOTOMOSAIC OF PACKAGES C TO G ALONG THE E-W CLIFFS 75
FIGURE 13: SCHEMATIC DIAGRAM OF THE IDEALIZED BOUMA SEQUENCE 76
FIGURE 14: COMPARISON OF DIFFERENT TYPES OF TURBIDITES 77
FIGURE 15: PETREL-GENERATED ISOPACH MAPS OF LARGE-SCALE PACKAGES 78
FIGURE 16: PETREL-GENERATED ISOPACH MAPS OF PACKAGES B AND Ba TO Bc 79
FIGURE 17: ANNOTATED PHOTO OF PACKAGE Bb EXHIBITING DOWNLAP ONTO PACKAGE A 80
FIGURE 18: ROSE DIAGRAMS OF PALEOCURRENT DATA. 81
FIGURE 19: DEPOSITIONAL EVOLUTION OF THE LOWER MEMBER OF THE EAGLE FM. 82
TABLE 1: FACIES DESCRIPTIONS AND DEFINITIONS 83
TABLE 2: TRACE FOSSIL ABUNDANCE FOR FACIES 1 THROUGH 5 84
TABLE 3: DESCRIPTION OF STRATIGRAPHIC SURFACES. 85
TABLE 4: TRACE FOSSIL ABUNDANCE FOR SURFACE TYPES 1 THROUGH 4 86

INTRODUCTION

Purpose

Deltaic successions record complex interactions between fluvial and basinal processes (Penland et al., 1988; Roberts, 1997; Serradji and Kamola, 2007; Warrick et al., 2009) and host productive hydrocarbon reservoirs (Kraft, 1979; Thom, 1983; Van Houten, 1984; Mancini, 2002). As a result, much research over the past 20 years has focused on the internal facies architecture of deltaic systems, the areal extent of architectural elements, and the processes that control their distribution (e.g., Pulham, 1989; Tye and Coleman, 1989; Dreyer, 1993; Lowry and Jacobsen, 1993; Rodriguez et al., 2000; Willis and Gabel, 2001; Ta et al., 2002; Bhattacharya and Giosan, 2003; Olariu, 2006; Charvin et al., 2010). Whereas facies and facies associations of modern deltas have been summarized by many workers (e.g., Fisher, 1969; Broussard, 1975; Coleman and Wright, 1975; Galloway; 1975; Postma 1990; Bhattacharya and Walker 1992; Reading and Collinson 1996; Giosan et al., 1999; Rodriguez et al., 2000; Bhattacharya and Giosan, 2003; Fielding et al., 2005) studies focusing on the internal facies variations and bed-scale facies architectures of ancient deltaic successions are not as common (Willis et al., 1999; Hori et al., 2002; Mellere et al., 2002; Anderson et al., 2004; Johnson and Graham, 2004; Ta et al., 2005; Olariu, 2005; Plink-Björklund and Steel, 2005; Gani and Bhattacharya, 2007).

Studies of modern deltaic systems have shown that deltaic deposits often record spatial and temporal variability in local depositional processes and facies distributions (i.e., intraparasequence-scale; *sensu* Rodriguez et al., 2000; Gani and Bhattacharya, 2007; Yoshida et al., 2007; Charvin et al., 2010). This small-scale variability observed in modern system is often not resolved in regional scale sequence stratigraphic analysis of ancient deltaic systems (i.e., parasequence-scale; *sensu* Bhattacharya and Walker, 1991; Plint and Kreitner, 2007;

Bhattacharya and Willis, 2001; Willis and Gabel, 2001; Porebski and Steel, 2003; Plink-Björklund and Steel, 2005), where such studies often average small-scale (i.e., intraparasequence-scale) facies variability and temporal trends for the purpose of regional correlation and to interpret the role of various allogenic forcing mechanisms (eustasy, tectonics and climate). As a result, subtle small-scale facies architecture variability in ancient deltaic successions may be underestimated by focusing on regional-scale sequence stratigraphic analysis, thereby compromising efforts to optimize exploration or development models involving these sedimentary systems.

Many studies use the plan view morphology of modern deltas and their surficial facies distributions as predictors of facies distributions in models of deltaic architectures away from outcrop and subsurface data control points (Busch, 1971; Duncan, 1983; Maguregui and Tyler, 1991; Bhattacharya and Willis, 2001). This approach assumes that the processes that shape delta surface morphologies also shaped the internal facies architectures of the delta (Wright and Coleman, 1973; Galloway 1975). Recent studies of internal facies architectures in modern deltas, however, reveal more complex interactions between river-, tide-, and wave processes than previously envisaged (Rodriguez et al., 2000; Charvin et al., 2010). For example, the Brazos River delta on the Texas coast has been interpreted as a wave-dominated delta based on its plan-view morphology, but recent investigations utilizing core data demonstrate that much of the delta was deposited during major river flood events with subsequent wave reworking of resulting surficial sediments (Rodriguez et al. 2000; Bhattacharya and Giosan, 2003). Similarly, the Burdekin River delta on the eastern Australian coast also exhibits a plan view morphology typically associated with wave dominance, but detailed internal facies analyses reveal that sharp-based river-dominated mouth-bar deposits dominate the depositional succession, underscoring

the importance of river-flood processes (Fielding et al., 2005). Because surficial delta morphology may not be an accurate predictor of internal facies architectures, it is critical that detailed three-dimensional outcrop-based studies be undertaken to develop more accurate internal facies architectur models within ancient delta deposits.

Three-dimensional exposures of the Upper Cretaceous Eagle Formation in south-central Montana provide an excellent opportunity to study in detail the bed-scale internal facies architectures within an ancient marine succession. This study presents a detailed internal facies architectural study of the informal lower member of the Eagle Formation and is centered on the hypothesis that a detailed internal facies architecture study can be used to infer the small-scale variability in depositional processes and temporal evolution within an ancient marine succession (Willis et al., 1999; Hori et al., 2002; Johnson and Graham, 2004; Ta et al., 2005). To this end, the primary objectives of this study include: 1) documentation of the lateral and vertical variability of facies and architectural elements, 2) determination of the nature and hierarchy of internal bounding surfaces, 3) interpretation of the depositional processes responsible for the emplacement of individual architectural elements, and 4) interpretation of the depositional environment(s) of the various architectural elements.

Geologic Framework

Convergence between the North American and Farallon plates during the Sevier Orogeny from Late Jurassic to Late Cretaceous time led to the formation of the north-south trending Sevier fold and thrust belt along the western margin of the North American craton (e.g., Armstrong, 1968; Price, 1973; Pang and Numendel, 1995). Orogenic loading, crustal shortening, and flexural subsidence associated with the Sevier thrust belt, in addition to dynamic subsidence associated with subduction of the Farallon Plate, resulted in the formation of a retroarc foreland basin, called the Western Interior Basin (WIB), east of the thrust front (e.g., Price, 1973; Jordan, 1981; DeCelles, 2004; Liu et al., 2008, 2011). The dynamics of this foreland basin were further influenced by compressional deformation during the Laramide Orogeny, beginning as early as the Campanian stage of the Late Cretaceous (DeCelles, 2004).

Due to the combined effects of flexural subsidence and high eustatic sea-levels, the WIB was periodically inundated by marine waters, forming the Cretaceous Western Interior Seaway (KWIS) (e.g., McGookey et al., 1972; Kauffman and Caldwell, 1993; Decelles, 2004). Variations in eustatic sea level (e.g., Miller et al., 2003, 2005; Plint and Kreitner, 2007), tectonic subsidence (e.g., Pang and Numendel, 1995; Catuneanu et al., 2000; White et al., 2002; DeCelles, 2004; Liu et al., 2008, 2011), and sediment supply (e.g., DeCelles and Currie, 1996; Catuneanu et al., 2000) during the Sevier Orogeny produced a series of third order regressive-transgressive depositional cycles within the WIB. These cycles are characterized by clastic wedges in which coastal plain and shallow marine strata record the western margin of the KWIS and extend eastward away from the orogenic front (Payenberg et al., 2002, 2003; Corbett et al., 2011; Kieft et al., 2011). According to Jordan (1981), during active deformation in the Sevier thrust belt, approximately 9 km of Cretaceous sediment accumulated in the Wyoming, Montana, and Idaho part of the

Cretaceous Western Interior Basin. During the Late Cretaceous, the stratal stacking patterns of these regressive-transgressive cycles became increasingly complex and amalgamated (DeCelles, 2004) as a result of fluctuations in rates of tectonic subsidence, eustasy, and sediment supply.

Various approaches have been used to determine the circulation patterns within the Cretaceous Western Interior Seaway, including oxygen- and carbon-isotope studies to infer density stratification and resulting circulation (Wright, 1987), numerical modeling of tidal circulation (Slater, 1985), qualitative predictions of current patters from inferred climatic conditions (Parrish and Curtis, 1982; Lloyd, 1982), characterizations of paleoceanography from the distribution of paleobiogeographic units (Kauffman, 1984), and numerical modeling of wind-driven flows over a portion of the Campanian shelf (Parrish et al., 1984). Most of these studies concluded that the net longshore drift and circulation patterns within the Cretaceous Western Interior Seaway were influenced by a strong counterclockwise gyre driven by Coriolis forcing, seasonal storms, and thermohaline-induced circulation (Kent, 1968; Scott and Taylor, 1977; Slingerland & Keen, 1999). Detailed numerical paleooceanographic modeling of the Cretaceous Western Interior Seaway (Ericksen and Slingerland, 1990; Slingerland et al., 1996) indicates that the seaway was generally wave-dominated with predominant southward longshore drift at the western margin and both winter storms and summer storms (hurricanes) affected the seaway in such a way that storm-driven currents generally were shore-parallel to the south with occasional oblique onshore and offshore directed flow.

Regional Background and Study Area

There have been many outcrop and subsurface studies that focused on the Late Cretaceous regressive-transgressive cycles in strata of the Bighorn Basin in central Wyoming, the

Powder River Basin in southeastern Montana and northeastern Wyoming, the San Juan Basin in New Mexico and Colorado, the Book Cliffs in north-central Utah, and the Canadian foreland basin in southern Alberta and Saskatchewan (e.g., Hollenshead and Pritchard, 1961; Sabins, 1963, 1972; Weimer, 1965; Asquith, 1970; Evans, 1970; Woncik, 1972; Palmer and Scott, 1984; Bergman and Walker, 1987; Cant, 1992; Bergman, 1994; Bhattacharya and Willis, 2001; Martinsen et al., 2001; Walker and Eyles, 2006; Gani and Bhattacharya, 2007). In contrast, relatively few detailed studies have been conducted on Late Cretaceous strata in south-central Montana.

The Cretaceous Eagle Formation of south-central Montana was deposited during Santonian to Campanian time along the northwest–southeast oriented western margin of the Cretaceous Western Interior Seaway as a result of sediments shed from the Sevier thrust belt (Figure 1; Gill and Cobban, 1973; Hearn and Hansen, 1989; Payenberg et al., 2003). The Eagle Formation is located stratigraphically above the Upper Santonian Telegraph Creek Formation and below the Lower Campanian Claggett Formation (Figure 2; Rice, 1980; Hearn and Hansen, 1989; Hanson and Little, 1989; Fishman et al., 2001; Payenberg et al., 2002). Outcrop exposures of these and equivalent formations extend along depositional strike from south-central Alberta and Saskatchewan to north-central Wyoming (Payenberg et al., 2002; 2003; Finn et al., 2010).

Outcrops of the Eagle Formation in south-central Montana wrap around the Pryor Mountains and in the study area strata dip approximately 4^0 to the northeast (Gill and Cobban, 1973; Olson and Smith, 2007). Exposures of the Eagle Formation in south-central Montana are interpreted to be the result of Laramide-Pryor uplift and subsequent down-cutting by the Yellowstone River and its tributaries (Shelton, 1965). Recent stratigraphic analyses of the Eagle Formation in and around Billings suggests that the Eagle Formation consists of three informal

members; a lower member, middle member, and upper member. This study focuses on the informal lower member of the Eagle Formation (herein known as the lower member of the Eagle Formation) in and near Billings, MT. The lower member outcrops along 30 km of cliff exposure (12 km in an E-W direction and 18 km in an N-S direction). Of these exposures, 16 km were examined in detail (9 km E-W and 7 km N-S) as part of this study.

In the study area, the Telegraph Creek Formation underlies the Eagle Formation and consists of interbedded shale and siltstone that coarsen upwards to interbedded siltstones and very fine grained sandstones. The upward transition from the Telegraph Creek Formation to the Eagle Formation is gradational and the Eagle Formation is defined as beginning with the first cliff forming sandstone above the Telegraph Creek Formation (Shelton, 1965; Hearn and Hansen, 1989).

Previous Work

The Eagle Formation in and around Billings, MT, has been studied previously (Olson, 1961; Shelton, 1965, Kendrick, 1985; Hearn and Hansen, 1989; Hanson, 1989; Hanson and Little, 1989) with various hypotheses suggested regarding its origin. Olson (1961) described four members in the Eagle Formation in Billings and inferred that the formation was exclusively marine in origin, based on the abundance of cross-bedding, glauconite, and the occurrence of well sorted sands.

Shelton (1965) subdivided the Eagle Formation into 5 units. He cited the low angle, southwest (paleolandward) inclined bedding, the coarsening upward grain size, and large width-to-thickness ratio as mapped in the subsurface as evidence that the informal lower member of the Eagle Formation studied here represents an emergent barrier bar or island. Shelton proposed

modern-day Galveston Island as an analog for his lowest unit. Because of the southwest dipping accretion surfaces in the lower member, Shelton concluded that the barrier island prograded in a landward direction. He also recognized the sharp contact at the top of the lower member and proposed it as a transgressive surface.

Kendrick (1985) studied the same interval as Shelton (1965) as well as the overlying basal sandstones of the informal middle member of the Eagle Formation. Kendrick noted the sharp contact at the top of the lower member but did not address its significance, and he interpreted the lower member and the basal part of the middle member as one depositional unit. Kendrick (1985) concluded that the interval he examined did not represent an emergent barrier island system, but rather inner shelf sand bar deposits. His interpretation was primarily based on the identification of hummocky cross stratification in the basal part of the middle member of the Eagle Formation indicating deposition within storm wave base.

Hanson and Little (1989) proposed nine different depositional sequences regionally within the Eagle Formation. They interpreted their first sequence (the lower member) as shoreline attached point-sourced plume sands that were deflected to the south by longshore and eddy currents. Hearn and Hansen (1989) suggested that there were only 3 depositional sequences within the Eagle Formation in the Billings area, and that the lowest one was the result of landward-migrating submarine shelf-bar sands.

METHODS

The lower member of the Eagle Formation typically outcrops as steep cliffs in and around Billings. Within the study area a total of fifteen stratigraphic sections were measured (Figures 1C, 3; Appendix A) in accessible ravines and one continuous HQ core (6.35 cm diameter) was described starting below the base of the Telegraph Creek Formation and ending above the lower member of the Eagle Formation. Sections and core were measured/described at centimeter to millimeter scale. Attributes recorded included grain size, bed thickness, sedimentary structures, ichnofauna, and bioturbation intensity. Bioturbation intensity was estimated using a numerical ranking from 0 (no bioturbation) to 6 (complete bioturbation) following the guidelines of MacEachern et al. (2005). At 50 additional locations (Figure 1C) composite bedset thicknesses were determined by suspending a rope down the side of vertical outcrop exposures and using binoculars to measure distances between bedset bottom and top from an accessible vantage point roughly at the same elevation. These bedset measurements were used as a proxy for stratigraphic sections, and plotted on photomosaics.

Because the underlying Telegraph Creek Formation is composed predominately of mudstone and typically is a slope former, the starting point of most outcrop measured sections was the first appearance of a cliff forming sandstone (Figure 4G). Both the Telegraph Creek and Eagle formations were described in detail in the available core. Paleocurrent indicator data was obtained by measuring orientations of ripple crests, trough axes, scour axes, and planar cross bedding. A gamma-ray profile of the informal lower member of the Eagle Formation was constructed using a Geometrics GR-101A handheld gamma-ray scintillometer (Figure 3) with readings recorded at 15 cm intervals on outcrop.

High-resolution photographic images (12 megapixel) were taken with a Nikon D5000 35 mm SLR camera and merged into photomosaics using Adobe Photoshop CS5. Photomosaics were used to trace laterally continuous surfaces in outcrop and to correlate all stratigraphic sections. Photomosaics covered approximately 25 km of continuous cliff exposure.

A Leica TC-307 total station and a Trimble TSC1 Asset Surveyor field GPS unit were used to determine the locations of all measured and rope drop sections as well as to survey laterally continuous surfaces identified in outcrop and in photomosaics (Figure 1C; Appendix B). A total of 282 x, y, z, data points were collected from 5 total station survey locations within the study area. All collected data were loaded into PETREL and used to generate plan view surface/contour maps and isopach maps.

The dip of all bedding planes and laterally continuous surfaces were corrected for an approximate dip of 4^0 towards the NE within the study area using the computer program Stereonet7 (Appendix C; Almendinger, 2011). The dip of 4^0 to the NE was obtained from field measurements of the Type 3 surface (see *Regional Scale Surfaces*).

Thin sections from 35 sandstone samples were examined petrographically using a Leitz Orthoplan polarizing microscope. Petrographic characteristics documented included composition, grain size, rounding, shape, and sorting as well as sample porosity (Appendix D). All samples were point-counted using a modified Gazzi (1966)-Dickinson (1970) method. Mineral grain types counted were quartz (mono- and polycrystalline), chert, plagioclase feldspar, orthoclase feldspar, biotite, muscovite, glauconite, and zircon as well as lithic fragments (metamorphic, sedimentary, and volcanic). A minimum of 500 framework grains were counted in each sample. The percentage of silt-sized particles, cement type(s), and number of counts on pore space were also recorded but was not included in the 500 framework grain counts per sample. A

QFL plot (following the methodologies outlined in Folk, 1974) was generated for the 35 samples examined to determine sandstone lithology (Figure 5).

RESULTS

Facies

Five facies were identified in the lower member of the Eagle Formation. These five facies were determined on the basis of their physical and ichnological characteristics (Tables 1 and 2; Figures 4, 6, and 7). Petrologic data (Figures 5, 8; Appendix D) is also included for facies 2, 4, and 5.

Facies 1 (F1): Bioturbated Interbedded Mudstone, Siltstone, and Sandstone

Facies 1 (F1) consists of interbedded siltstone and mudstone that coarsens upward into interbedded siltstone and sandstone. Facies 1 was infrequently observed in outcrop and seen in detail in core. Mudstone and siltstone beds contain uncommon soft sediment deformation structures (e.g., poorly developed dish structures and convolute bedding). Sand beds within F1 are subordinate to siltstone and mudstone, are sharp based, moderately sorted, very fine grained, and show little internal grading. Individual sand beds vary between <1 and 10 cm thick. Sand beds in F1 are either structureless, planar laminated, or hummocky cross-stratified (HCS) (Figure 4A, B, C). F1 beds have a corrected/depositional dip $<0.5^{o}$ to the NE. The percentage of sandstone present increases as F1 coarsens upward and gradationally transitions into F2. Lopez (2000) mapped F1 as the Telegraph Creek Formation in the study area.

Bioturbation intensity in F1 varies from 1 to 6, with the most intense burrowing occurring in siltstone and mudstone. Ichnofauna identified in F1 include *Ophiomorpha, Terebellina, Palaeophycus tubularis,* and *Planolites. Ophiomorpha* burrows are typically sand filled. Bedding parallel burrows of *Planolites* and *Palaeophycus tubularis* dominate the lower part of F1,

whereas the upper part is dominated by sub-horizontal and sub-vertical burrows of *Ophiomorpha* and *Terebellina*.

Facies 2 (F2): Bioturbated Massive Sandstone

Facies 2 is a yellow to gray bioturbated (Figure 4D, E, F), well-sorted, sub-rounded, lithic arkose to feldspathic litharenite (Figures 5, 8; Appendix D). Grain size varies from lower very fine near the base to upper very fine sand toward the top. F2 averages 5% silt sized particles and 4% of sand sized grains are accessory minerals that consist of glauconite, muscovite, and biotite. Calcite is the primary cement in F2 with iron oxide subordinate.

The BI of F2 is 5 to 6, and bedding boundaries have been disrupted by a high trace density. While trace abundance is high, diversity is low. *Ophiomorpha* and *Terebellina* traces are common, whereas as *Skolithos* and *Cylindrichnus concentricus* traces are rare. *Ophiomorpha* burrows are packed densely along distinct horizons which can be traced laterally for tens of meters. Vertical feeding traces of *Skolithos* and *Ophiomorpha* commonly are truncated along these horizons (Figure 4F). The vertical distance between *Ophiomorpha* horizons varies between 10 and 80 cm and these horizons have an average corrected/depositional dip of $<0.5^{o}$ to the NE.

Red-brown spherical and ellipsoidal carbonate concretions are common in F2. These concretions occur along multiple horizons and range from about 30 to 300 cm in diameter. Many concretions contain a recognizable ichnofauna such as *Ophiomorpha*.

Facies 3 (F3): Mudstone and Siltstone

Facies 3 consists of tan to gray laminated mudstones or planar to ripple laminated siltstones (Figure 4H, I). In outcrop it is difficult to observe sedimentary structures in F3.

Laminated mudstones range from <10 to 40 cm thick and contain rare carbonate laminae. The BI of the laminated mudstones varies between 0 and 4 and the only identified burrow type is *Palaeophycus tubularis*. Where the BI is 4, the laminated mudstones have a mottled appearance. Within F3 siltstones sedimentary structures observed grade from planar laminated bases upward to ripple laminated tops. The siltstones range from 20 to 40 cm thick, have sharp basal and upper contacts, and have a BI of 0.

Facies 4 (F4): Planar and Ripple Laminated Sandstone

Facies 4 is a tan to gray well sorted, sub-rounded lithic arkose to feldspathic litharenite (Figures 5, 8; Appendix D). Grain size varies from lower fine to upper very fine sand. Individual beds are normally graded, sharp based, and contain planar and ripple laminations (Figure 6). F4 averages 3% silt sized particles and 2% of sand sized grains are accessory minerals consisting of glauconite, muscovite, and biotite. Calcite is the primary cement with subordinate iron oxide.

Individual F4 beds range in thickness from 20 to 80 cm and can be traced laterally for hundreds of meters and have maximum corrected/depositional dips of 6° to the SW. About 65% of F4 beds are characterized by planar laminated bases and a ripple laminated tops (Figure 6B, E). About 5% of ripple laminated sandstones contain ripples that are symmetric in cross section and have non-rounded crests. Symmetric ripples are found only in the upper part of these beds. Approximately 10% of F4 beds consist of a planar laminated base, a ripple laminated middle, and are capped by a silty-sandstone layer that sometimes contains planar laminations and detrital organic fragments.

The remaining 25% of F4 consist of fine-grained sandstone up to 80cm thick, which contain only planar laminations (Figure 6A, F). At two locations, beds were observed with

planar laminated bases, small-subcritically-climbing trough cross-beds with roughly 10cm of vertical relief, and ripple laminated tops. The majority of the ripple laminated sandstone beds contain slightly asymmetric ripples with rounded crests and, locally, convex-upward lee and stoss sides (Figure 6D). Load casts were also observed in F4 beds (Figure 6C). When present, basal scours within F4 average 60 cm wide and 20 cm deep (Figure 6I) but can reach dimensions up to 185 cm in width by 90 cm deep (Figure 6G).

The BI of F4 is 0 to 3 and is characterized by a low diversity ichnofauna assemblage (Table 2) which most closely resembles a mixed *Cruziana-Skolithos* ichnofacies (*sensu* Seilacher, 1967). About 60% of the assemblage in F4 consists of the bedding parallel deposit feeding traces of *Planolites* and *Palaeophycus tubularis*. About 40% of the assemblage consists of suspension feeding traces of *Ophiomorpha* and *Skolithos* in addition to *Fugichnia* (escape traces) between beds (Figure 6H).

F4 beds commonly contain discontinuous calcite concretion horizons that are tens of meters in length, as well as isolated round to oblong calcite concretions up to 80 cm in diameter. Both concretion types occur along bedding horizons, and exhibit slightly increased bioturbation intensities (BI 3 to 4).

Facies 5 (F5): Graded, Massive, Planar Laminated and Planar Cross Laminated Sandstone

Facies 5 is a tan to gray well-sorted, sub-rounded lithic arkose to feldspathic litharenite (Figures 5, 8; Appendix D). Grain size varies from upper fine to lower fine sandstone. Individual beds are normally graded, sharp based, and either massive to planar laminated or massive to planar cross laminated (Figure 7). F5 averages 1% silt sized particles and approximately 1% of

sand sized grains are accessory minerals consisting of glauconite, muscovite, and biotite. Calcite is the primary cement in F5 with subordinate iron oxide.

Individual F5 beds range in thickness from 60 to 110 cm, can be traced laterally for hundreds of meters and are characterized by a maximum depositional dip of 6° to the SW. The majority of beds (> 50%) consist of a massive base and a planar laminated top (Figure 7A, B). Roughly 20% of F4 consist of massive bedding only (Figure 7E), whereas about 15% consist of a massive base, a planar laminated middle and a planar cross or ripple laminated top (Figure 7D). The remaining 15% consist of repetitions of these sedimentary structures (e.g., planar laminated, massive, planar laminated) (Figure 7C). Approximately 30% of all these bed types are capped by thin (1-2 cm) silt drapes (Figure 7A). Soft sediment deformation features occur in all bed types, but are not common.

The BI of F5 is 0 to 2 and is characterized by a low diversity ichnofauna assemblage (Table 2) which most closely resembles a mixed *Cruziana-Skolithos* ichnofacies assemblage (*sensu* Seilacher, 1967). About 90% of the assemblage is dominated by traces from suspension feeding organisms such as *Ophiomorpha*, *Skolithos*, and *Monocraterion* (Figure 7F) in addition to *Fugichnia* (near vertical escape traces) between beds. The remaining 10% of the assemblage consist of deposit feeding traces of *Planolites* and these are found in the silt drapes that cap roughly 30% of F5 beds.

Discontinuous calcite concretion horizons and isolated round to oblong concretions are also common in F5 beds and their distribution is similar to that previously described for F4 beds.

Petrographic Data

Petrographic analyses of 35 sandstone samples from facies 2, 4, and 5 indicate that each facies contains lithic arkoses and/or feldspathic litharenites (*sensu* Folk, 1974). A QFL plot (Figure 5) demonstrates lithologic grouping by facies and compositional variations between and within each facies type. F2 is the least mineralogically mature with an average composition of Q54, F23, L23. F4 is Q61, F20, L19, and F5 is the most mineralogically mature with a composition of Q66, F19, L15 (Figure 8; Appendix D).

Pore space varies by facies type. In F2 pore space ranges from 3% to 21% with an average porosity of 13%. Porosity in F4 ranges from 1% to 25% and averages 12%. In F5 beds pore space ranges from 1% to 20% with an average pore space of 16%. Calcite cement dominates representing about 95% of the cement present.

The petrographic data can be found in Appendix D.

Stratigraphic Surfaces

Laterally continuous surfaces were observed in outcrop and mapped in the study area (Figure 9). Surfaces in the study area occur at two scales; those that can be used to package outcrop-scale architectural elements (hundreds to thousands of meters) and those that can be used to construct regional frameworks (tens of kilometers) (Tables 3 and 4). Plan view surface/contour maps were generated for the outcrop-scale surface types described below (Figure 10).

Outcrop Scale Surfaces

Type 1 surfaces

Type 1 surfaces are the smallest scale and can be traced along cliff exposures for hundreds of meters (Figure 10). These surfaces slope up to 6° to the SW, are bedding parallel, typically do not truncate underlying sediments, and are under- and overlain by F4, and F5. Sandstone beds immediately underlying Type 1 surfaces include framework constituents (70 to 80%), matrix-cement (20 to 25%) and pore spaces (0 to 10%). Bioturbation intensity along Type 1 surfaces is 3 and the assemblage consists of bedding parallel burrows of *Planolites* and *Palaeophycus tubularis*, which most closely resembles the Cruziana ichnofacies (*sensu* Seilacher, 1967)

Type 2 Surfaces

Type 2 surfaces are of intermediate scale and can be traced along cliff exposures for thousands of meters (Figure 10, 11). These surfaces slope up to 6° to the SW, are bedding parallel, typically do not truncate underlying deposits, and are underlain by F4 and F5. Sediments immediately underlying Type 2 surfaces include framework constituents (70 to 80%), matrix-cement (20 to 30%) and pore spaces (0 to 5%, typically 0%). Type 2 surfaces function as hydrologic barriers (Figure 9B). Bioturbation intensity along Type 2 surfaces is increased (BI of 4) relative to underlying deposits, and the assemblage consists of bedding parallel burrows of *Planolites* and *Palaeophycus tubularis* which most closely resembles that of the Cruziana ichnofacies (*sensu* Seilacher, 1967). Type 2 surfaces were consistently observed to be overlain by F3 laminated mudstones. The contact with overlying F3 is sharp. Above Type 2 surfaces, F3

varies in thickness from <10 cm in the east, where they are composed entirely of silt, to 40 cm in the west where they are finer grained and contain significant amounts of clay.

Regional Scale Surfaces

Type 3 surface

One Type 3 surface, corresponding to the lower of the two regional surfaces, was mapped over an area of 60 km^2 (Figure 8D, 9D, E, 11, and 12). This surface has a gentle depositional dip to the NE (< 0.5°). The 10 to 20 cm immediately underlying the surface has a BI of 5 to 6, is dominated by *Planolites , Palaeophycus tubularis* and *Ophiomorpha*, is always underlain by F2 deposits, and includes framework constituents (75 to 80%), pore spaces (0 to 10%) and calcite cement (5 to 15%). In the eastern part of the study area it is directly overlain by F4 or F5 deposits. In the western part of the study area this surface is directly overlain by laminated mudstone with a mottled appearance and a BI of 4 from F3 that is up to 20 cm thick, and F3 siltstones, F4, or F5 deposits overlie the laminated mudstones above this surface. All, F3, F4, and F5 deposits directly overlying this surface show evidence of downlap.

Type 4 surface

The Type 4 surface occurs as the upper of the two regional surfaces and was mapped over the same 60 km^2 area as the Type 3 surface (Figure 8D, 9C, 11, and 12). The Type 4 surface represents the top of the lower member of the Eagle Formation, has a depositional dip of approximately 1° to the NE, and truncates the underlying west- (landward) dipping Type 1 and 2 surfaces as well as underlying F4 and F5 deposits. This surface is erosional and truncates older deposits in the northeast and successively younger deposits to the southwest (Figure 11, 12). The

Type 4 surface is very well cemented (porosity values typically 0%; where all void space is typically filled with calcite cement), and is a significant hydrologic barrier to flow. The 10 to 20 cm of sandstone immediately underlying this surface is characterized by a *Glossifungites* ichnofacies (*sensu* Seilacher, 1967; Yang, 2009) and has a BI of 6. The burrows within this interval are filled primarily with sediments from the immediately overlying units of the middle member of the Eagle Formation.

DEPOSITIONAL PROCESSES AND ENVIRONMENTS

Depositional Processes:

Facies 1 (F1)

The high degree of bioturbation observed in the mudstones and siltstones of F1 (up to BI of 6) resulted in the destruction of most sedimentary structures. The high bioturbation intensity in these sediments indicate that deposition resulted from suspension settleout in a low energy environment where benthic organisms could rework the sediments (*sensu* Pemberton et al., 2001). The occurrence of sparsely bioturbated (BI of 1) thin (<10 cm) structureless and planar laminated sandstone beds within an overall highly bioturbated (BI up to 6) mud- and siltstone dominated succession indicates that sand deposition resulted from episodic high energy events such as sediment gravity flows of varying strength (Brenchley et al., 1979; Dott and Bourgeois, 1982; Mulder et al., 2003; MacEachern et al., 2005; Pattison, 2005; Haughton, 2009). The hummocky cross stratified sandstone beds within F1, however, likely were formed from a combination of unidirectional and oscillatory flow and can be attributed to formation by the action of storm waves (Dott and Bourgeois, 1982; Surlyk and Noenygaard, 1986; Arnott and Southard, 1990; Yang et al., 2005). The soft sediment deformation structures locally preserved in the mudstone and siltstone (poorly developed dish structures and convolute bedding) likely formed during the emplacement of overlying sandstone beds where loading during rapid sedimentation events caused the upward escape of over-pressured fluids through cohesionless sediment (Lowe, 1975; Allen, 1982; Pemberton et al., 1992).

The amount of sandstone beds increases vertically in F1 suggesting that the frequency of high energy events increased through time as did proximity to the sediment source.

Facies 2 (F2)

F2 is characterized by a very high degree of bioturbation (BI 5 to 6) and a lack of preserved sedimentary structures. As a consequence, the interpretation of depositional processes is limited to what can be inferred from the observed ichnofauna.

Within F2, the trace fossil *Ophiomorpha* is distributed throughout, but commonly occurs as densely clustered groups of burrows along discrete horizons. These horizons likely reflect bedding surfaces where ichnofauna colonized the substrate (Pollard et al., 1993). Additionally, *Ophiomorpha* burrows are commonly truncated along specific horizons, suggesting that burrow truncation resulted from erosion during high-energy events (Pemberton et al., 2001; MacEachern et al., 2005). The ichnofauna assemblage of F2 is characterized strictly by traces indicative of suspension feeding behavior (Table 2). The colonization of such high energy deposits by a strictly suspension feeding trace assemblage is characteristic of opportunistic colonization of event beds by ichnofauna (Pemberton et al., 1992; MacEachern et al., 2005). Along with the erosional nature of depositional events in F2, the ichnofauna and its occurrence within the facies strongly suggests that it was deposited as the result of sediment gravity flows.

Facies 3 (F3)

The laminated mudstones with rare carbonate laminae of F3 indicate deposition from suspension settleout in a low energy environment (e.g., Cotter, 1975; Agrawal and Pottsmith, 2000). A BI of up to 4 with a mottled appearance also indicates a low energy setting that allowed organisms to rework and destroy laminae (*sensu* Pemberton et al., 2001).

The sharp based beds of siltstone indicate deposition from high energy episodic events (Brenchley et al., 1979; Dott and Bourgeois, 1982; MacEachern et al., 2005; Pattison, 2005). A BI of 0 in these siltstone beds also indicates high energy, which inhibited bioturbation

(Pemberton et al., 1992; MacEachern et al., 2005). The upward transition from upper flow regime planar lamina to lower flow regime asymmetric ripples (Bouma Tb to Tc) is indicative of deposition resulting from unidirectional decelerating currents. These siltstones are interpreted to represent the waning stages of turbidity currents (Bouma, 1962; Middleton and Hampton, 1976; Allen, 1984; Baas et al., 2000; Gani 2004; Haughton et al, 2009).

Facies 4 and 5 (F4 and F5)

Both F4 and F5 contain partial Bouma-like sequences (Bouma, 1962) (Figure 13), can be erosionally based or scoured, exhibit soft sediment deformation structures, and contain *Fugichnia* (ichnofauna escape burrows). All of these characteristics have been described from turbidites (Bouma, 1962; Middleton and Hampton, 1976; Collinson and Thompson 1989; Hiscott et al., 1997; Gani 2004). As such, F4 and F5 are interpreted to have resulted from deposition by turbidity currents.

The sedimentary structures and characteristics observed in F4 and F5 are similar to both low- and high-density turbidites, but the deposits more closely resemble turbidites resulting from sustained flow generated during storms (i.e., storm surges) (Figure 14). Such storm generated flows can produce fully turbulent waxing to waning flows characterized by high concentrations of sediment where individual surges can be sustained for multiple hours (Inman et al., 1976; Shepard et al., 1977; Dengler et al., 1984 Mulder et al., 2003; Plink-Björklund et al., 2004). The characteristics exhibited by F4 and F5 which are consistent with an origin as storm generated turbidites are (1) the abundance of thick sand beds (up to 80 cm thick in F4 and 110 cm in F5), (2) prevalence of traction related sedimentary structures (i.e., ripples and planar cross beds), (3) presence of combined flow ripples, and (4) evidence of sustained flow and changes in flow

behavior through time (i.e., waxing to waning flow) (Piper and Savoye, 1993; Kneller and Buckee, 2000; Mulder and Alexander, 2001; Plink-Björklund et al., 2004; Zavala et al., 2006; Lamb et al., 2008). Waxing to waning flow characteristics are observed in F5 deposits where 15% of beds exhibit repetitions of Bouma-like turbidite divisions within a bed (i.e. Tb-Ta-Tb; Figure 7C). These variations reflect temporal changes in flow velocity and sediment flux within the same current. The alternation of Tb and Ta intervals indicates alternation of low and high fallout rates where the ungraded intervals reflect rapid fallout rates and the laminated intervals represent decreases in sediment flux (Arnott and Hand, 1989; Kneller and Branney, 1995).

Sustained flows generally are thought to result from hyperconcentrated sediment discharged by rivers into receiving basins during high-flow or runoff events (Bates, 1953). In this case the excess density provided by the suspended sediment results in a flow with a bulk density greater than that of the ambient water and the flow plunges (Bates 1953; Mutti et al., 1996) generating a subaqueous extension of the fluvial channel, and basinward delivery of large volumes of sediment (Zavala et al., 2006). The resulting deposits are typically referred to as hyperpycnites (*sensu* Mulder et al., 2003)

Sustained flows and their resulting deposits can, however, be generated by mechanisms other than hyperconcentrated rivers, including (1) instability during volcanic eruptions and the consequent remobilization of unconsolidated material (Lipman and Mullineaux, 1981; Kokelaar, 1992); (2) seismically triggered sliding within the drainage basin (Syvitski and Schafer, 1996); (3) storm surges (e.g., Inman et al., 1976; Shepard et al., 1977; Dengler et al., 1984); and (4) retrogressive slope failure (e.g., Andresen and Bjerrum, 1967).

Recent studies have shown that sustained flows do not require autosuspension from a hyperconcentrated river source for initiation and sustainment of flow, but can be initiated by

sediment flux convergence (i.e., sediment load increase due to heightened wave orbital velocities and near-bottom currents) and maintained by wave and current-induced suspension (combined flow processes) (Hill et al., 2003; Wright and Friedrichs, 2006). The term 'combined flow' is generally used to indicate a combination of geostrophic unidirectional currents and strong wave driving oscillatory motion at the bed, commonly associated with storms (Arnott and Southard, 1990; Dumas et al., 2005). As these sustained flows move under the influence of gravity, they deposit sediment in response to decreases in wave and current induced near-bed shear velocity or bed slope, or both.

Only trace amounts of organic material were identified within F4 and F5, and time equivalent river effluents or channels were not found; thus F4 and F5 cannot be linked conclusively to a fluvial source. However, the occurrence of Bouma-like Tc ripple laminations consisting of slightly asymmetric ripples with rounded crests, and convex-upward lee and stoss sides is consistent with current-dominated combined flow ripples (Harms, 1969; Yokokawa, 1995; Yokokawa et al., 1995; Myrow et al., 2002; Hill et al., 2003). This suggests a combined flow origin for F4 and F5 where rounded crests arise from small vortices that form in the troughs of these ripples during combined flow (Yokokawa 1995; Yokokawa et al. 1995). Thus, the turbidites of F4 and F5 are interpreted as the result of combined flow origin rather than the direct result of fluvial discharge.

In addition, F4 and F5 beds display depositional dips to the S-SW, which is normal to oblique to the NW-SE trending paleoshoreline (Gill and Cobban, 1973; Payenberg et al., 2003). The landward primary dip direction of these facies suggests that they were generated during storms when effects of combined flows typically result in sediments being transported and

deposited in onshore directions (Swift and Rice, 1984; Penland et al., 1988; Snedden et al., 1988).

Facies Architecture

Analyses of the 5 facies and 4 surface types resulted in the delineation of sediment packages within the lower member of the Eagle Formation. These sediment packages are delineated based on the type(s) of stratigraphic surfaces which bound them into different geometries with distinct internal characteristics. Isopach maps were generated for packages that could be documented in 3-dimensions and correlated between the E-W and N-S trending cliffs. Packages occur at 3 scales; those that can be traced along outcrop exposures for hundreds of meters and are bounded by Type 1 surfaces (three analyzed), those that can be traced along outcrop exposures for thousands of meters and that are bounded by Type 2 surfaces (six analyzed), and those that can be traced along outcrop exposures for tens of kilometers and that are bounded by Type 3 and 4 surfaces (two analyzed).

Package A

Package A is the stratigraphically oldest and largest of the packages and is comprised of facies 1 and 2. Package A gradationally coarsens upwards from F1 to F2. The upper part of package A (consisting entirely of F2) makes up the lower half of the cliff forming lower member of the Eagle Formation (Figure 4G). The lower half of the gamma-ray profile, which was measured through the entire lower member of the Eagle Formation, begins at the first appearance of cliff forming sandstone and indicates that the upper part of package A exhibits an overall coarsening upward pattern (Figure 3).

The lower part of package A (facies 1) normally is covered by the talus slope below the overlying cliff forming sandstone. Because F1 was rarely observed in outcrop, thickness measurements of package A were taken from the upper cliff forming part only.

The upper part of package A was observed along the E-W trending cliffs for 12 km and along N-S trending cliffs for 18 km, but only studied in detail for 9 km in an E-W direction and 7 km in a N-S direction. This cliff-forming part of package A averages 15 m thick and is thickest in the northeastern part of the study area where it is 20 m. Where observed, it thins to 5m thick 18 km south of downtown Billings and is 8m thick 9 km west of downtown (Figure 15). The top of package A is the Type 3 surface.

Packages B to G

Overlying package A and the Type 3 surface are 6 sandstone packages (packages B to G) that are stacked en-echelon. Each is comprised of facies 3, 4, and 5. Packages B to G are sigmoidal in shape, coarsen upward from muddy to planar and cross laminated F3, and exhibit an east to west or down-slope fining of facies (proximal to distal) from F5 in the east to F4 in mid-slope to down-slope locations to F3 in distal locations in the west. Not all facies types are preserved in each package, but each package demonstrates a proximal to distal fining. Each of these packages thins and pinches out to the west along the E-W trending cliffs (Figures 11, 12), and each downlaps onto the Type 3 surface. Packages B to G have gentle depositional dips to the SW. Each package is capped by a Type 2 surface and overlying F3 laminated mudstones, and each is truncated at its most up-slope location by the Type 4 surface.

The E-W cliff exposures in Billings are oblique to paleoslope and dip sub-parallel to packages B to G. In contrast, the N-S cliffs are aligned strike sub-parallel. In an E-W direction

these packages occur over 12 km outcrop exposure. Each package is between 2 and 3 km in length down depositional dip, and each package has a maximum thickness of about 12 m.

Of the 6 en-echelon stacked packages, only package B (the oldest) could be correlated with certainty between the E-W and N-S trending cliffs, allowing for study in both dip sub-parallel and strike sub-parallel exposures. Package B was mapped along the E-W trending cliffs for 3 km and the N-S trending cliffs for 2.7 km. An isopach map of package B illustrates that it thins to the southwest (Figure 16).

Packages Ba, Bb, and Bc

Package B can be subdivided into three (3) smaller sandstone packages (Ba, Bb, and Bc) or sub-packages. Each is composed of facies 3, 4, and 5. Packages Ba to Bc each coarsen upward from fine-lower sandstone to fine-upper sandstone. The upper half of the gamma-ray profile encompasses package Bb and suggests a upward coarsening succession (Figure 3).

Packages Ba to Bc have a maximum thickness of about 10 m and can be correlated between the E-W and N-S cliffs. Similar to the larger packages, packages Ba to Bc are sigmoidal in shape, have gentle dips to the SW, and exhibit down-slope facies transition from F5 through F4 and F3. Each package downlaps onto the Type 3 surface (Figure 17). Along the E-W trending cliffs, packages Ba to Bc stack en-echelon, thin, and pinch out to the west and along the N-S trending cliffs, packages Ba to Bc stack en-echelon to the south and pinch out to the south. The package overlying package Bc along the N-S trending cliffs could not be correlated with complete confidence to the E-W trending cliffs. It is unclear if deposition of this package is contemporaneous with, or occurred before or after deposition of package C along the E-W trending cliffs. Paleocurrent indicator measurements from packages Ba to Bc reflect an average

sediment transport direction of about 210°. Paleocurrent indicators from Ba to Bc vary between 207° and 220° (Figure 18). Packages Ba to Bc are separated from each other by Type 1 surfaces and are truncated in an up-slope direction by the Type 4 surface.

Depositional Environment and Evolution

The lower member of the Eagle Formation is interpreted as a regressive to transgressive wave-dominated deltaic system with 1) a regressive phase characterized by delta progradation, and 2) a transgressive phase characterized by wave and storm generated deposits. The evolution of this deltaic succession (Figure 19) is discussed in terms of the significance of stratigraphic surfaces, geometry of sand packages between surfaces, and changes in depositional setting.

Regressive Phase

The regressive phase of delta evolution is represented by Package A. The overall high bioturbation intensity in package A (up to BI 6 in F1 and 5 to 6 in F2) indicates that deposition occurred in what was an overall low energy environment with a relatively low sedimentation rate. The overall low energy setting allowed for organisms to re-work and destroy bedding structures (*sensu* Pemberton et al., 2001). This suggests that deposition was below normal fair-weather wave base, where ichnofauna could flourish (MacEachern et al., 2005). The sparsely bioturbated (BI 1) nature of the thin sandy beds within F1, however, suggests that the episodic events which emplaced these sand beds were associated with higher environmental energy, which inhibited extensive bioturbation (Pemberton et al., 1992; MacEachern et al., 2005). The HCS beds within package A (in the upper part of F1) suggest that deposition of part of package A occurred above storm wave base (Dott and Bourgeois, 1982; Surlyk and Noenygaard, 1986; Yang et al., 2005).

Both prograding deltas and non-deltaic shoreface successions produce coarsening upward sequences similar to the trend observed in package A (e.g., Oomkens, 1970; Coleman and Wright, 1975; Bhattacharya and Willis, 2001; Bhattacharya and Giosan, 2003; Olariu et al., 2010; Bhattacharya and Walker, 1991). Recognition of this attribute alone is not sufficient for distinguishing between these two depositional setting. The low diversity ichnofauna assemblage that characterizes package A is, however, more typical of deltaic settings where the close proximity to a fluvial source results in salinity fluctuations that inhibit ichnofauna diversity (Pemberton et al., 2001; MacEachern et al., 2005). Based on its 1) coarsening upward profile, 2) restricted ichnofauna assemblage, and 3) extensive bioturbation, package A is interpreted as part of a regressive delta in a pro-delta (F1) to distal delta front (F2) environment below fair weather wave base but above storm wave base.

The upper 10 to 20 cm of package A has a BI of 6, suggesting a period of reduced sedimentation that allowed for ichnofauna to flourish (Pemberton et al., 1992, Pemberton and MacEachern, 2005; MacEachern et al., 2005). The increased bioturbation of the upper parts of package A and the Type 3 surface which caps it represent a period of slowed or non-deposition that occurred as the delta lobe underwent abandonment. The intense bioturbation of the upper 10 to 20 cm of package A likely developed subsequent to delta lobe abandonment when fluvial discharge was reduced before the transgressive phase started. The Type 3 surface which separates underlying prograding deltaic deposits from overlying transgressive deposits is interpreted as a maximum regressive surface (MRS). Such surfaces mark the upper limit of coarsening-upward regressive sediments and the first appearance of transgressive sediments. In sequence stratigraphy a maximum regressive surface is often used to separate an underlying regressive systems tract from an overlying transgressive systems tract (Catuneanu, 2002).

Additionally, the MRS in the western part of the study area is overlain by laminated to mottled F3 with a BI of 4 (*Paleophycus tubularis*) indicating that the depositional environment energy was low (Buatois et al., 2005).

Transgressive Phase

The transgressive phase of delta evolution is characterized by the southwest dipping (paleolandward) packages B to G. The storm generated turbidites that compose packages B to G occur in various depositional environments such as deltas (Nelson, 1982; Pattinson, 2005), shoreface successions (McCrory and Walker, 1986; Stine and Schmitt, 1987; Winn, 1989; Duke et al., 1991), barrier islands and shoals (Schwartz, 1982), as well as lagoons and estuaries (Sexton, 1995; Savrda and Nanson, 2003; Williams, 2010). Paleolandward dipping deposits, however, are not a common occurrence and landward directed deposition is restricted to only a few depositional settings such as the landward components of barrier island complexes (Shelton, 1965; Schwartz, 1982; Penland et al., 1988; Sedwick and Davis, 2003; Horwitz and Wang, 2005; Wang and Horwitz, 2007; Switzer and Jones, 2008; Allen and Johnson, 2010), sand ridges (Lee et al., 1994), sandy spits (Davidson-Arnott and Fisher, 1992), and sandy shoals (Rice and Shurr, 1983; Penland et al., 1988; Percival, 1992).

Shelton (1965) previously interpreted packages B-G as barrier island deposits. He cited low-angle inclined bedding, an upward increase in grain size, and gradational lower and lateral boundaries of packages B to G as evidence for the barrier island interpretation. Packages B to G, however, contain no evidence of subaerial exposure and contain only trace amounts of organics (<1%), favoring an interpretation that packages B to G were deposited landward of a submerged feature such as non-emergent shoal.

Strong wave energy and longshore drift are the main mechanisms driving the formation and development of sub-aqueous sandy shoals (Huthnance, 1982). Sandy shoals can form from transgressive submergence and wave reworking of abandoned deltaic headlands (Fisk and McFarlan, 1955; Frazier, 1967; Penland et al., 1988), the remnants of wave reworked ebb tidal deltas and shoreface-attached ridges (McBride and Moslow, 1991; Snedden and Dalrymple, 1999; Snedden et al., 1999), shoreface processes that transport sandy sediment to the lower shoreface (Neodoroda et al., 1984; Snedden et al., 1988), or they develop from sea floor irregularities that were created by wave erosion and reworking of older exposed inner shelf deposits (Clark, 2010).

In a shoal environment, during storm events when currents are generally unidirectional and sustained, sediments previously deposited alongshore from a nearby fluvial source, or that have been eroded from a pre-existing feature (e.g. basinward flank of the shoal, shoreface/deltaic sediments), are resuspended and deposited in a landward direction by storm surge driven turbidity currents that flow over the crest of the shoal and then downslope (Greenwood, 1985; Horwitz, 2005; Wang, 2007; Switzer, 2008). These types of deposits are generally referred to as overwash deposits (Schwartz, 1982; Sedwick and Davis, 2003; Horwitz, 2005).

Most of what is known about overwash deposits has come from modern studies of large storm events and their effects on barrier islands (Morton, 1978; Schwartz, 1982; Greenwood, 1985; Sedwick and Davis, 2003; Wang, 2007; Horwitz, 2005) and to a lesser extent, on spits, shoals, and sand ridges (Schwartz, 1982; Lee et al., 1994; Jose et al., 2009; Rogers, 2009; Snedden et al., 2011). As a result of variation in hydraulic competence during storm surges, overwash deposits exhibit different characteristics depending on proximity to the feature they were deposited behind (Ritchie and Penland, 1988; Sedwick, 2003; Horwitz, 2005). Deposits in

overwash proximal areas contain massive and planar laminated beds that are generally thicker than their distal counterparts, where the flow regime is lower and bedforms, such as lingoid ripples (e.g. Schwartz, 1982), straight-crested mega-ripples (Davis et al., 1989), and straight-crested ripples (Deery and Howard, 1977) prevail. Such sediment packages are present in packages B to G, where F5 exhibits characteristics of being deposited in overwash proximal areas, F4 beds exhibit mid- to distal- overwash characteristics, and F3 is finer grained and thinner than the preceding facies, suggesting deposition most distal to the flow source. In F5, a majority of the beds contain Ta and Tb Bouma divisions and are up to 110 cm thick. Whereas F4 contains only lower flow regime related sedimentary structures (Tb and Tc divisions with subordinate Td divisions), and are thinner (only up to 80 cm thick). The abundance of Ta and Tb Bouma divisions in F5 indicates that these deposits were emplaced close to the flow source where the flow strength was greatest and sediment concentration the highest. The lack of Td intervals in F5 indicates that these beds either never accumulated or were eroded by subsequent flow (Haughton et al, 2009). The lack of Ta divisions in F4 and prevalence of sandy Tb and Tc divisions indicates that these deposits represent the mid to distal parts of overwash events, where the flow decreased in velocity (Haughton et al, 2009). In these instances F3 is composed entirely of planar to ripple-laminated silt and mud with a BI of 0 to 1, indicating that it was deposited most distal to the flow source.

The overwash packages B to G are separated from each other by Type 2 surfaces. The occurrence of F3 laminated mudstone drapes above Type 2 surfaces suggests that the Type 2 surfaces formed as a result of the termination of coarse-grained sedimentation events. The F3 drapes accumulated subsequent to the deposition of the individual sand packages B to G, when energy was greatly reduced and sedimentation was restricted to sediment settle-out. The

increasing thickness of the F3 silt beds (up to 40 cm) to the west indicates increasing water depth and/or lower energy conditions landward of the shoal area. Development of Type 2 surfaces during periods of reduced sedimentation is also supported by the increased bioturbation of the sediments immediately below the Type 2 surfaces relative to underlying and overlying deposits. The increased bioturbation below Type 2 surfaces is interpreted to represent a period of slowed or reduced deposition which allowed for the establishment of ichnofaunal communities (*sensu* MacEachern et al., 2005).

The coarsening upward profiles within each of the packages Ba to Bc suggest a vertical increase in depositional energy within the packages that is interpreted here as representing a vertical transition from distal to proximal conditions. Relative to facies contained, the oldest of the subpackages (Ba) has a higher proportion of F4 beds (~ 50% of all beds) than the overlying two sub-packages (Bb and Bc) (~30% of beds). The modestly coarser sands of Bb and Bc relative to Ba suggests that Bb and Bc were deposited more proximal to the shoal position than Ba, and demonstrates that the entire larger package B has an overall coarsening upward profile. The vertical decrease in BI observed within sub-packages Ba to Bc also reflects a vertical increase in the sedimentation rate indicating increasing depositional energy (Howard and Frey, 1975; Leithold, 1993, 1994; Leithold and Dean, 1998; MacEachern et al., 2005). In addition, the trace *Monocraterion* is only found in F5 beds (Figure 7F). It is typically associated with moderate to high energy conditions (Seilacher, 1967; Frey and Mayou, 1971; Crimes, 1975; Rhoads, 1975; Yang et al., 2009), suggesting that the upper parts of packages Ba to Bc, where *Monocraterion* traces are located, experienced higher energy conditions than the more basal parts.

The overall low to moderate bioturbation intensities of sub-packages Ba to Bc (BI 0-3) suggest that overwash events were frequent and inhibited extensive bioturbation (Buatois et al., 2005; MacEachern et al., 2005). The combination of low- to moderate bioturbation intensities and low ichnofauna diversity within packages Ba to Bc is consistent with storm dominated deposition (sensu MacEachern et al., 2005). The occurrence of deposit feeding traces from the *Cruziana* ichnofacies (*Planolites* and *Palaeophycus tubularis*) on top of bedding planes is suggestive of colonization of storm event beds after overwash deposition during low-energy, fair weather conditions. Similarly, *Skolithos* ichnofacies indicative of suspension feeding behavior suggests opportunistic colonization of the high energy event beds (Pemberton et al., 1992; MacEachern et al., 2005).

Paleocurrent indicators measured from the storm generated overwash deposits within package B (Figure 18) indicate an average sediment transport direction of 210° degrees to the S-SW. According to Gill and Cobban (1973), the paleoshoreline at the time of deposition followed a trend of N-NW to S-SE, indicating that the SW sediment transport direction for packages Ba to Bc was directed onshore, but obliquely towards the south. This sediment transport direction is likely the result of a combination of shore-parallel to the south storm-driven currents (Ericksen and Slingerland, 1990; Slingerland, 1996) and onshore (westerly) directed waves; where, such a combination would result in a net sediment transport direction to the SW.

Within package B, paleocurrent indicators from packages Ba to Bc illustrate different sediment transport directions. Sub-package Ba contains indicators recording an overall southwest transport direction, while sub-packages Bb and Bc record a south- southwesterly sediment transport direction (Figure 18). The isopach maps generated for packages Ba and Bb illustrate this shift between sediment transport directions, whereas the isopach map generated for Bc

suggests there are two different overwash depositional centers contained within the package of sediment (Figure 16).

The sediments immediately below Type 1 surfaces which separate packages Ba to Bc have increased amounts of bioturbation relative to underlying and overlying deposits, suggesting that episodes of reduced sedimentation allowed for the establishment of ichnofaunal communities (MacEachern et al., 2005). Therefore, the Type I surfaces are interpreted as hiatal surfaces. The separation of overwash packages with differing sediment transport directions by hiatal surfaces strongly suggests that Type 1 surfaces developed as a result of overwash fan abandonment in favor of locations with greater accommodation. This lateral offset of overwash fan packages Ba to Bc resulted in an overlapping amalgamated fan complex, package B. Packages C to G are also likely overwash fan complexes composed of amalgamated overwash fans similar to packages Ba-Bc, although these packages, however, were not examined in sufficient detail to allow for the delineation of sub-packages.

The westerly en-echelon stacking of packages B-G is indicative of migration towards the paleoshoreline, the location of which is suggested by Gill and Cobban (1973) to be southwest of the study area. Landward migrating shoals are common along transgressive deltaic coastlines (Penland et al., 1988; Kobashi et al., 2007; Rogers, 2009), and the landward migration of packages B to G is interpreted to reflect transgressive conditions during deposition.

The Type 4 surface unconformably overlies packages B to G and truncates older packages in the east and successively younger packages to the west, clearly demonstrating that this surface is time transgressive. The sediments immediately underlying the Type 4 surface are colonized by a *Glossifungites* ichnofacies. This ichnofacies is typically associated with erosionally exhumed, dewatered and compacted or cemented substrates corresponding to

erosional discontinuities, suggesting that the Type 4 surface was formed by wave scour (Pemberton and MacEachern et al., 2005).

The development of time transgressive wave scour surfaces on top of landward migrating and prograding sand bodies is evidence of relative sea level rise and an accompanying decrease in sediment supply (Nummedal and Swift, 1987; Thorne and Swift, 1991). The field relationships indicate that the Type 4 surface is a transgressive ravinement surface (TRS).

Implications for Reservoir Development

Ancient regressive to transgressive deltaic successions are well documented in the strata of the Cretaceous Western Interior Seaway of North America (e.g., MacEachern et al., 1998; Bhattacharya, 2001; Gani and Bhattacharya, 2007) and include intervals in the Almond Formation (e.g., Weimer, 1965; Hendricks, 1994) and Cardium Formation (e.g., Bergman and Walker, 1987), both late Cretaceous in age. Such sand bodies are characterized by an internal stratigraphy that records both spatial and temporal variations in shoreline morphology and physical processes (Charvin et al., 2010). Identification of ancient regressive to transgressive deltaic successions in the geologic record is important due to their ability to host large quantities of water and hydrocarbons (Kraft and John, 1979; Thom, 1983; Van Houten et al., 1984; Mancini and Puckett, 2002).

Many hydrocarbon producing reservoirs within regressive to transgressive successions are interpreted in the literature to be transgressive linear sand bodies that are ancient barrier island complexes, sand ridges, and sandy shoals that paralleled paleoshorelines. These include the Cretaceous Viking sands of Alberta and Saskatchewan (Evans, 1970; Cant, 1992), the Upper Cretaceous Sussex Sandstone in the Powder River Basin of Montana and Wyoming (Asquith,

1970), the Lower Cretaceous Dakota Formation in the Denver Basin in Colorado (Tobison, 1972), and the Late Cretaceous Mesaverde Formation and Gallup Sandstone in the San Juan Basin of New Mexico (Hollenshead and Pritchard, 1961; Sabins, 1963, 1972). These transgressive linear sand bodies tend to make excellent hydrocarbon reservoirs because they are typically encased in reservoir sealing facies such as shale, (e.g., Sussex-Shannon sandstone; Berg, 1975; Brenner, 1978; Gaynor and Swift, 1988) or are capped by cemented surfaces (Hollenshead and Pritchard, 1961; Sabins, 1963, 1972; Asquith, 1970; Evans, 1970; Woncik, 1972; Palmer and Scott, 1984; Cant, 1992). Furthermore, transgressive linear sand bodies commonly consist of clean, well-sorted sand that exhibits upward coarsening trends and is characterized by high permeability and porosity values (Penland et al., 1988; Percival, 1992; Berne et al., 1998).

The Eagle Formation contains a series of well-preserved regressive to transgressive deposits; several of which host active producing gas reservoirs outside the study area. These include the Tiger Ridge and Battle Creek fields in north-central Montana, Eagle-equivalent units on the Cedar Creek anticline, the Pumpkin Creek Field, and the Liscom Creek field in southeastern Montana (Shurr and Ridgley, 2002). These reservoirs have estimated porosities of up to 25% and effective permeability up to 150 md (Bayliff, 1975). As of 2002, approximately 880 BCF of biogenic gas had been produced from shallow Cretaceous reservoirs in Montana; of the 880 BCF, 50 BCF had been produced from the Eagle Formation at the Battle Creek Field, and 525 BCF produced from the Tiger Ridge Field where most of the production was from the Eagle Formation (Shurr and Ridgley, 2002).

The Milk River Formation, an Eagle Formation equivalent which occurs along depositional strike to the north in Alberta and Saskatchewan, is estimated to host 15 tcf of

biogenic gas (Rice and Claypool, 1981; Fishman et al., 2001). Additionally, to the south, in the Bighorn Basin, the lower member of the Mesaverde Formation (an Eagle Formation equivalent), is a producing gas reservoir (Finn et al., 2010). As of 2008 in the Bighorn Basin of northern Wyoming and south-eastern Montana, a minimum cumulative production of 833 BCF of gas has come from Upper Cretaceous-Tertiary reservoirs (Finn et al., 2010).

Along-strike correlations between the Eagle Formation in south-central Montana and equivalents to the north in Canada and north-central Montana and to the south in the Bighorn Basin in northern Wyoming are poorly documented, and as a result, the reservoir potential of the Eagle Formation in south-central Montana is not well known. Clearly, stratigraphic architectures, lateral and vertical facies trends, and nature of bounding surfaces observed in the lower member of the Eagle Formation in south-central Montana have important implications for regional subsurface reservoir prediction and development.

The lower member of the Eagle Formation in south-central Montana is similar to many of the hydrocarbon producing sand bodies in the Cretaceous Western Interior Seaway in that it is encased in sealing facies; the lower member grades laterally to siltstones and shale (Hanson and Little, 1989), is underlain by the shales and siltstones of F1, and is capped by a regional scale impermeable transgressive ravinement surface (TRS). Internally however, the lower member of the Eagle Formation exhibits a more complex architecture that must be considered when evaluating the reservoir potential of the system.

The outcrop-scale Type 1 and Type 2 surfaces which bound both large- and small-scale shoal overwash packages are nearly continuously cemented and would likely inhibit fluid flow in the subsurface. Likely, these surfaces will seal and compartmentalize each shoal sand body.

Thus, individual shoal overwash package should be treated as a separate reservoir units from the standpoint of production.

Each shoal overwash reservoir unit, both large (packages B to G) and small (packages Ba to Bc) exhibits a coarsening upward profile, vertical increase in lithologic maturity, proximal to distal fining of facies. These characteristics indicate that the greatest fluid flow pathways and best reservoir potential would be at the stratigraphically highest positions within each shoal overwash unit, where the reservoir is coarsest, and permeability highest (Krumbein and Monk, 1942; Dodge and Loucks, 1979; Loucks et al., 1979; Shepherd, 1989; Forster et al., 2003). The average porosity in the upper parts of each shoal package below the cemented horizons is 16% (average porosity for F5 deposits), which is good (Hyne, 2001). The occurrence of discontinuous calcite concreted horizons along beds within the shoal overwash units may also reduce effective vertical permeability (Hurst, 1987) and inhibit fluid flow in the subsurface (e.g., Hurst, 1987; Gibbons et al., 1993)

The well-cemented transgressive ravinement surface (Type 4 surface) truncates packages B-G at their most up-dip locations and dips in an opposite direction to the Type 1 and 2 surfaces, indicating that it will likely be trap and seal geological fluids in the underlying packages.

High resolution control on the vertical and lateral relationship between architectural elements and temporally distinct compartmentalizing surfaces may prove instrumental in correctly predicting the highest reservoir potential in a regressive to transgressive wave-dominated deltaic reservoir. This study offers an important analysis of the internal architecture of a regressive to transgressive delta in that within an overall regressive to transgressive wave dominated deltaic succession. Specifically, it is the upper confines of individual shoal overwash units (both small and large) that have the highest reservoir quality and likely the highest sweep

efficiency. These most porous, permeable facies occur just below low-permeability compartmentalizing surfaces (Pranter et al., 2007). Thus, a single vertical well drilled into a to a transgressive shoal overwash unit would not provide the maximum reservoir depletion from the transgressive shoal reservoir system. To achieve maximum resource recovery from a transgressive shoal reservoir system, the landward stacking of these compartmentalized sandstone packages, and their sealing surfaces must be considered. In this instance, it would be most advantageous to place a directional well below and oriented parallel to the capping ravinement surface in order to penetrate and drain all of the underlying shoal packages.

CONCLUSIONS

The informal lower member of the Eagle Formation in south-central Montana is interpreted to have been deposited in a regressive to transgressive wave-dominated deltaic system. The deltaic succession records a two-phase depositional evolution: 1) a regressive phase characterized by delta progradation, and 2) a transgressive phase characterized by landward migrating shoal overwash deposits. Detailed mapping of the internal stratigraphy, lateral facies variations, bed-scale facies architecture, and bounding surface hierarchy within the three-dimensionally exposed informal lower member of the Eagle Formation illustrates an internal complexity typically not documented in most regional-scale wave-dominated deltaic studies. Because this type of sedimentary system forms reservoirs in the subsurface, sand body stacking patterns, lithologic trends, three-dimensional thickness variations, and associated connectivity were documented in order to develop an overall outcrop based reservoir analog of an offshore wave-dominated deltaic succession. Comprehensive understandings of such reservoir types require detailed field investigations, because outcrop-based reservoir models provide valuable insight into reservoir properties that might otherwise be overlooked in regional scale studies derived primarily from seismic reflection, well logs, and/or core.

The key findings of this study are as follows:

1. The regressive phase of delta evolution is characterized by prograding pro-delta to distal delta front deposits emplaced below fair weather wave base but above storm wave base.
2. The prograding deltaic deposits of the regressive phase are capped by a maximum regressive surface (MRS) which developed after delta lobe abandonment and before transgressive deposition began.

3. The transgressive phase of delta evolution is characterized by landward dipping shoal overwash deposits which stack en-echelon westward towards the paleoshoreline, indicating landward migration of the shoal during delta transgression.
4. Shoal overwash deposition was driven by storm-generated turbidity currents.
5. Transgressive shoal overwash packages occur at two scales; small scale (those that are up to 1 km wide) and large scale (those that are between 2 and 3 km wide). Small-scale shoal overwash packages are defined as individual overwash fans, whereas large-scale shoal overwash packages consists of a series of amalgamated overwash fans which form an overwash fan complex.
6. Transgressive shoal packages (both large and small) are separated from each other by paleolandward dipping outcrop-scale surfaces which hydraulically compartmentalize the sand bodies, making them individual reservoir units.
7. The vertical and lateral facies trends observed within the shoal packages indicates increased permeability and porosity at the upper and most proximal parts of the shoal overwash fan deposits.
8. Wave scour generated a time transgressive ravinement surface (TRS) on the basinward side of the transgressive shoal. This erosional surface migrated landward with the retreating shoal, truncating all of the shoal overwash deposits at their most up-dip locations. This TRS has the potential to serve as an updip seal for fluids in the shoal overwash packages.

REFERENCES

Allen, J.R.L, Sedimentary Structures, Their Character and Physical Basis. Vol. 2. Amsterdam: Elsevier Scientific Pub., 1982.

Allen, J.R.L, 1984, (unabridged one-volume edition) Sedimentary Structures: Their Character and Physical Basis: Elsevier, Amsterdam (1984) (pp. 593–663)

Allen, J.R.L., and Johnson, C.L., 2010, Facies control on sandstone composition (and influence of statistical methods on interpretations) in the John Henry Member, Straight Cliffs Formation: Sedimentary Geology, v. 230, p. 60-76.

Andresen, A., Bjerrum, L., 1967, Slides on subaqueous slopes in loose sands and silts, *in* Richards, A.F., ed., Marine Geotechnique: Univ. Illinois Press, Urbana, p. 221– 239.

Anderson, J.B., and Fillon, R.H., eds., 2004, Late Quaternary Stratigraphic Evolution of the Northern Gulf of Mexico Margin: SEPM, Special Publication 79, 311 p.

Anderson, P.B., Chidsey, T.C., Ryer, T.A., Adams, R.D., and Mclure, K., 2004, Geologic Framework, facies, paleogeography, and reservoir analogs of the Ferron Sandstone in the Ivie Creek Area, East Central Utah, in Chidsey, T.C., Jr., Adams, R.D., and Morris, T.H., eds., The fluvial–deltaic Ferron Sandstone: regional to wellbore-scale outcrop analog studies and application to reservoir modeling: American Association of Petroleum Geologists, Studies in Geology 50, p. 331–356.

Agrawal, Y.C., and Pottsmith, H.C., 2000, Instruments for particle size and settling velocity observations in sediment transport: Marine Geology, v. 168, i. 1-4, p. 89-114.

Armstrong, R.L., 1968, Sevier orogenic belt in Nevada and Utah. Geol. Soc. Am. Bull., 79, 429–458.

Arnott, R., and Hand, B., 1989, Bedforms, primary structures and grain fabric in the presence of suspended sediment rain: Journal of Sedimentary Petrology, v. 59, p. 1062–1069.

Arnott, R., and Southard, J., 1990, Exploratory flow-duct experiments on combined-flow bed configurations, and some implications for interpreting storm event stratification: Journal of Sedimentary Petrology, v. 60, p. 211–219.

Asquith, D. O., 1970, Depositional topography and major marine environments late Cretaceous, Wyoming: American Association of Petroleum Geologists Bulliten, v. 54, no. 7, p. 1184-1224.

Baas, J.H., van Dam, R.L., and Storms, J.E.A., 2000, Duration of deposition from decelerating high-density turbidity currents: Sedimentology, v. 136, i. 1-2, p. 71-88.

Bates, C., 1953, Rational theory of delta formation: American Association of Petroleum Geologists Bulletin, v. 37, p. 2119-2161.

Bayliff, W.H., 1975, Performance review of Tiger Ridge and Bullock gas units. In: Energy resources of Montana: Montana Geological Society 22nd Annual Publication, p. 31-37.

Berg, R.R., 1975, Depositional environment of Upper Cretaceous Sussex Sandstone, House Creek Field, Wyoming; American Association of Petroleum Geologists Bulletin, v. 59, p. 2099-2110.

Bergman, K.M. and Walker, R.G., 1987, The importance of sea level fluctuations in the formation of linear conglomerate bodies: Carrot Creek Member, Cretaceous Western Interior Seaway, Alberta, Canada: Journal of Sedimentary Petrology, v. 57, p. 651–665.

Bergman, K.M., 1994, Shannon sandstone in Hartzog Draw– Heldt Draw fields reinterpreted as detached lowstand shoreface deposits: Journal of Sedimentary Research, v. B64, p. 184–201.

Berne, S., Lericolais, G., Marsset, T., Bourillet, J.F., and De Batist, M., 1998, Erosional offshore sand ridges and lowstand shorefaces; examples from tide- and wave-dominated environments of France: Journal of Sedimentary Reserarch, v. 68, p. 540-555.

Bhattacharya, J.P. and Walker, R.G., 1991, Allostratigraphic subdivision of the Upper Cretaceous Dunvegan, Shaftesbury, and Kaskapau Formations in the subsurface of northwestern Alberta: Bulliten of Canadian Petroleum Geology, v. 39, p. 145–164.

Bhattacharya, J.P., and Walker, R.G., 1992, Deltas, *in* Walker, R.G., and James, N.P., eds., Facies Models: Response to Sea Level Change: St. John's, Newfoundland, Geological Association of Canada, p. 157–177.

Bhattacharya, J., and Willis, B., 2001, Lowstand deltas in the Frontier Formation, Powder River basin, Wyoming: Implications for sequence stratigraphic models: American Association of Petroleum Geologists Bulletin, v. 85, no. 2, p. 261-294.

Bhattacharya, J., and Giosan, L., 2003, Wave-influenced deltas: geomorphological implications for facies reconstruction: Sedimentology, v. 50, p. 187–210.

Bouma, A.H., 1962, Sedimentology of Some Flysch Deposits: A Graphic Approach to Facies Interpretation. Elsevier, Amsterdam. 168 pp.

Brenchley, P. J., Newall, G., and Stanistreet, I. G., 1979, A storm surge origin for sandstone beds in an epicontinental platform sequence, Ordovician, Norway: Sedimentary Geology, v. 22, i. 3-4, p 185-217.

Brenner, R.L., 1978, Sussex sandstone of Wyoming – example of Cretaceous offshore sedimentation: American Association of Petroleum Geologists Bulletin, v. 62, p. 181-200.

Broussard, M.L., 1975, *in* Broussard, M.L. ed., Deltas, Models for Exploration: Geologic Society, Houston, TX, p. 99–149.

Buatois, L. A., Gingras, M. K., MacEachern, J., Mangano, M. G., Zonneveld, J., Pemberton, S. G., Netto, R. G., and Martin, A., 2005, Colonization of brackish-water systems through time: evidence from the trace-fossil record: PALAIOS, v. 20, p. 321-347.

Busch, D.A., 1971, Genetic Units in Delta Prospecting: American Association of Petroleum Geologists, v. 55, i. 8, p. 1137 – 1154.

Cant, D. J., 1992, The stratigraphic and palaeogeographic context of shoreline-shelf reservoirs. i*n* Rhodes, E.G., and Moslow, T.F., eds., Marine Clastic reservoirs: Springer-Verlag, Berlin: p. 3-38.

Catuneanu, O., Sweet, A. R., and Miall, A. D., 2000, Reciprocal stratigraphy of the Campanian-Paleocene Western Interior of North America: Sedimentary Geology, v. 134, p. 235-255.

Catuneanu, O., 2002, Sequence stratigraphy of clastic systems: concepts, merits, and pitfalls: Journal of African Earth Sciences, v. 35, i. 1, p. 1-43.

Charvin, K., Hampson, G., Gallagher, K, and Labourdette, R., 2010, Intra-parasequence architecture of an interpreted asymmetrical wave-dominated delta: Sedimentology, v. 57, p. 760-785.

Clark, C.K., 2010, Stratigraphy, sedimentolog, and ichnology of the Upper Cretaceous Frontier Formation in the Alkali Anticline region, Bighorn County, Wyoming [Masters thesis]: Lincoln, University of Nebraska, 76 p.

Coleman, J.M. and Wright, L.D., 1975, Modern river deltas variability of processes and sand bodies, *in* Broussard, M.L. ed., Deltas, Models for Exploration: Geologic Society, Houston, TX, p. 99–149.

Collinson, J., and Thompson, D., 1989, Sedimentary Structures [Second Edition]: London, U.K., Unwin Hyman, 207 p.

Corbett, M.J., Fielding, C.R., and Birgenheier, L.P., 2011, Stratigraphy of a Cretaceous coastal-plain fluvial succession: the Campanian Masuk Formation, Henry Mountains Syncline, Utah, USA: Journal of Sedimentary Research, v. 81, p. 80-96.

Cotter, E., 1975, Late Cretaceous Sedimentation in a Low-Energy Coastal Zone: The Ferron Sandstone of Utah: Journal of Sedimentary Petrology, v. 45, n. 3, p. 669-685.

Crimes, T. P., 1975, The stratigraphical significance of trace fossils: Springer-Verlag, New York, p. 109-130.

Currie, B.S., 1997, Sequence Stratigraphy of nonmarine Jurassic-Cretaceous rocks, central Cordilleran foreland-basin system: GSA Bulletin, v. 109, no. 9, p. 1206-1222.

Davidson-Arnott, R.G.D., and Fisher, J.D., 1992, Spatial and temporal controls on overwash occurrence on a Great Lakes barrier spit: Canadian Journal of Earth Sciences, v. 29, p. 102-117.

Davis, R.A., Jr., Andronaco, M., Gibeaut, J.C., 1989, Formation and development of a tidal inlet from a washover fan, west-central Florida coast, USA: Sedimentary Geology, v. 65, p. 87-94.

DeCelles, P.G., and Currie, B.S., 1996, Long-Term sediment accumulation in the Middle Jurassic-early Eocene Cordilleran retroarc foreland-basin system: Geology, v. 24, no. 7, p. 591-594.

Decelles, P., 2004, Late Jurassic to Eocene evolution of the Cordilleran thrust belt and foreland basin system, western U.S.A.: American Journal of Science, v. 304, p. 105-168.

Deery, J.R., Howard, J.D., 1977. Origin and character of washover fans on the Georgia Coast, U.S.A.: Gulf Coast Association of Geological Societies transactions, v. 27, p. 259-271.

Dengler, A.T., Noda, E.K., Wilde, P., Normark, W.R., 1984, Turbidity currents generated by Hurricane Iwa: Geo-Marine Letters, v. 4, p. 5 – 11.

Dickinson, W.R., 1970, Interpreting detrital modes of greywacke and arkose: Journal of Sedimentary Petrology, v. 40, p. 695-707.

Dickinson, W.R., and Suczek, C.A., 1979, Plate tectonics and sandstone compositions: American Association of Petroleum Geologists Bulletin, , v. 63, p. 2164-2182.

Dodge, M.M., and Loucks, R.G., 1979, Mineralogic composition and diagenesis of Tertiary sandstones along Texas Gulf Coast: American Association of Petroleum Geologists Bulletin, v. 63, p. 440.

Dott, R.H., and Bourgeois, J., 1982, Hummocky Stratification: Significance of Its Variable Bedding Sequences: Geological Society of America Bulletin, v. 93, p. 663-680.

Dreyer, T., 1993, Geometry and facies of large-scale flow units in fluvial-dominated fan-delta-front sequences: Geological Society Special Publications, v. 69, p, 135-174.

Duke et al., W., Arnott, R., and Cheel, R., 1991, Shelf sandstones and hummocky cross-stratification: New insights on a stormy debate: Geology, v. 19, p. 625-628.

Dumas, S., Arnott, R., and Southard, J., 2005, Experiments on oscillatory-flow and combined-flow bed forms: implications for interpreting parts of the shallow-marine sedimentary record: Journal of Sedimentary Research, v. 75, n. 3, p. 501-513.

Duncan, E.A., 1983, Delineation of delta types: Norias delta system, Frio Formation, South Texas: Gulf Coast Association of Geological Societies, Transactions, v. 33, p. 269–273.

Ericksen, M. and R.L. Slingerland, 1990. Numerical Simulations of Tidal and Wind-driven Circulation in the Cretaceous Interior Seaway of North America, *Geol. Soc. Amer. Bull.*, 102:1499-1516

Evans, W.E., 1970, Imbricate linear sand bodies of Viking formation in Dodsland – Hoosier area of southwestern Saskatchewan, Canada: American Association of Petroleum Geologists Bulletin, v.54, p. 469-486.

Fielding, C.R., Trueman, J., and Alexander, J., 2005, Sedimentology of the modern and Holocene Burdekin River Delta of north Queensland, Australia—controlled by river output, not by waves and tides, *in* Giosan, L., and Bhattacharya, J.P., eds., River Deltas: Concepts, Models, and Examples: SEPM, Special Publication 83, p. 467–496.

Finn, T.M., Kirschbaum, M.A., Roberts, S.B., Condon, S.M., Roberts, L.N.R., and Johnson, R.C., 2010, Cretaceous–Tertiary Composite Total Petroleum System (503402), Bighorn Basin, Wyoming and Montana: U.S. Geological Survey Digital Data Series DDS–69–V, 157 p.

Fisher, W.L., Brown, L.F., Scott, A.J. and McGowen, J.H., 1969, Delta Systems in the Exploration for Oil and Gas, a Research Colloquium: Bureau of Economic Geology, Univ. Texas, Austin, 204 pp.

Fishman, N., Ridgley, J., and Hall, D., 2001, Timing of gas generation in the Cretaceous Milk River Formation, southeastern Alberta and southwestern Saskatchewan—evidence from authigenic carbonates; Summary of investigations 2001, v. 1, Saskatchewan Geological Survey, Sask. Energy Mines, Misc. Rep. 2001-4.1, p, 125-136

Fisk, H. N., and McFarlan, E.,Jr., 1955, Late quaternary deltaic deposits of the Mississippi river [Louisiana]; local sedimentation and basin tectonics: Special Paper - Geological Society of America, , 279-302.

Folk, R., 1974, Petrology of sedimentary rocks: Hemphill, Austin, Tex. 182 p.

Forster, S., Bobertz, B., and Bohling, B., 2003, Permeability of sands in the coastal areas of the southern Baltic Sea: mapping a grain-size related sediment property : Aquatic Geochemistry, v. 9, no. 3, p. 171-190.

Frazier, D.E., 1967, Recent Deltaic Deposits of the Mississippi River: Their Development and Chronology: Transaction

Frey, R. W. and Mayou, T. V., 1971. Decapod burrows in Holocene barrier island beaches and washover fans, Georgia: Senckenberg. Marit., 3: 53--77.

Galloway, W.E., 1975, Process framework for describing the morphologic and stratigraphic evolution of deltaic depositional systems, *in* Broussard, M.L., ed., Deltas; Models for Exploration: Houston Geological Society: Houston, p. 87–98.

Gani, M.R., 2004, From turbid to lucid: a straightforward approach to sediment gravity flows and their deposits: The Sedimentary Record, v. 2, p. 4–8.

Gani, R., and Bhattacharya, J., 2007, Basic building blocks and process variability of a Cretaceous delta: Internal facies architecture reveals a more dynamic interaction of river, wave, and tidal processes than is indicated by external shape: Journal of Sedimentary Research, v. 77, p. 284-302.

Gaynor, G.C., and Swift, D.J.P., 1988, Shannon Sandstone depositional model; sand ridge dymnamics on the Campanian Western Interior Shelf; Journal of Sedimentary Research, v. 58, no. 5, p. 868-880.

Gazzi, P., 1966, Le aernarie del flysch sopracretaceo dell'Appennino modenese; correlazioni con il flysch di Monghidoro: Mineralogica e Petrografica Acta, v. 12, p. 69-97.

Gibbons, K, Hellem, T., Kjemperund, A., Nio, S.D., and Vebenstad, K., 1993, Sequence architecture, facies development and carbonate-cemented horizons in the Troll Field reservoir, offshore Norway: Special Publications, Geological Society of London, v. 69, p. 1-32.

Gill, J.R., and Cobban, W.A., 1973, Stratigraphy and geologic history of the Montana Group and equivalent rocks, Montana, Wyoming, and North and South Dakota: U.S. Geological Survey Professional Paper 776, 37 p.

Giosan, L., Bokuniewicz, H., Panin, N. and Postolache, I., 1999, Longshore sediment transport pattern along the Romanian Danube delta coast: Journal of Coastal Research, v. 15, p. 859-871.

Greenwood, B., 1985, Vertical sequence and lateral transitions in the facies of a barred nearshore environment: Journal of Sedimentary Petrology, v. 55, n. 3, p. 366-375.

Hanson, M.H., 1989. Utilization of genetic sequence analysis in the prediction of Eagle Sandstone reservoir facies distributions, Montana: M.Sc. thesis, Colorado School of Mines, Golden, Colorado, USA, 150 p.

Hanson, M., and Little, L., 1989, Distributions of genetic sequences, Eagle Sandstone, Billings, Montana, *in* French D.E., ed., Geologic Resources of Montana: Montana Geological Society Centennial Field Symposium, p. 141-150.

Harms, J. C., 1969, Hydraulic significance of some sand ripples: Geological Society of.America Bulletin, v. 80, p. 363-396.

Harms, J.C., Southard, J.C., and Walker. R., G., 1982, Structures and Sequences, *in*, Clastic Rocks. Society of Economic Petrology and Mineralogy, Short Course 9.

Haughton, P., Davis, C., McCaffrey,W., Barker, S., 2009, Hybrid sediment gravity flow desposits – classification, origin and significance: Marine and Petroleum Geology, v. 26, p. 1900–1918.

Hendricks, M.L., 1994, Ravinement surface control on hydrocarbon accumulation in transgressive systems tracts: Almond Formation, Green River Basin, Wyoming, *in* Dolson, J.C., Hendricks, M.L., and Westcott, W.A., eds., Unconformity-Related Hydrocarbons in Sedimentary Sequences: Rocky Mountain Association of Geologists, p. 209–218.

Hearn, D., and Hansen, W., 1989, Reexamination of the Cretaceous (Campanian) Eagle Sandstone at Billings, Montana, *in* French D.E., ed., Geologic Resources of Montana: Montana Geological Society Centennial Field Symposium, p. 131-138.

Hesselbo, S.P., 1996, Spectral gamma-ray logs in relation to clay mineralogy and sequence stratigraphy, Cenozoic of the Atlantic margin, offshore New Jersey, *in* Mountain, G.S., Miller, K.G., Blum, P., Poag, C.W., and Twichell, D.C., eds., Proceedings of the Ocean Drilling Program, Scientific Results, v. 150, p. 411-422.

Hill, P., Meule, S., and Longuepee, H., 2003, Combined-flow processes and sedimentary structures on the shoreface of the wave-dominated Grande-Riviere-De-La-Baleine Delta: Journal of Sedimentary Research, v. 73, n. 2, p. 217-226.

Hiscott, R.N., Pickering, K.T., Bouma, A.H., Hand, B.M., Kneller, B.C., Postma, G., Soh, W., 1997, Basin-floor fans in the North Sea: sequence stratigraphic models vs. sedimentary Facies: discussion: American Association of Petroleum Geologists Bulletin 81, 662– 665.

Hollinshead, C. T., and Pritchard, R. L., 1961, Geometry of producing Mesaverde sandstones, San Juan basin. *In* Peterson, J.A., and Osmond, J.C., eds., Geometry of Sandstone Bodies: AAPG, Tulsa, OK, p. 98-118. AAPG, Tulsa, OK.

Hori, K., Saito, Y., Zhao, Q., and Wang, P., 2002, Architecture and evolution of the tide-dominated Changjiang (Yangtze) River delta, China: Sedimentary Geology, v. 146, p. 249–264.

Horwitz, M., and Wang, P., 2005, Sedimentological characteristics and internal architecture of two overwash fans from hurricanes Ivan and Jeanne: Gulf Coast Association of Geological Societies Transactions, v. 55, p. 343-352.

Howard, J. D., and Frey, R. W., 1975, Regional animal-sediment characteristics of Georgia estuaries: *Senckenbergiana Maritima, 7*, 33-103.

Hurst, A., 1987, Problems of reservoir characterization in some North Sea sandstone reservoirs solved by the application of microscale geological data. *In* Kleppe, J., Berg, E.W., Hjelmeland, O., and Torsaeter, O., eds., North Sea Oil and Gas Reservoirs Graham and Trotman, London, p. 153-167.

Huthnance, J.M., 1982, On one mechanism forming linear sand banks: Estuarine and Marine Coastal Science, v. 14, 79–99.

Hyne, N.J., 2001, Nontechnical guide to petroleum geology, exploration, drilling, and production, PennWell Corporation, 2nd ed., 598 p.

Inman, D.L., Nordstrom, C.E., Flick, R.E., 1976, Currents in submarine canyons: an air– sea– land interaction: Annual Review of Fluid, p. 273– 310.

Johnson, C.L., and Graham, S.A., 2004, Sedimentology and reservoir architecture of a synrift lacustrine delta, southeastern Mongolia: Journal of Sedimentary Research, v. 74, p. 770–785.

Jordan, T., 1981, Thrust loads and foreland basin evolution, Cretaceous, Western United States: American Association of Petroleum Geologists Bulletin, v. 65, no. 12, p. 2506-2520.

Jose, F., Stone, G., Kobashi, D., SiadatMousavi, S., and Liu, B., 2009, Hydrodynamic response of a transgressive shoal to the proposed mining for restoring adjacent beaches and barriers: Sabine Bank, off Louisana-Texas coast, United States. Coastal Dynamics, n. 146

Kauffman, E.G., 1984, Paleobiogeography and evolutionary response dynamics in the Cretaceous Western Interior Seaway of North America, *in* Westermann, G.E.G., ed., Jurassic-Cretaceous biochronology and paleogeography of North America: Geological Association of Canada Special Paper 27, p. 273-306.

Kauffman, E. G., and Caldwell, W.G.E., 1993, The Western Interior Basin in space and time, in Caldwell, W.G.E., and Kauffman, E.G., eds., Evolution of the Western Interior Basin: Geological Association of Canada, Special Paper v. 39, p. 1-30.

Kendrick, K., 1985, Depositional environment of the Eagle Sandstone, Billings, Montana [Unpublished Bachelors Thesis]: Billings, MT, Rocky Mountain College, p. 30.

Kent, H. C., 1968, Biostratigraphy of Niobrara-equivalent part of Mancos Shale (Cretaceous) in northwestern Colorado: American Association of Petroleum Geologists Bulletin, v. 52, p. 2098–2115

Kieft, R.L., Hampson, G.J., Jackson, C.A.L., and Larsen, E., 2011; Stratigraphic Architecture of a net-transgressive marginal- to shallow-marine succession: Upper Almond Formation, Rock Springs Uplift, Wyoming, USA.: Journal of Sedimentary Research, v. 81, p. 513-533.

Kneller, B., and Branney, M., 1995, Sustained high-density turbity currents and the deposition of thick massive sands: Sedimentology, v. 42, p. 607-616.

Kneller, B.C., and Buckee, M.J., 2000, The structure and fluid mechanics of turbidity currents: a review of some recent studies and their geological implications: Sedimentology, v. 47, p. 62–94

Kobashi, D., Jose, F., and Stone, G.W., 2007, Impacts of Fluvial Fine Sediments and Winter Storms on a Transgressive Shoal: Journal of Coastal Research, Special Issue 50

Kokelaar, B.P., 1992, Ordovician marine volcanic and sedimentary record of rifting and volcanotectonism: Snowdon, Wales, United Kingdom: Geological Society of America Bulletin 104, 1433–1455.

Kraft, J.C. and John, C.J., 1979, Lateral and vertical facies relations of transgressive barrier: American Association of Petroleum Geologists Bulletin, v. 63, p. 2145-2163.

Krumbein, W.C., and Monk, G.D., 1942, Permeability as a function of the size parameters of unconsolidated sands: American Institute of Mining, Metallurgical and Petroleum Engineers, Technical Publication. 1492, p. 1-11.

Lamb, M., Myrow, P., Houck, C., and Strauss, J., 2008, Deposits from wave-influenced turbidity currents: Pennsylvanian Minturn Formation, Colorado, U.S.A.: Journal of Sedimentary Research, v. 78, p. 480-498.

Lee, H., Chun, S., Chang, J., and Han, S., 1994, Landward migration of isolated shelly sand ridge (chenier) on the macrotidal flat of Gosmo Bay, west coast of Korea: controls of storms and typhoon: Journal of Sedimentary Research, v. 64, n. 4, p. 886-893.

Leithold, E.L., 1993, Preservation of laminated shale in ancient clinoforms; comparison to modern subaqueous deltas: Geology, v. 21, p. 359-362.

Leithold, E.L., 1994, Stratigraphical architecture at the muddy margin of the Cretaceous Western Interior Seaway, southern Utah: Sedimentology, v. 41, p. 521-542.

Leithold, E.L., and Dean, W. E., 1998, Depositional processes and carbon burial on a Turonian prodelta at the margin of the Western Interior Seaway, *in* Dean, W. E., and Arthur, M. A., eds., Stratigraphy and Paleoenvironments of the Western Interior Seaway, SEPM Concepts in Sedimentology and Paleontology no. 6, p. 189–200.

Lipman, P.W., Mullineaux, D.R., 1981, The 1980 eruption of mount St. Helens, Washington. United States Geological Survey Professional Paper 1250. 844 p

Liu, L., Spasojevic, S., Gurnis, M., 2008, Reconstructing Farallon Plate subduction beneath North America back to the Late Cretaceous: Science, v. 232, no. 5903, p. 934-938.

Liu, S., Nummedal, D., and Liu, L., 2011, Migration of dynamic subsidence across the Late Cretaceous United States Western Interior Basin in response to Farallon plate subduction: Geology, v. 39, no. 6, p. 555-558.

Lloyd, C. R., 1982, The mid-Cretaceous earth: Paleogeography; ocean circulation and temperature; atmospheric circulation: Journal of Geology, v. 90, p. 393-413.

Lopez, D. A., 2000, Geologic map of the billings 30' x 60' quadrangle, Montana. Butte, MT, United States (USA): Montana Bureau of Mines and Geology, Butte, MT.

Loucks, R. G., M. M. Dodge, and W. E. Galloway, 1979, Importance of secondary leached porosity in lower Tertiary sandstone reservoirs along the Texas Gulf Coast: Gulf Coast Association of Geological Societies Transactions, v. 29, p. 164–171

Lowe, D. R., 1975, The origin of convolute lamination: Annual Meeting Expanded Abstracts - American Association of Petroleum Geologists, v. 2, p. 92-92.

Lowry, P., and Jacobsen, T., 1993, Sedimentological and reservoir characteristics of a fluvial-dominated delta-front sequence; ferron sandstone member (turonian), east-central utah, USA: Geological Society Special Publications, v. 69, p, 81-103.

MacEachern, J.A., Zaitlin, B.A., and Pemberton, S.G., 1998, High-resolution sequence stratigraphy of early transgressive deposits, Viking Formation, Joffre Field, Alberta, Canada: American Association of Petroleum Geologists Bulletin, v. 82, p. 729-756.

MacEachern, J., Bann, K., Bhattacharya, J., and Howell, C., 2005, Ichnology of deltas: organism responses to the dynamic interplay of rivers, waves, storms, and tides, *in* Giosan, L., and Bhattacharya, J.P., eds., River Deltas: Concepts, Models, and Examples: SEPM, Special Publication, v. 83, p. 49–85.

Maguregui, J.A., and Tyler, N., 1991, Evolution of middle Eocene tide-dominated deltaic sandstones, Lagunillas Field, Maracaibo Basin, western Venezuela, in Miall, A.D., and Tyler, N., eds., The Three Dimensional Facies Architecture of Terrigenous Clastic Sediments, and its Implications for Hydrocarbon Discovery and Recovery: SEPM, Concepts in Sedimentology and Paleontology, 3, p. 233–244.

Mancini, E.A., and Puckett, T.M., 2002, Transgressive-regressive cycles: application to petroleum exploration for hydrocarbons associated with Cretaceous shelf carbonates and coastal and fluvial-deltaic siliciclastics, northeastern Gulf of Mexico, *in* Armentrout, John

M., and Rosen, Norman C. (eds.), Sequence stratigraphic models for exploration and production, GCSSEPM Foundation 22nd Annual Research Conference, p. 173-199.

Martinsen, R.S., Steel, R.J., Martinsen, O.J., and Krystinik, L.F., 2001, Improved sequence stratigraphic and reservoir characterization models; Mesaverde Group, southwestern Wyoming; 2001 Annual Meeting Expanded Abstracts - American Association of Petroleum Geologists, p, 199.

McBride, R., and Moslow, T., 1991, Origin, evolution, and distribution of shoreface sand ridges, Atlantic inner shelf, U.S.A.: Marine Geology, v. 97, p. 57–85.

McCroy, V. L., and Walker, R. G., 1986, A storm and tidally-influenced prograding shoreline – Upper Cretaceous Milk River Formation of southern Alberta, Canada: Sedimentology, v. 33, p. 47-60.

McGookey, D., Haun, J., Hale, L., Goodell, H., McCubbin, D., Weimer, R., and Wulf, G., 1972, Cretaceous Systems. *In* Mallory, W., ed., Geologic atlas of the Rocky Mountain region: Denver, Colorado: Rocky Mountain Association of Geologists, p. 190-228.

Mellere, D., Plink-Bjorklund, P., and Steel, R., 2002, Anatomy of shelf deltas at the edge of a prograding Eocene shelf margin, Spitsbergen: Sedimentology, v. 49, p. 1181–1206.

Middleton, G.V., and Hampton, M.A., 1976, Subaqueous sediment transport and deposition by sediment gravity flows, *in*, Stanley, D.J., Swift, D.J.P., eds., Marine Sediment Transport and Environmental Management: Wiley, New York, p. 197-218.

Miller, K.G., Sugarman, P.J., Browning, J.V., Kominz, M.A., Hernandez, J.C., Olsson, R.K., Wright, D.W., Feigenson, M.D., and Van Sickel, W., 2003, Late Cretaceous chronology of large, rapid sea-level changes: glacioeustasy during the greenhouse world: Geology, v. 31, p. 585-588.

Miller, K.G., Wright, J.D, and Browning, J.V., 2005, Visions of ice sheets in a greenhouse world. Marine Geology, v. 217, p. 215-231: Journal of Sedimentary Research, v. 67, no. 6, p. 994-1000.

Morton, R., 1978, Large-scale rhomboid bed forms and sedimentary structures associated with hurricane washover: Sedimentology, v. 25, p. 183-204.

Mulder, T., Syvitski, P., Migeon, S., Faugères, J., and. Savoye, B., 2003, Marine hyperpycnal flows: Initiation, behavior and related deposits: A review: Marine and Petroleum Geology, v. 20, p. 861–882.

Mulder, T., and Alexander, J., 2001, The physical character of subaqueous sediment gravity flows and their deposits: Sedimentology, v. 48, p. 269-299.

Mutti, E., Davoli, G., Tinterri, R. and Zavala, C., 1996, The importance of ancient fluvio-deltaic systems dominated by catastrophic flooding in tectonically active basins: Mem. Sci. Geol. (Padova), v. 48, p. 233–291.

Myrow, P.M., Fischer, W., and Goodge, J.W., 2002, Wave-modified turbidites: combined-flow shoreline and shelf deposits, Cambrian, Antartica: Journal of Sedimentary Research, v. 72, no. 5, p. 641–656

Neodoroda, A. W., Swift, D. J. P., Hopkins, T. S. and Ma, C. M., 1984, Shoreface morphodynamics on wave dominated coasts: Marine geology, v. 60, p. 331-354.

Nelson, H., 1982, Modern shallow-water graded sand layers from storm surges, Bering Shelf: a mimic of Bouma sequences and turbidite systems: Journal of Sedimentary Petrology, v. 52, no. 2, p. 537-545

Nummedal, D., and Swift, D., 1987, Transgressive stratigraphy at sequence-bounding unconformities: Some principles derived from Holocene and Cretaceous examples, *in Pilkey, D., Pilkey, O.H., Howard, J.D., eds.,* Sea Level Fluctuation and Coastal evolution: Society of Economic Paleontologists and Mineralogists Special Publication, v. 41, p. 241-260.

Odin, G. S. and Fullagar, P. D., 1988, Geological significance of the glaucony facies, *in* Odin, G. S., ed., Green Marine Clays: Amsterdam, Elsvier, p. 295-232.

Olariu, C., Bhattacharya, J.P., Xu, X., Aiken, C.L.V., Zeng, X., and McMechan, G.A., 2005, Integrated study of ancient delta front deposits, using outcrop, ground penetrating radar and three dimension photorealistic data: Cretaceous Panther Tongue Sandstone, Utah, *in* Giosan, L., and Bhattacharya, J.P., eds., River Deltas: Concepts, Models, and Examples: SEPM, Special Publication 83, p. 155–177.

Olariu, C., and Bhattacharya, J.P., 2006, Terminal distributary channels and delta front architecture of river-dominated delta systems: Journal of Sedimentary Research, v. 76, p. 212–233.

Olariu, C., Steel, R., and Petter, A., 2010, Delta-front hyperpycnal bed geometry and implications for reservoir modeling: Cretaceous Panther Tongue delta, Book Cliffs, Utah: American Association of Petroleum Geologists Bulletin, v. 94, n. 6, p. 819-845.

Olson, N.K., 1961. Depositional factors of the upper Cretaceous Eagle Formation, south-central Montana: M.Sc. thesis, University of Iowa, Iowa City, Iowa, USA, 128 p.

Olson, J., and Smith, L. N., 2007, Geography and geology of the middle Yellowstone River Area, Treasure and Yellowstone counties, Montana: Montana Bureau of Mines and Geology Ground-water Assessment Atlas 3B-02 (open-file version), 1 sheet(s), 1:250,000

Oomkens, E., 1970, Depositional sequences and sand distribution in the postglacial Rhone delta complex, *in* Morgan, J.P., eds., Deltaic Sedimentation, Modern and Ancient, SEPM Special Publication, v. 15, p. 198-212.

Palmer, J.J. and Scott, A.J., 1984, Stacked shoreline and shelf sandstones of the La Ventana Tongue (Campanian), Northwestern New Mexico: American Association of Petroleum Geologists Bulletin, v. 68, p. 74–91.

Pang, M., and Nummedal, D., 1995, Flexural subsidence and basement tectonics of the Cretaceous Western Interior Basin, United States: Geology, v. 23, p. 173–176.

Parrish, J. T., and Curtis, R. L., 1982, Atmospheric drculation, upwetling and organic-rich rocks in the Mesozoic and Cenozoic Eras: Palaeogeography, Palaeochmatology, Palaeoecology, v. 40, p. *31-66.*

Parrish, J. T,, Gaynor, G. C., and Swift, D.J.P., 1984, Circulation in the Cretaceous Western Interior Seaway of North America, a review, *in* Stott, D. F., and Glass, D. J., eds.. The Mesozoic of middle North America: Canadian Society of Petroleum Geologists Memoir 9, p. 221-231.

Pattison, A., 2005, Storm-influenced prodelta turbidite complex in the lower Kenilworth Member at Hatch Mesa, Book Cliffs, Utah, U.S.A.: implications for shallow marine facies models: Journal of Sedimentary Research, v. 75, p. 420–439.

Payenberg, T., Braman, D., Davis, D., and Miall, A., 2002, Litho- and chronostratigraphic relationships of the Santonian/Campanian Milk River Formation in southern Alberta and Eagle Formation in Montana utilizing stratigraphy, U-Pb geochronology and palynology: Canadian Journal of Earth Sciences, v. 39, p. 1553-1577.

Payenberg, T., Braman, D., and Miall, A., 2003, Depositional environments and stratigraphic architecture of the Late Cretaceous Milk River and Eagle formations, southern Alberta and north-central Montana: relationships to shallow biogenic gas: Bulletin of Canadian Petroleum Geology, v.51, no. 2, p. 155-176.

Pemberton, S.G., MacEachern, J.A., and Ranger, M.J., 1992, Ichnology and event stratigraphy: The use of trace fossils in recognizing tempestites, *in* Pemberton, S.G., ed., Applications of Ichnology to Petroleum Exploration, A Core Workshop: SEPM, Core Workshop, v. 17, p. 85–117.

Pemberton, S., Spila, M., Pulham, A., Saunders, T., MacEachern, J., Robbins, D., and Sinclair, I., 2001, Ichnology and Sedimentology of Shallow to Marginal Marine Systems: Geological Association of Canada, Short Course, v. 15, p. 343.

Pemberton, S., and MacEachern, J., 2005, Significance of ichnofossils to applied stratigraphy,*in* Koutsoukos, E.A.M., eds., Applied Stratigraph, p. 279-300.

Penland, S., Boyd, R., and Sutter, J., 1988, Transgressive depositional systems of the Mississippi delta plain: A model for barrier shoreline and shelf sand development: Journal of Sedimentary Petrology, v. 58, no. 6, p. 932-949.

Percival, C., 1992, The Harthope Ganister – a transgressive barrier island to shallow-marine sand-ridge from the Namurian of Northern England: Journal of Sedimentary Petrology, v. 62, n. 3, p. 442-454.

Piper, D.J.W., Savoye, B., 1993, Processes of late Quaternary turbidity current flow and deposition on the Var fan, north-west Mediterranean Sea: Sedimentology 40, 557– 582.

Plink-Björklund, P., and R. J. Steel, 2004, Initiation of turbidity currents: Outcrop evidence for Eocene hyperpycnal flow turbidites: Sedimentary Geology, v. 165, p. 29–52.

Plink-Björklund, P., and R. J. Steel, 2005, Deltas on falling-stage and lowstand shelf margins, the Eocene Central Basin of Spitsbergen: Importance of sediment supply, *in* Giosan, L., and Bhattacharya, J.P., eds., River Deltas: Concepts, Models, and Examples: SEPM, Special Publication 83, p. 179–206.

Plint, G.A., and Kreitner, M.A., 2007, Extensive thin sequences spanning Cretaceous foredeep suggest high-frequency eustatic control: Late Cenomanian, Western Canada foreland basin: Geology, p. 735-738.

Plint, A.G., Walker, R.G. and Bergman, k.M., 1986, Cardium Formation 6. Stratigraphic Framework of the Cardium in Subsurface, Bulletin of Canadian Petroleum Geology, v. 34, n. 2, p. 213-225.

Pollard, J.E., Goldring, R., and Buck, S.G., 1993, Ichnofabrics containing Ophiomorpha: Significance in shallow-water facies interpretation: Journal of the geological society, London, vol. 150, pp. 149-164.

Porbeski, S.J., and Steel, R.J., 2003, Shelf-margin deltas: their stratigraphic significance and relationship to deepwater sands: Earth-Science Reviews, v. 62, p. 283–326.

Postma, G., 1990, Depositional architectures and facies of river and fan deltas, *in* Colella, A., and Prior, D.B., eds., Coarse-Grained Deltas: International Association of Sedimentologists, Special Publication 10, p. 13–27.

Powers, M.C., 1953, A new roundness scale for sedimentary particles. Journal of Sedimentary Petrology, v. 23, p. 117-119.

Pranter, M.J., Ellison, A.L, Cole, R.D., and Patterson, P.E., 2007, Analysis and modeling of intermediate-scale reservoir heterogeneity based on a fluvial point-bar outcrop analog, Williams Fork Formation, Piceance Basin, Colorado: American Association of Petroleum Geologists Bulletin, v. 91, p. 1025-1051.

Price R.A. 1973, Large-scale gravitational flow of supracrustal rocks, southern Canadian Rockies, *in* DeJong K.A., Scholten R.A. eds., Gravity and tectonics: New York John Wiley p. 491– 502.

Pulham, A. J., 1989, Controls on internal structure and architecture of sandstone bodies within upper carboniferous fluvial-dominated deltas, county clare, western Ireland: *Geological Society Special Publications, 41*, 179-203.

Reading, H.G., and Collinson, J.D., 1996, Clastic coasts, *in* Reading, H.G., ed., Sedimentary Environments; Processes, Facies and Stratigraphy: Oxford, U.K., Blackwell, p. 154–231.

Rhoads, D. C., 1975, The palaeoecological and environmental significance of trace fossils, *in* Frey, R.W., ed., The Study of Trace Fossils: Springer-Verlag, Berlin, p. 147-160.

Rice, D., 1980, Coastal and deltaic sedimentation of Upper Cretaceous Eagle Sandstone: Relation to shallow gas accumulations, north-central Montana: American Association of Petroleum Geologists Bulletin, v.64, no. 3, p. 316-338.

Rice, D.D., and Claypool, G.E., 1981, Generation, accumulation, and resource potential of biogenic gas. American Association of Petroleum Geologists Bulletin, b. 93, p. 1379-1401.

Rice, D.D., and Shurr, G.W., 1983, Patterns of sedimentation and paleogeography across the Western Interior Seaway during time of deposition of Upper Cretaceous Eagle Sandstone and equivalent rocks, Northern Great Plains: In: Mesozoic paleogeography of West-Central United States. M. W. Reynolds and E. D. Dolly (eds). Society of Economic Paleotologists and Mineralogists Rocky Mountain Section Meeting, Denver, Colorado, p. 337-358.

Ritchie, W., and Penland, S., 1988, Rapid dune changes associated with overwash processes on the deltaic coast of South Louisiana: Marine Geology, v. 81, p. 97-122.

Roberts, H. H., 1997, Dynamic changes of the holocene mississippi river delta plain; the delta cycle: Journal of Coastal Research, v. 13, i. 3, p. 605-627.

Rodriguez, A.B., Hamilton, M.D., and Anderson, J.B., 2000, Facies and evolution of the modern Brazos Delta, Texas: wave versus flood influence: Journal of Sedimentary Research, v. 70, p. 283–295

Rogers, B. E., 2009, Framework and evolution of a transgressed delta lobe: Bernard shoals, northern Gulf of Mexico, USA [Master's thesis]: University of New Orleans, p. 101.

Sabins, F. F., 1963, Anatomy of a stratigraphic trap: American Association of Petroleum Geologists Bulletin, v. 47, p. 193-228.

Sabins, F. F., 1972, Comparison of Bisti and Horseshoe Canyon stratigraphic traps, San Juan basin, New Mexico: American Association of Petroleum Geologists Memoirs, v. 10, p. 610-22.

Savrda, C. E., and Nanson, L. L., 2003, Ichnology of fair-weather and storm deposits in an Upper Cretaceous estuary (Eutaw Formation, western Georgia, USA): Palaeogeography, Palaeoclimatology, Palaeoecology, v. 202, p. 67-83.

Schwartz, R., 1982, Bedform and stratification characteristics of some modern small-scale washover sand bodies: Sedimentology, v. 29, p. 835-849.

Scott, R.W., and Taylor,A. M., 1977, Upper Cretaceous environments and paleocommunities in the southern Western Interior, *in* Kauffman, E. G., ed., Cretaceous facies, faunas and paleoenvironments across the Western Interior Basin: Mountain Geologist, v. 14, p. 155–173.

Sedwick, P., and Davis, R., 2003, Stratigraphy of washover deposits in Florida: implications for recognition in the stratigraphic record: Marine Geology, v. 200, p. 31-48.

Seilacher, A., 1967, Bathymetry of trace fossils: Marine Geology, v. 5, p. 189-200.

Serradji, H., and Kamola, D., 2007, Depositional environments and sequence stratigraphy of the lower cretaceous dakota sandstone, SW colorado. Abstracts: Annual Meeting - American Association of Petroleum Geologists, 2007, p. 126-126.

Sexton, W. J., 1995, The post-storm hurricane Hugo recovery of the undeveloped beaches along the South Carolina coast, "Capers Island to the Santee Delta": Journal of Coastal research, v. 11, no. 4, p. 1020-1025.

Shelton, J., 1965, Trend and genesis of lowermost sandston unit of Eagle Sandston at Billings, Montana: American Association of Petroleum Geologists Bulletin, v.49, no.9, p. 1385-1397.

Shepard, F.P., McLoughlin, P.A., Marshall, N.F., Sullivan, G.G., 1977, Current-meter recordings of low speed turbidity currents: Geology v. 5, p. 297– 301.

Shepherd, R.G., 1989, Correlations of Permeability and Grain Size: Ground Water, v. 27, no. 5, p. 633-638.

Shurr, G.W., and Ridgley, J.L., 2002, Unconventional shallow biogenic gas systems: American Association of Petroleum Geologists Bulletin, v. 86, n. 11, p. 1939-1969.

Slater, R. D., 1985, A numerical model of tides in the Cretaceous Seaway of North America: Journal of Geology, v. 93, p. 333-345.

Slingerland, R.L., Keen, T.R., 1999. Sediment transport in the Western Interior Seaway of North America: Predictions from a climate-ocean-sediment model. In: Bergman, K.M., Snedden, J.W. (Eds.), Isolated Shallow Marine Sand Bodies: Sequence Stratigraphic Analysis and Sedimentologic Interpretation. SEPM Special Publication No. 64, P. 179-190.

Slingerland, R.L., Kump, L.R., Arthur, M.A., Fawcett, P. J., Sageman, B.B., and Barron, E.J., 1996, Estuarine Circulation in the Turonian Western Interior Seaway of North America: Geological Society of America Bulletin, v. 108, p. 941-952.

Snedden, J.W., Dalrymple, R.W., 1999, Modern shelf sand ridges: from historical perspective to a unified hydrodynamic and evolutionary model, *in* Bergman, K.M., Snedden, J.W. eds., Isolated Shallow Marine Sand Bodies: Sequence Stratigraphic Analysis and Sedimentologic Interpretation: SEPM Special publication, v. 64, p. 13–28.

Snedden J., Kreisa, R., Tillman, R., Culver, S., and Schweller, W., 1999, An expanded model for modern shelf sand ridge genesis and evolution on the New Jersey Atlantic shelf, *in* Bergman, K.M., and Snedden, J.W., eds., Isolated Shallow Marine Sand Bodies; Sequence Stratigraphic Analysis and Sedimentologic Interpretation: SEPM, Special Publication 64, p. 147–163.

Snedden, J., Nummendal, D., and Amos, A., 1988, Storm- and fair-weather combined flow on the central texas continental shelf: Journal of Sedimentary Petrology, v. 58, n. 4, p. 580-595.

Snedden, J., Tillman, R., and Culver, S., 2011, Genesis and evolution of a mid-shelf, storm-built sand ridge, New Jersey continental shelf, U.S.A: Journal of Sedimentary research, v. 81, i. 81, p. 534-552.

Stine, A., and Schmitt, J., 1987, Storm-influenced shelf deposition of the lower sandstone member, Lower Cretaceous Thermopolis Shale, southwestern Montana. Contributions to Geology, Unversity of Wyoming, v. 25, p. 35-53.

Surlyk, F., and N. Noenygaard, 1986, Hummocky cross-stratification from the Lower Jurassic Hasle Formation of Bornholm, Denmark: Sedimentary Geology, v. 46, no. 3-4, p. 259-73.

Swift, D.J.P., and Rice, D.D., 1984, Sandbodies on muddy shelfs: a model for sedimentation in the Western Interior Cretaceous seaway, North America, *in* Tillman, R.D., and Seimers, C.T., eds., Siliclastic Shelf Sediments: SEPM Special Publications, v. 34, P. 43-62.

Switzer, A., and Jones, B., 2008, Large-scale washover sedimentation in a freshwater lagoon from the southeast Australian coast: sea-level change, tsunami or exceptionally large storm?: The Holocene, v. 18, p. 787-803.

Sydow, J., and Roberts, H.H., 1994, Stratigraphic framework of a late Pleistocene shelf-edge delta, northeast Gulf of Mexico: American Association of Petroleum Geologists, Bulletin, v. 78, p. 1276–1312.

Syvitski, J.P.M., Schafer, C.T., 1996. Evidence for an earthquake-triggered basin collapse in Saguenay fjord, Canada: Sedimentary Geology 104, 127– 153.

Ta., T. K.O., Nguyen, V.L., Tateishi, M., Kobayashi, I., Tanabe, S., and Saito, Y., 2005, Holocene delta evolution and dispersal models of the Mekong River, southern Vietnam, *in* Giosan, L., and Bhattacharya, J.P., eds., River Deltas: Concepts, Models, and Examples: SEPM, Special Publication 83, p. 453–466.

Ta, T.K.O., Nguyen Van, L., Tateishi, M., Kobayashi, I., Saito, Y., and Nakamura, T., 2002, Sediment facies and late holocene progradation of the mekong river delta in bentre province, southern vietnam; an example of evolution from a tide-dominated to a tide- and wave-dominated delta: Sedimentary Geology, v. 152, i. 3-4, p. 313-325.

Thom, B.G., 1983, Transgressive and regressive stratigraphies of coastal sand barriers in southeast Australia: Marine Geology, v. 56, p. 137-158.

Thorne, J., and Swift, D., 1991, Sedimentation on continental margins, VI: A regime model for depositional sequencês, their component systems tracts, and bounding surfaces, *in* Swift, D., Oertel, G., Tillman, R., and Thorne, J., eds., Shelf Sand and Sandstone Bodies: International Association of Sedimentologists Special Publication, v. 14, p. 189-255.

Tobison, N. H., 1972, Boxer field, Morgan County, Colorado, 1972. American Association of Petroleum Geologists Memoirs, v. 30, p. 383-388.

Tye, R. S., and Coleman, J. M., 1989, Depositional processes and stratigraphy of fluvially dominated lacustrine deltas; mississippi delta plain: Journal of Sedimentary Petrology, v. 59, i. 6, p. 973-996.

Van Houten, F.B., Bhattacharya, D., and Mansour, S.E.I., 1984, Cretaceous Nubia Formation and correlative deposits, eastern Egypt: major regressive-transgressive complex: Geological Society of America Bulliten, v. 95, p. 397-405.

Walker, R.G., and Eyles, C.H., 2006, Topography and significance of a basinwide sequence-bounding erosion surface in the Cretaceous Cardium Formation, Alberta, Canada: Journal of Sedimentary Research, v. 61, no. 4, p. 473-496.

Wang, P., and Horwitz, M., 2007, Erosional and depositional characteristics of regional overwash deposits caused by multiple hurricanes: Sedimentology, v. 54, p. 545-564.

Warrick, J.A., George, D.A., Gelfenbaum, G., Ruggiero, P., Kaminsky, G.M., and Beirne, M., 2009, Beach morphology and change along the mixed grain-size delta of the dammed Elwha River, Washington: Geomorphology, v. 111, p. 136-148.

Weimer, R.J., 1965, Stratigraphy and petroleum occurrences, Almond and Lewis Formations (Upper Cretaceous), Wamsutter Arch, Wyoming: Wyoming Geological Association Guidebook, 19th Annual Field Conference, p. 65-81.

Wentworth, C.K., 1922, A scale of grade and class terms for clastic sediments. The Journal of Geology, v. 30, no. 5, p. 377-392.

White, T., Furlong, K., and Arthur, M., 2002, Forebulge migration in the Cretaceous Western Interior basin of the central United States: Basin Research, v. 14, p. 43-54.

Williams, H. F. L., 2010, Storm surge deposition by hurricane Ike on the Mcfaddin National Wildlife Refuge, Texas: implications for paleotemestology studies: Journal of Foraminiferal Research, v. 40, no. 3, p. 210-219.

Willis, B.J., Bhattacharya, J.P., Gabel, S.L., and White, C.D., 1999, Architecture of a tide-influenced river delta in the frontier formation of central wyoming, USA: Sedimentology, v 46, i. 4, p. 667-688.

Willis, B.J., and Gabel, S.L., 2001, Sharp-based tide-dominated deltas of the Sego Sandstone, Book Cliffs, Utah, USA: Sedimentology, v. 48, p. 479–506.

Winn, R. D., 1989, Storm deposition in marine sand sheets: Wall Creek Member, Frontier Formation, Powder River Basin, Wyoming: Journal of Sedimentary Petrology, v. 61, no. 1, p. 86-101.

Wonick, J, 1972, Recluse Field, Campbell County, Wyoming: American Association of Petroleum Geologists Memoirs, v. 16, p. 376-382.

Wright, L.D. and Coleman, J.M., 1973, Variations in morphology of major river deltas as functions of ocean wave and river discharge regimes: American Association of Petroleum Geologists Bulletin, v. 57, p. 370–398.

Wright, E. K., 1987, Stratification and paleodrculation of the Late Cretaceous Western Interior Seaway of North America: Geological Society of America Bulletin, v. 99, p. 480-490.

Wright, L., and Friedrichs, C., 2006, Gravity-driven sediment transport on continental shelves: A status report: Continental Shelf Research, v. 26, p. 2092-2107.

Yang, B. C., Dalrymple, R. W., and Chun, S. S., 2005, Sedimentation on a wave-dominated, open-coast tidal flat, south-western korea; summer tidal flat-winter shoreface: Sedimentology, v. 52, i. 2, p. 235-252.

Yang, B., Dalrymple, R., Gingras, M., and Pemberton, S., 2009, Autogenic occurrence of Glossifungites ichnofacies: examples from wave-dominated, macrotidal flats, southwestern coast of Korea: Marine Geology, v. 26, p. 1-5.

Yokokawa, M., 1995. Combined-flow ripples: genetic experiments and applications for geologic records: Kyushu University, Faculty of Science, Memoirs, Series D, Earth and Planetary Sciences, v. 29, p. 1–38.

Yokokawa, M., Masuda, F., and Endo, N., 1995, Sand particle movement on migrating combined-flow ripples: Journal of Sedimentary Research, v. 65, p. 40–44.

Yoshida, S., Steel, R.J. and Dalrymple, R.W., 2007, Changes in depositional processes – an Ingredient in a new generation of sequence-stratigraphic models: Journal of Sedimentary Research, v. 77, p. 447–460.

Zavala, C., Ponce, J., Arcuri, M., Drittanti, D., Freue, H., and Asensio, M., 2006, Ancient lacustrine hyperpycnites: a depositional model from a case study in the Rayoso Formation (Cretaceous) of west-central Argentina: Journal of Sedimentary Research, v. 76, p. 41–59.

Zingg, T., 1935, Beitrag zur Schotteranalyse: Sehweizerische Mineralogische and zetrographische Mitteilungen, v. 15, p. 39-140.

FIGURES AND TABLES

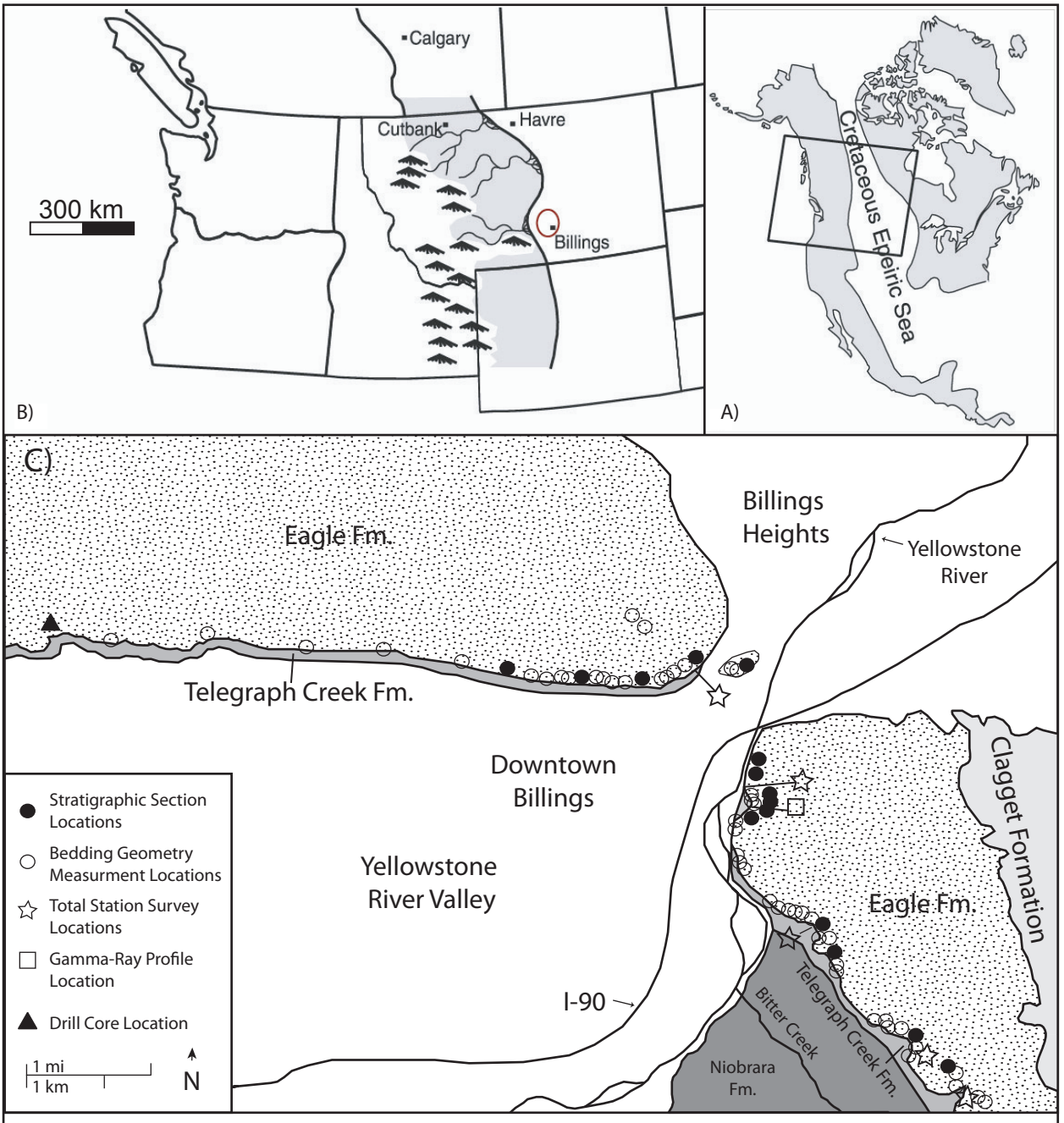

Figure 1: Map of study area. (A) Outline of the Late Cretaceous Western Interior Seaway; (B) the location of the Santonian-Campanian Eagle Formation in south-central Montana relative to the Sevier orogenic front (modified from Payenberg et al., 2002) and the location of the study area within Montana (circled in red); (C) Geologic line drawing of the study area in Billings, MT, (modified from Lopez, 2000) where downtown Billings is flanked to the North and East by the Cretaceous cliff-forming Eagle Formation referred to locally as the the "rimrocks".

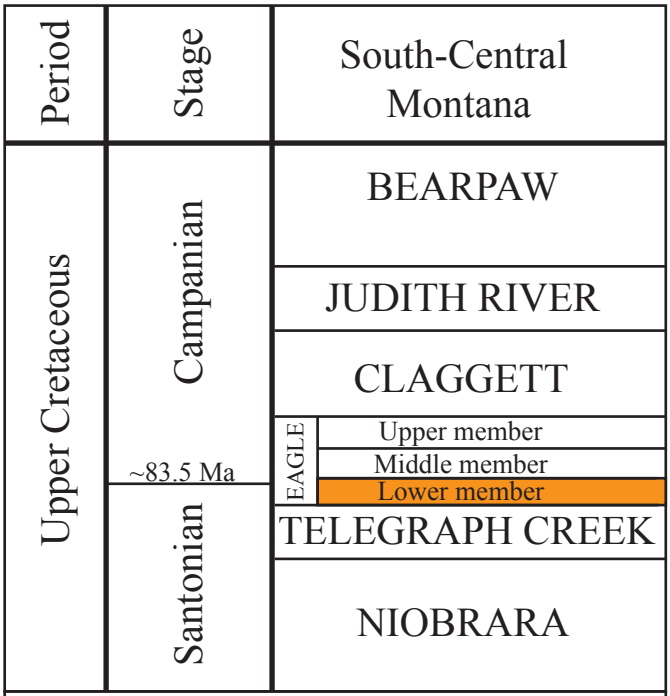

Figure 2: Upper Cretaceous Stratigraphy in south-central Montana. Orange box indicates the informal lower member of the Eagle Formation and the focus of this study (Modified from Payenberg, 2002).

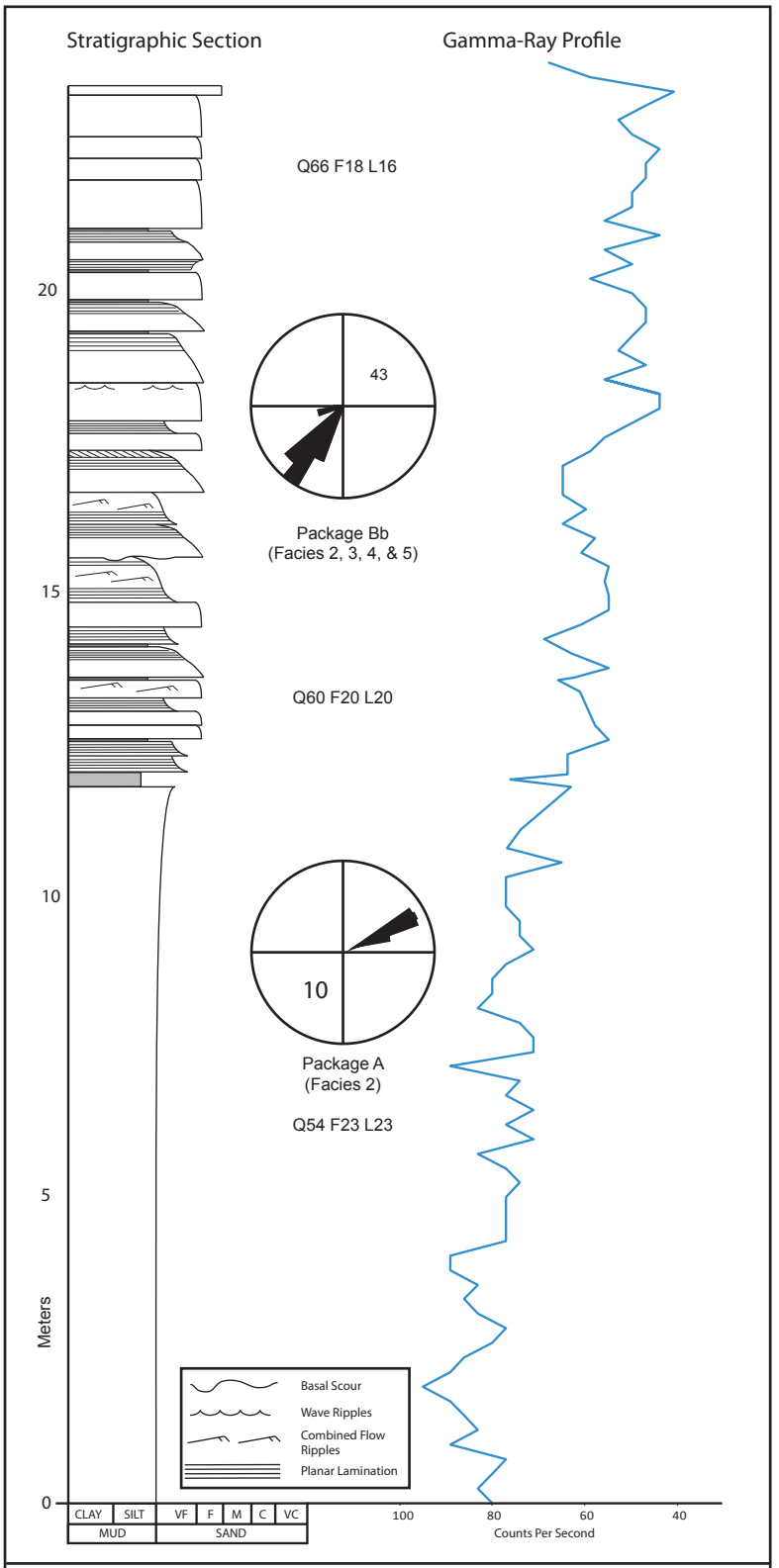

Figure 3: Stratigraphic section and gamma-ray profile of package A and Bb. Stratigraphic section and gamma ray profile measured at a gully exposure where package A is overlain by pacakge Bb. Rose diagrams illustrate paleocurrent measurments and bedding dip orientations obtained from each package. The gamma-ray profile exhibits an overall vertical decrease in counts per second which reflects a vertical decrease in the amount of gamma radiation emitted from the rocks within the stratigraphic section. A vertical decrease in gamma radiation can be used to infer a vertical decrease in clay content within packages A and Bb (Hesselbo, 1996). Note the vertical increase in quartz content and grain size coniciding with the vertical decrease in clay content.

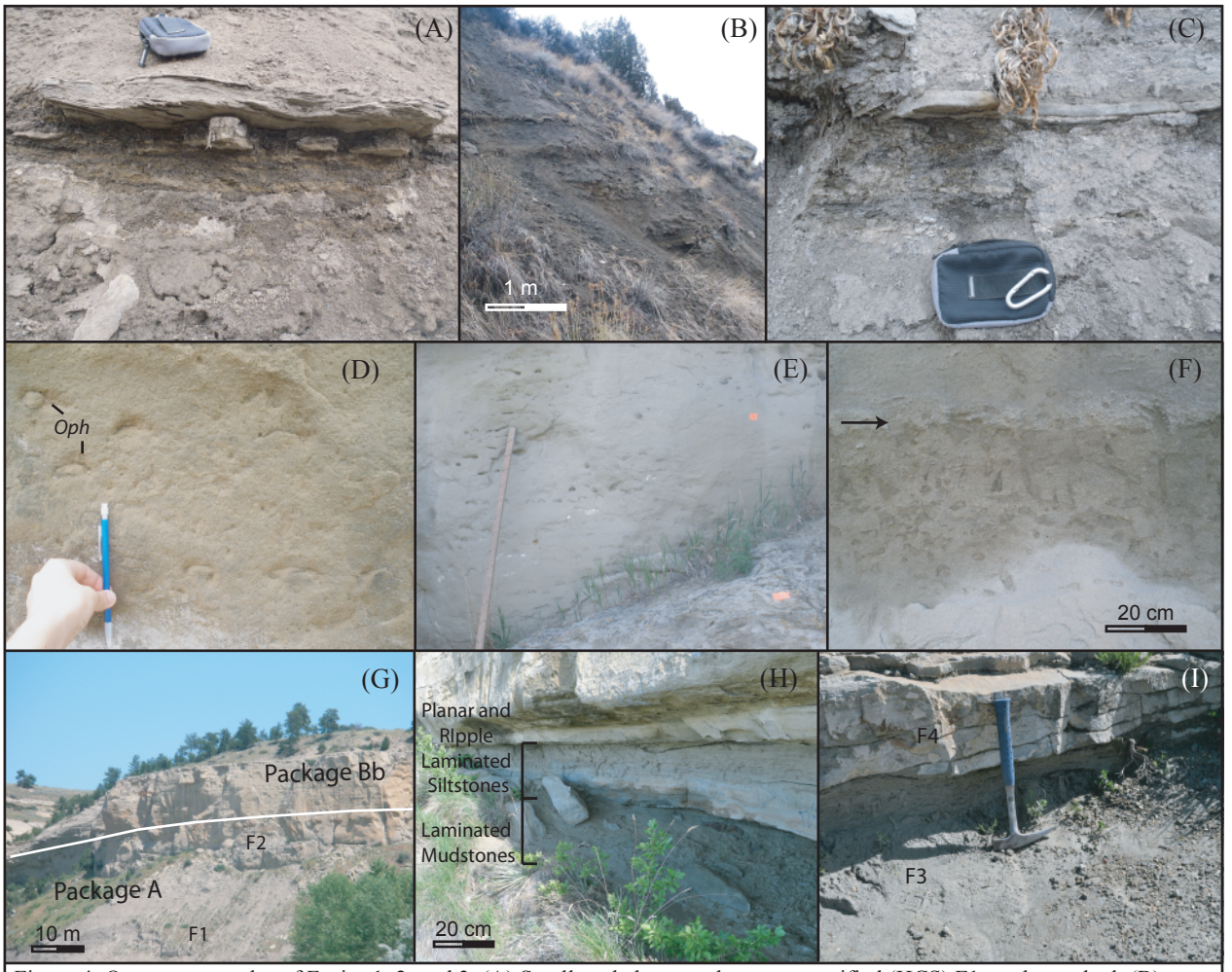

Figure 4: Outcrop examples of Facies 1, 2, and 3. (A) Small-scale hummocky cross stratified (HCS) F1 sandstone bed; (B) NE dipping F1 siltstones and planar laminated and structurless sandstones; (C) Structureless sandstone bed within F1; (D) Close-up picture showing the bioturbated massive nature of F2 sandstones. Preserved ichnofauna burrows in this picture are of *Ophiomorpha* (*Oph*); (E) Typical outcrop exposure of the bioturbated massive appearance of Facies 2 sandstones (2-meter stick for scale); (F) Example of *Ophiomorpha* burrows packed densely along a distinct horizon within F2. Note the truncation of the near vertical feeding feeding traces along the upper contact of this horizon marked by the black arrow. Burrow truncation likely resulted from erosion during a high-energy flow event (Pemberton et al., 2001; MacEachern, 2005); (G) Annotated photo showing package A overlain by Package Bb. In this picture the talus slope forming nature of F1can be observed, and the first appearance of cliff forming sandstone is marked by F2. Note that the starting point for most outcrop measured sections began with the first appearance of cliff forming sandstone (F2) above the talus slope (F1); (H) F3 outcrop exposure of laminated mudstones overlain by planar and ripple laminated siltstones; (I) F3 Laminated mudstones overlain by ripple laminated F4 sandstones.

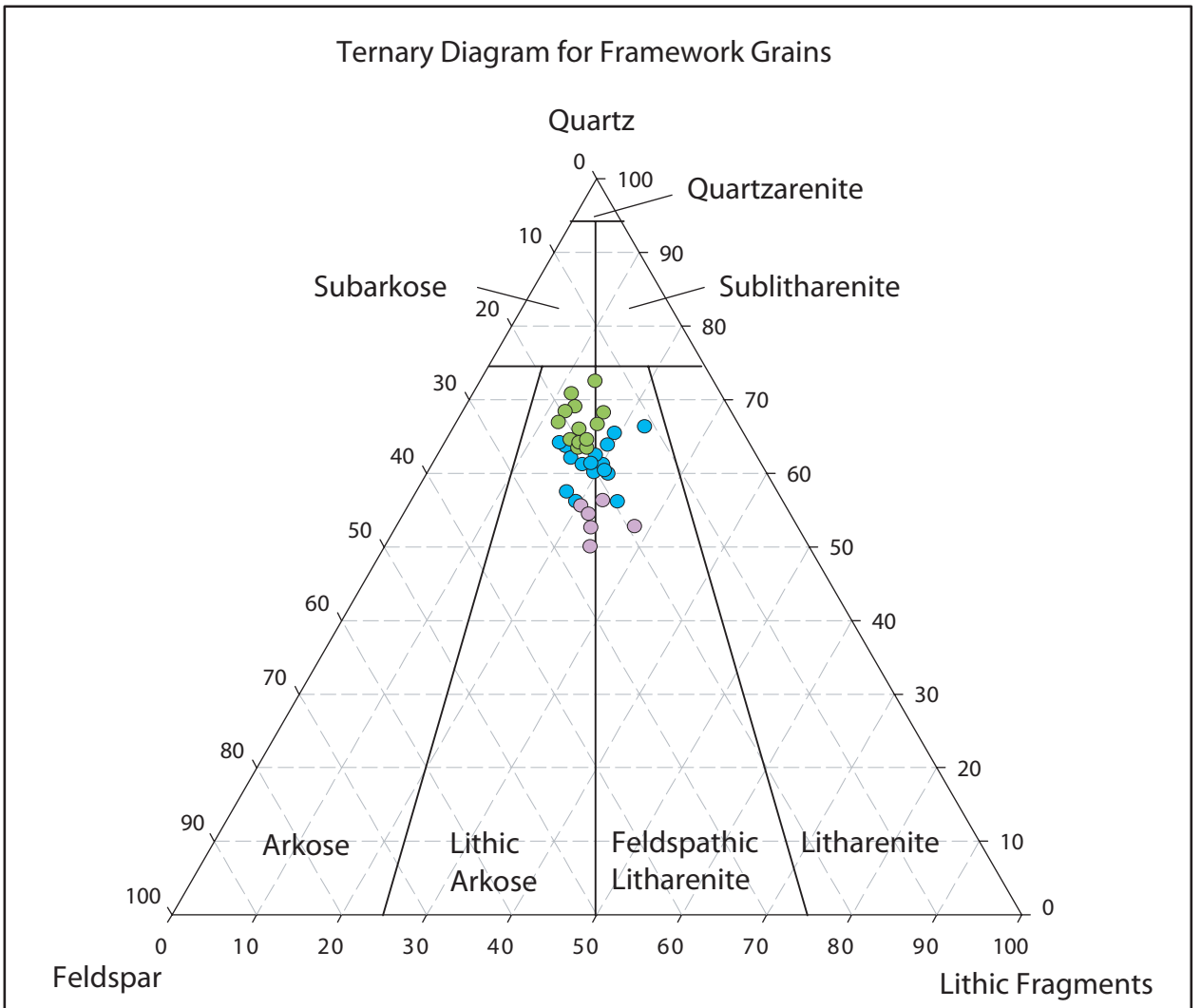

Figure 5: Modal compositional data for sandstone samples from the lower member of the Eagle Formation plotted on QFL diagrams. (A) Ternary diagram showing the modal QFL composition and sandstone classification nomenclature (after Folk, 1974), of all analyzed samples . The lithologic composition of each sample is colored based on the facies which they were collected from; ○ represent F2 samples; ● F4 samples; and ● F5 samples. This figure demonstrates distinct compositional grouping of samples by faices type and an increase in lithologic maturity of the samples from F2 through F4 and F5.

Figure 6: Outcrop examples of facies 4. (A) Sandstone bed consisting of Bouma-like Tb planar laminations; (B) Normally graded sandstone bed consisting of a Tb planar laminated base and Tc ripple laminated top; (C) Poorly developed load casts; (D) Slightly asymmetric ripple with rounded crests, and convex-upward lee and stoss sides (combined-flow ripple); (E) Typical exposure of stacked beds with Tb planar laminated bases and Tc ripple laminated tops (30 cm ruler for scale in center of picture); (F) Bed consisting of a thick succession of Tb planar laminations; (G) Large scour that has eroded through underlying F4 beds and is filled with Tb planar and Tc ripple laminated sandstones. Note the upper fill surface of the scour is conformable with the sharp base of the overlying bed. Scour is 185 cm in width by 90 cm deep; (H) *Fugichnia (*Escape trace) through Tb planar laminations; (I) Average scale (60 cm wide and 20 cm deep) and appearance of basal scoured surface.

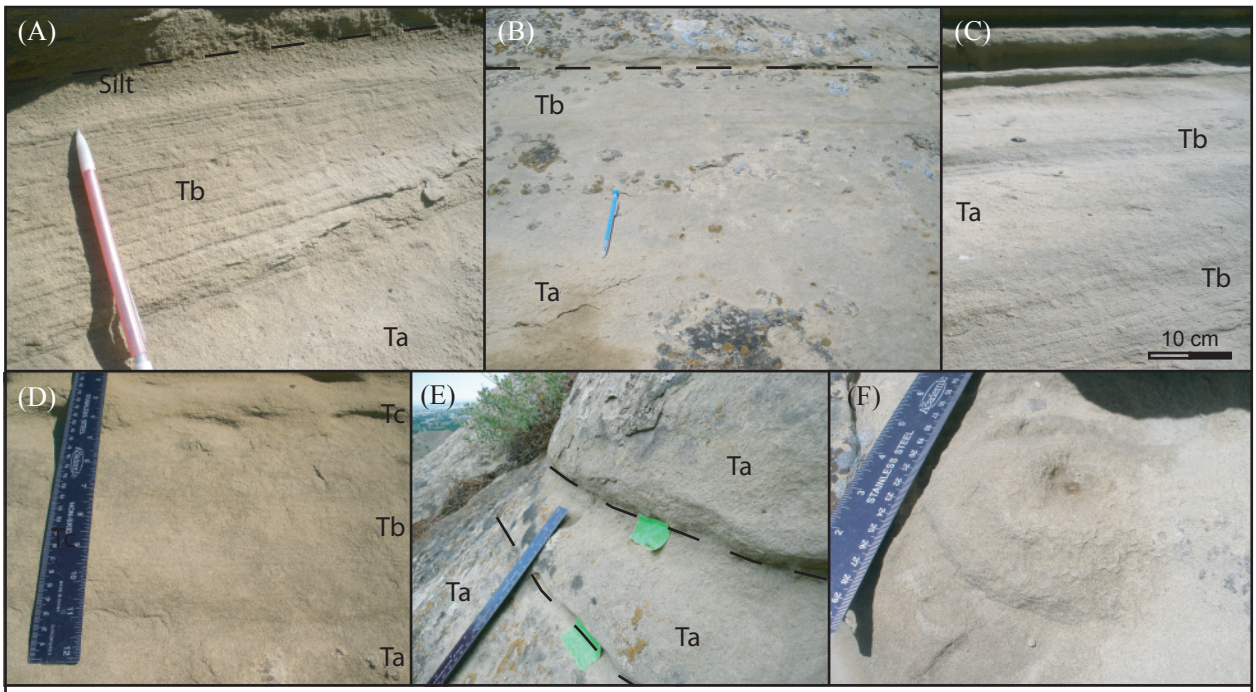

Figure 7: Outcrop examples of Facies 5. (A) Bed containing a Bouma-type Ta massive base, and aTb planar laminated top. A thin silt drape caps the bed; (B) Sandstone with a Ta massive base and Tb planar laminated top; (C) Repetition of sedimentary structures within an individual bed (Tb-Ta-Tb) indicates deposition from waxing to waning flow; (D) F5 bed containing a Ta massive base, Tb planar laminated middle, and Tc ripple laminated top; (E) Three beds consisting of massive bedding only; (F) Example of a Monocraterion burrow, where *Monocratierion* is a simple vertically oriented burrow that shows a funnel-like projection at the top of the burrow (Frey, 1985) and only occurs in F5 sandstones.

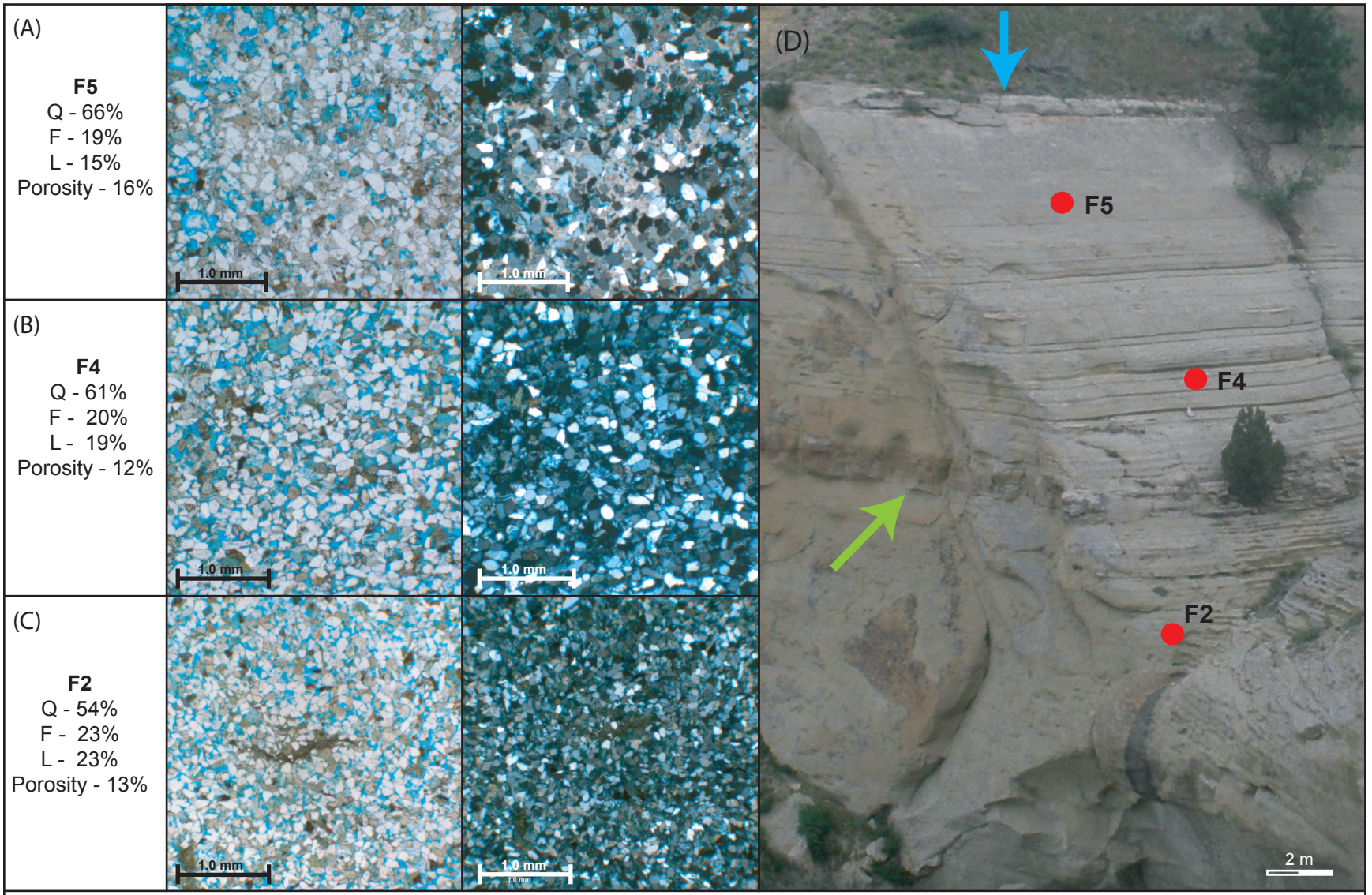

Figure 8: Petrographic images of facies 2, 4, and 5. Plane-polarized light and cross-polarized light petrographic images of samples collected from F5 (A), F4 (B), and F2 (C) in a vertical succession through a gully exposure (D) where package A is overlain by package Ba. Red circles represent the locations where petrographic image samples were collected from. The petrographic images are representative of each facies. The QFL and porosity percentages are average values for each facies type.The green arrow indicates the location of the Type 3 MRS surface which separates package A from Ba, and the blue arrow indicates the location of the Type 4 TRS surface. Note the vertical increase in grain size, and quartz content.

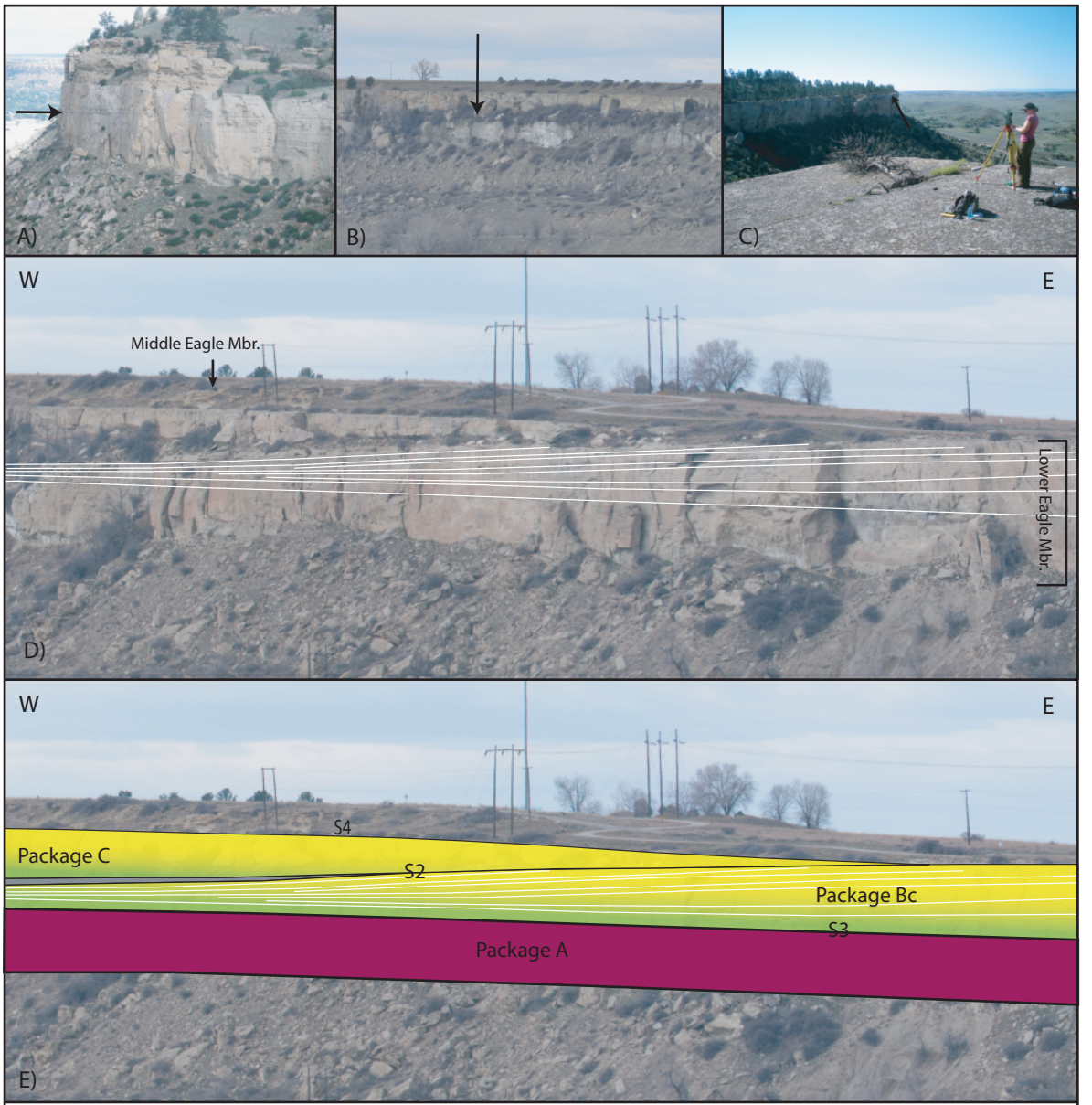

Figure 9: Outcrop examples of stratigraphic surfaces. (A) Cliff exposure of a Type 1 surface as indicated by arrow; (B) Type 2 surface as indiated by the arrow (note that the Type 2 surface is a hydrologic barrier as evidenced by vegetation growing above this surface); (C) Conducting a total station survey of the Type 4 surface (surface in foreground and surface marked by arrow; (D) Photomosaic of the E-W trending cliffs in Billings, MT, where white lines denote composite bedset boundaries (note that bedsets thin towards the W); (E) Photomosaic of the E-W trending cliffs with depositional packages and surfaces types illustrated (Type 2 surfaces - S2; Type 3 surface - S3; and Type 4 - S4; Type 1 surfaces not in picture). Green shading denotes distal overwash deposits and yellow shading denotes proximal overwash deposits. Note the sigmoidal shape of package Bc, and the en-echelon stacked nature of package C to the west.

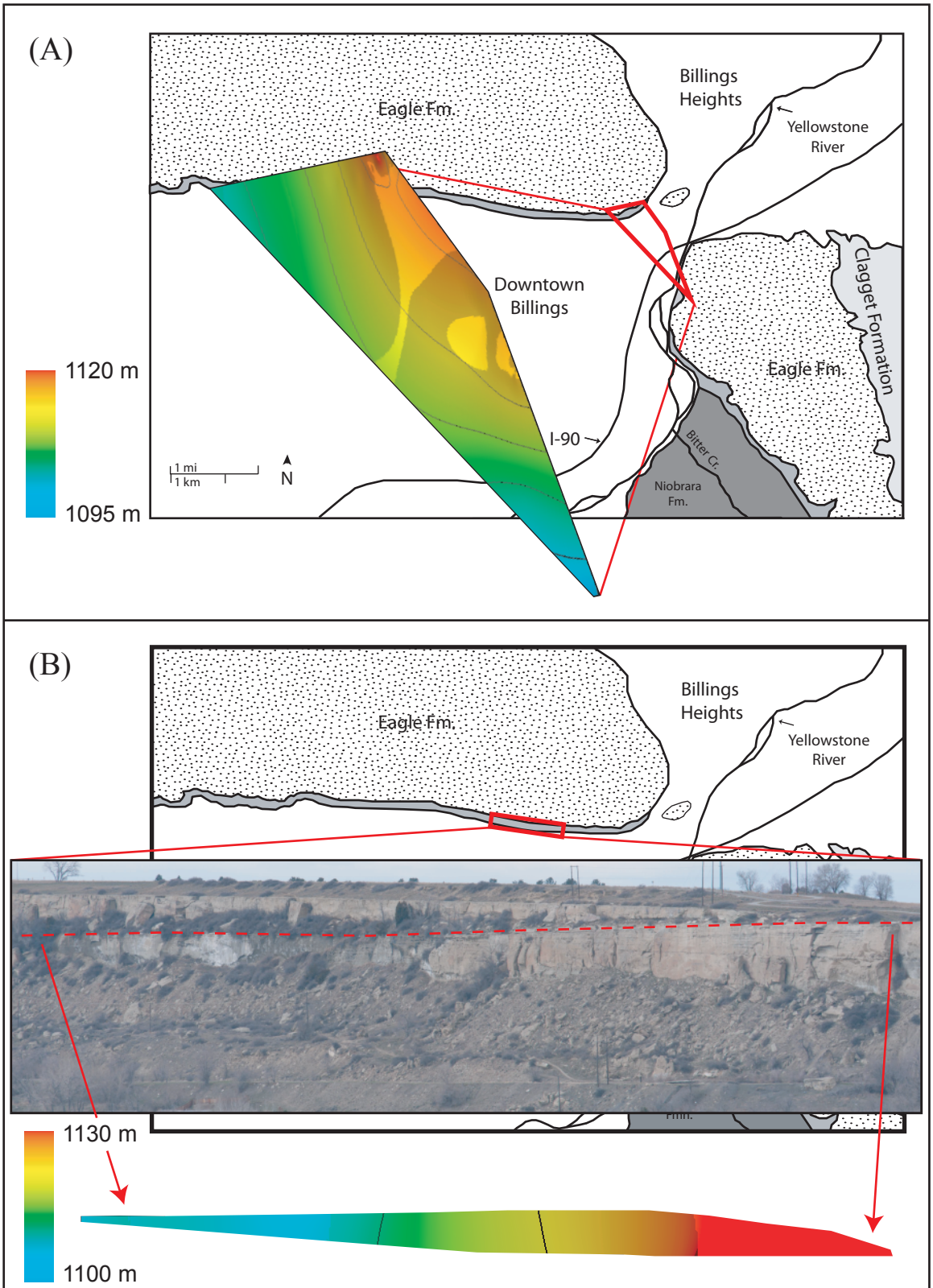

Figure 10: Plan view contour maps of outcrop-scale surfaces. (A) PETREL generated plan view contour map of the Type 1 surface which separates package Ba from overlying Package Bb (B) Outcrop photo of the Type 2 surface which separates package B from package C (red dashed line on picture) and a PETREL generated plan view contour map of that Type 2 surface.

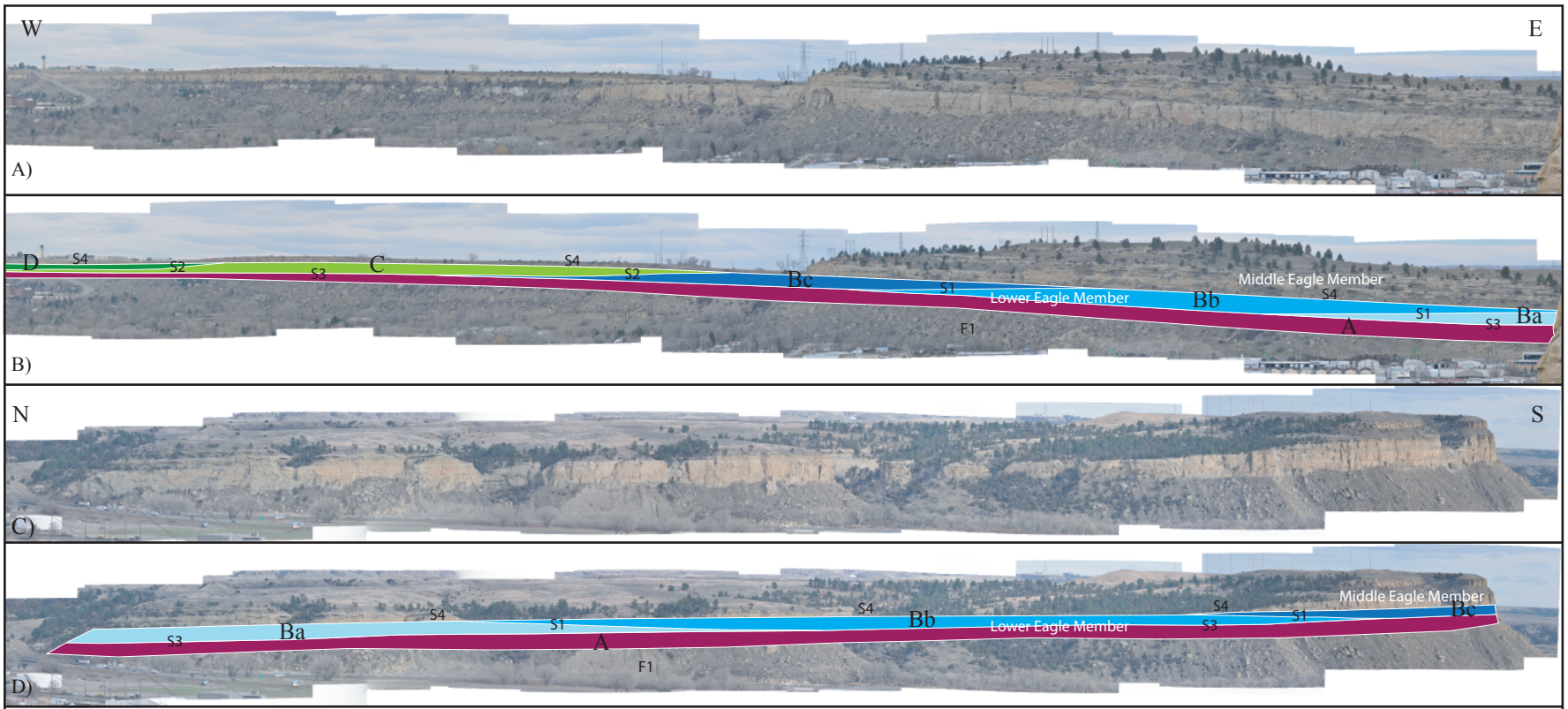

Figure 11: Annotated photomosaics of the E-W and N-S trending cliffs in Billings, MT. (A) E-W trending cliff exposures in Billings; B) Packages A, Ba to Bc, C and D depicted on photomosaics of the E-W trending cliffs, dipping and stacking of packages B-D is towards the west; C) Photomosaic of the N-S trending cliff exposures in Billings; D) Packages A and Ba-Bc depicted on a photomosaic of the N-S trending cliffs, dipping and stacking of packages Ba to Bc is towards the S-SW. Note that the Type 3 surface (S3) separates package A from overlying packages, Ba-Bc are separated by Type 1 surfaces (S1), Packages B-D are separated by a Type 2 surfaces (S2), and the Type 4 surface (S4) caps the entire lower member.

Figure 12: Annotated photomosaics of Packages C-G along the E-W trending cliffs. A) Photomosaic of the E-W trending cliffs in Billings; B) Packages C-G dipping and stacking towards the west (paleolandward) above Package A. Packages C-G are separated from eachother by Type 2 surfaces. Note the time transgressive nature of the Type 4 surface (S4 - red line) by its truncation of older deposits to the east and successively younger deposits to the west.

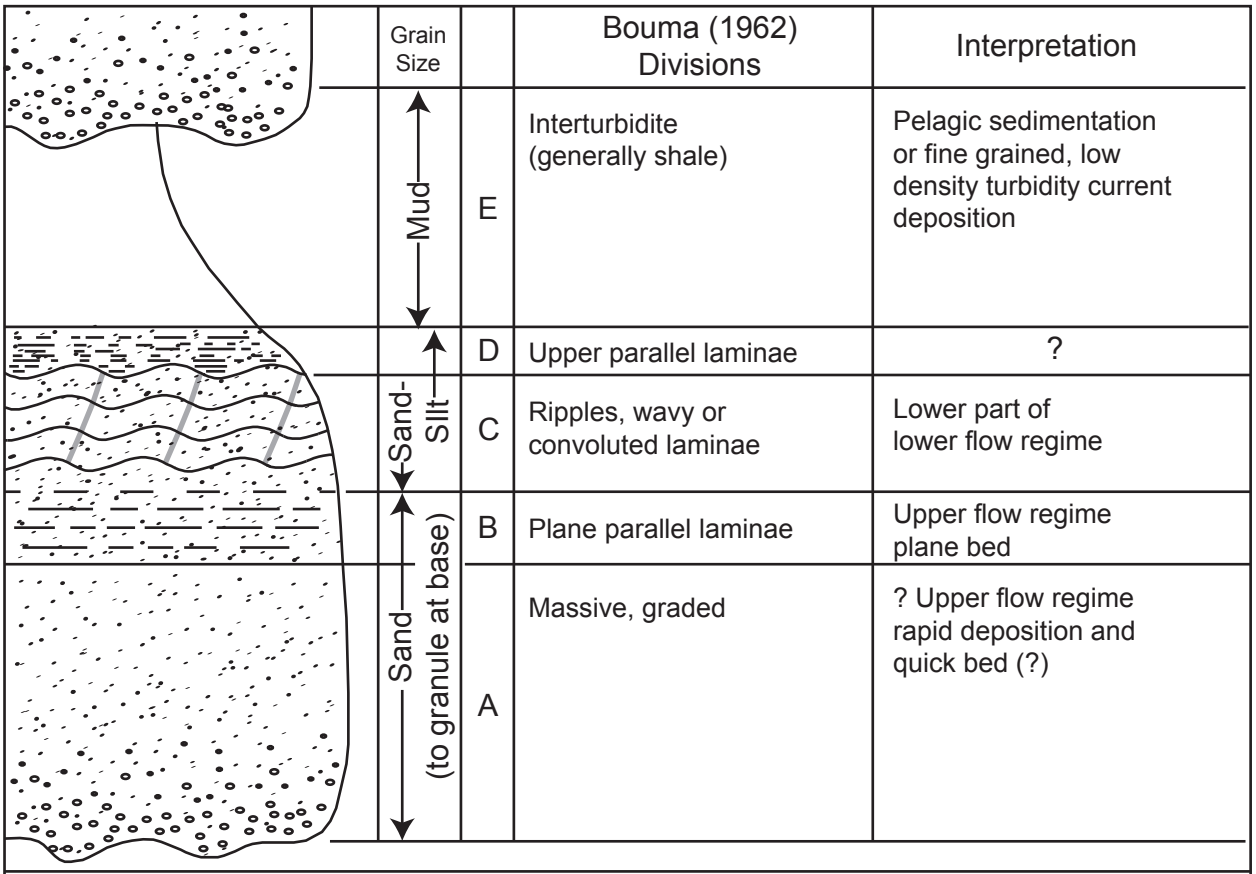

Figure 13: Schematic diagram of the idealized Bouma Sequene. Ideal sequence of structures in a turbidite bed (the Bouma sequence). Modified from Bouma (1962) and Blatt et al. (1972).

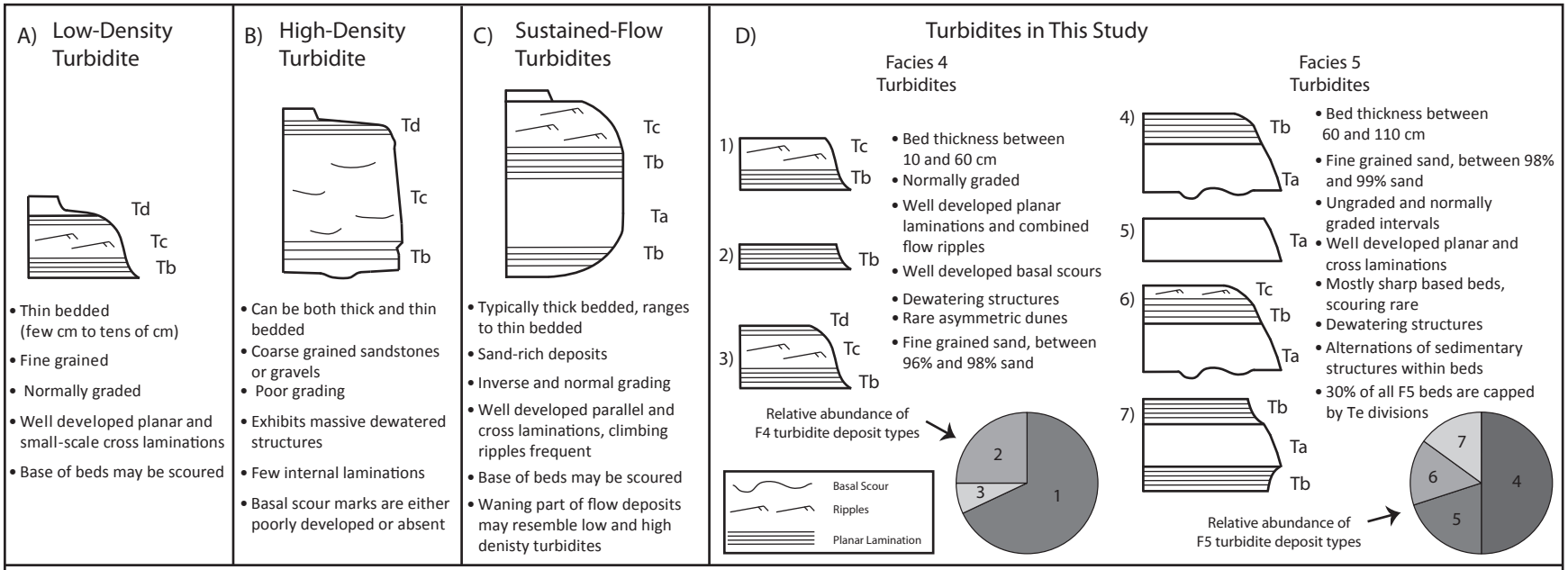

Figure 14: A comparison of different types of tubitie deposits and the tubidites in this study. The deposits of F4 and F5 have characteristics that resemble those of low- and high-density turbidity currents (e.g., Middleton, 1967; Middleton and Hampton, 1973; Lowe, 1982; Mulder and Alexander, 2001), however, based on the thick nature, sand-rich character, and repetition of sedimentary structures, the beds of F4 and F5 more closely match turbidites deposited during sustained flow (e.g., Mulder and Alexander, 2001; Plink-Björklund, 2004; Zavala, 2006; Lamb, 2008). Due to the presence of combined flow ripples and landward dipping beds, F4 and F5 are interpreted to be storm-surge generated turbidites.

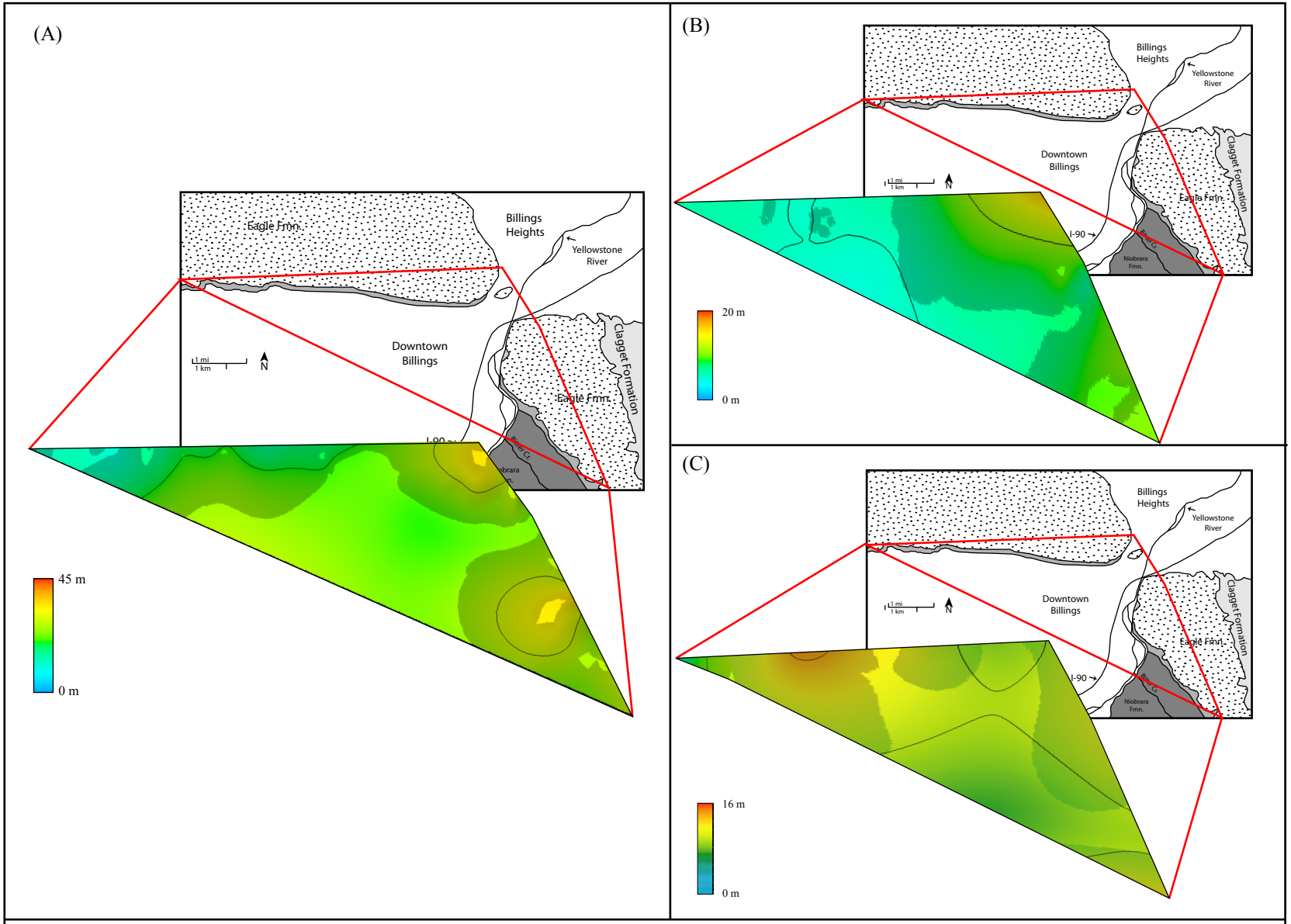

Figure 15: PETREL generated isopach maps of large-scale packages identified in the study area. (A) Isopach map of the enitre lower member of the Eagle Formation; (B) Isopach map of the regressive succession, package A; (C) Isopach map of the transgressive succesion, packages B to G (entire shoal succession).

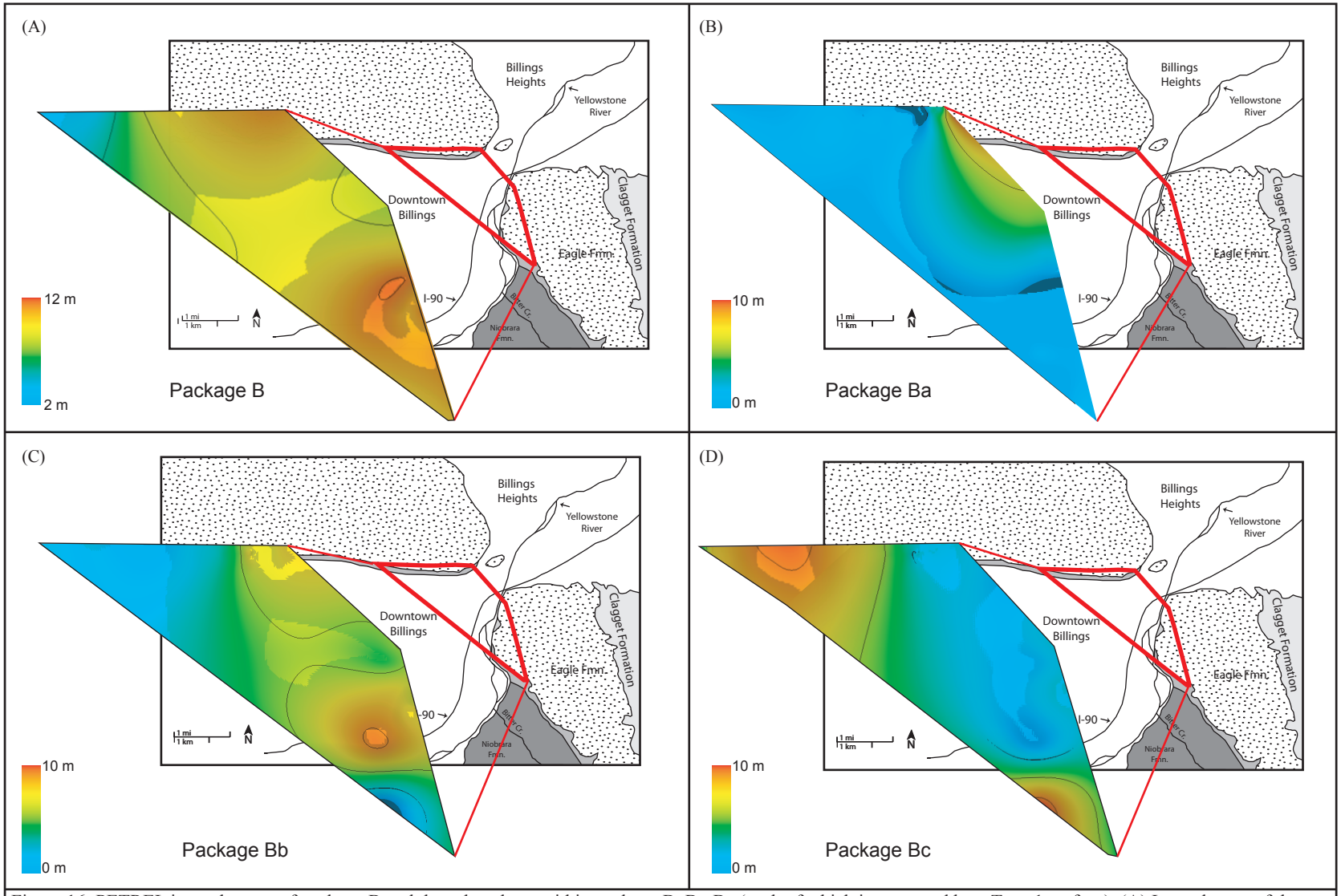

Figure 16: PETREL isopach maps of package B and the subpackges within package B, Ba-Bc (each of which is separated by a Type 1 surface). (A) Isopach map of the oldest shoal package, package B; (B) Isopach map of sub-package Ba, the oldest and north-easternmost sub-package within package B; C) Isopach map of package Bb which is the second oldest sub-package within package B; D) Isopach map of Package Bc, the youngest and south-westernmost sub-package within Package B. Notice the overall thinning of package B to the west-southwest, and changes in depositional centers between sub-packages Ba through Bc, reflecting infilling of areas of greater accomodation.

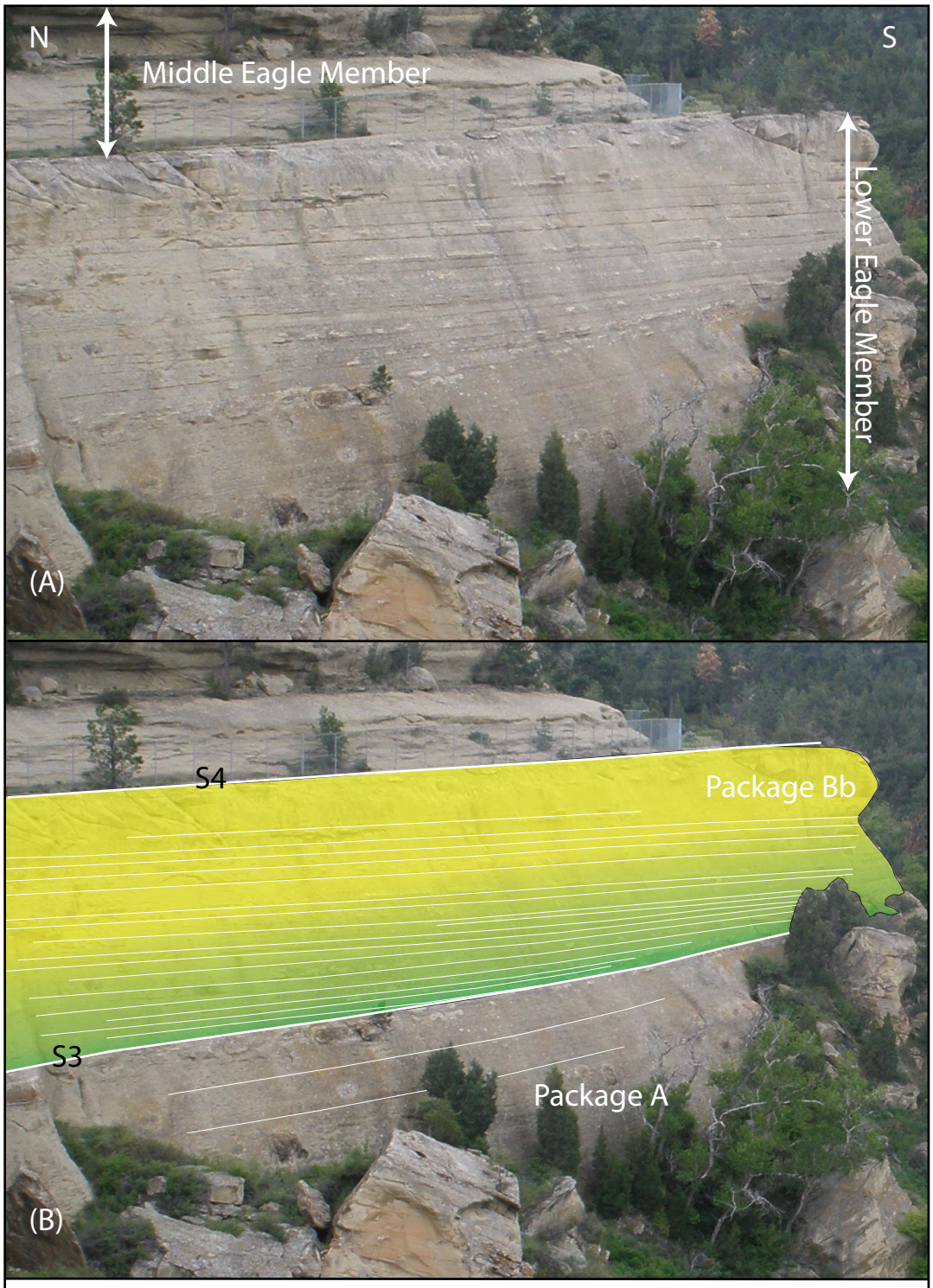

Figure 17: Annotated photo of package Bb exhibitiing downlap onto package A. (A) Exposure of the lower member of the Eagle Formation, and the overlying middle member; (B) Annotation of package A and overlying package Bb. Green shading denotes distal overwash deposits and yellow shading indicates proximal overwash deposits. Package A is separated from Bb by the Type 3 MRS surface (S3) and the lower member is separated from the middle by the Type 4 TRS surface (S4).White lines in package A denote horizons of intense bioturbation by the trace *Ophiomorpha* and white lines in package Bb are distinct bedding planes. Note the gentle southward dipping beds in package Bb which exhibit downlap onto package A and the east-northeast dip of *Ophiomorpha* horizons in package A.

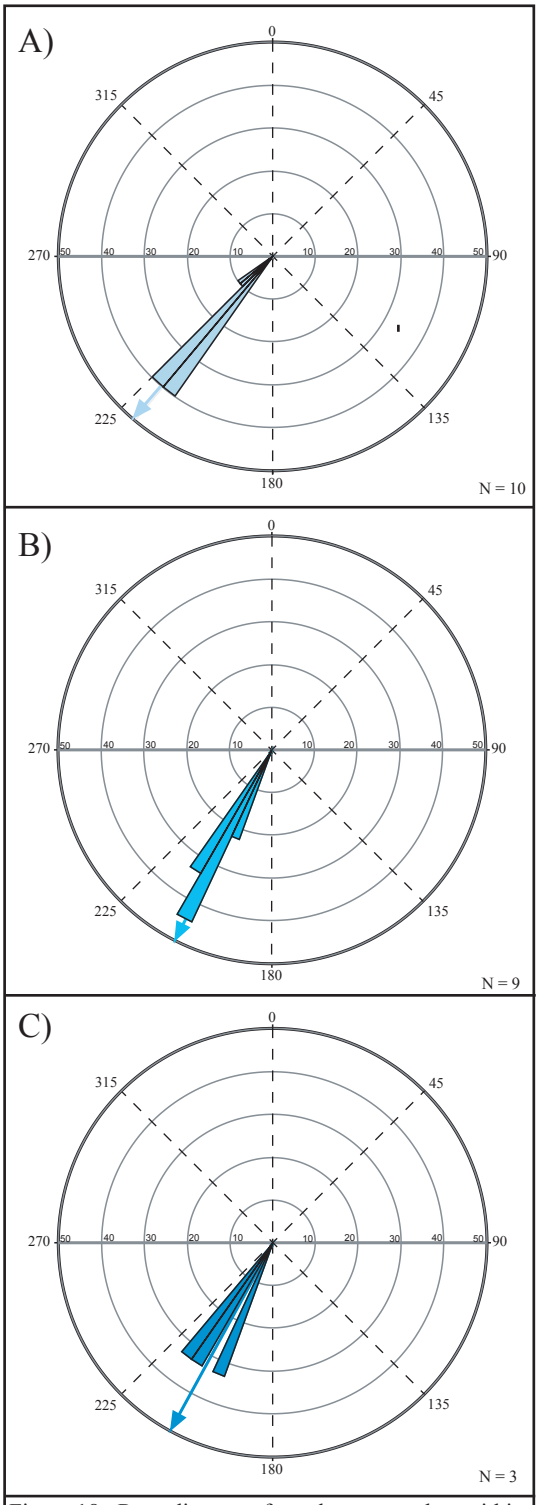

Figure 18: Rose diagrams for paleocurrent data within the study area. (A) paleocurrent measurments from package Ba; (B) paleocurrent measurments from package Bb; and (C) paleocurrent measurments from package Bc. Note that the scale for each rose diagram is based upon the percent of total paleocurrent measurments from 0-50%. Arrows indicate mean paleocurrent direction. Paleocurrent measurments were obtained from measuring ripple crest, cross bedding, and trough axis orientations. Rose diagrams generated with the program Stereonet7 (Allmendinger, 2011).

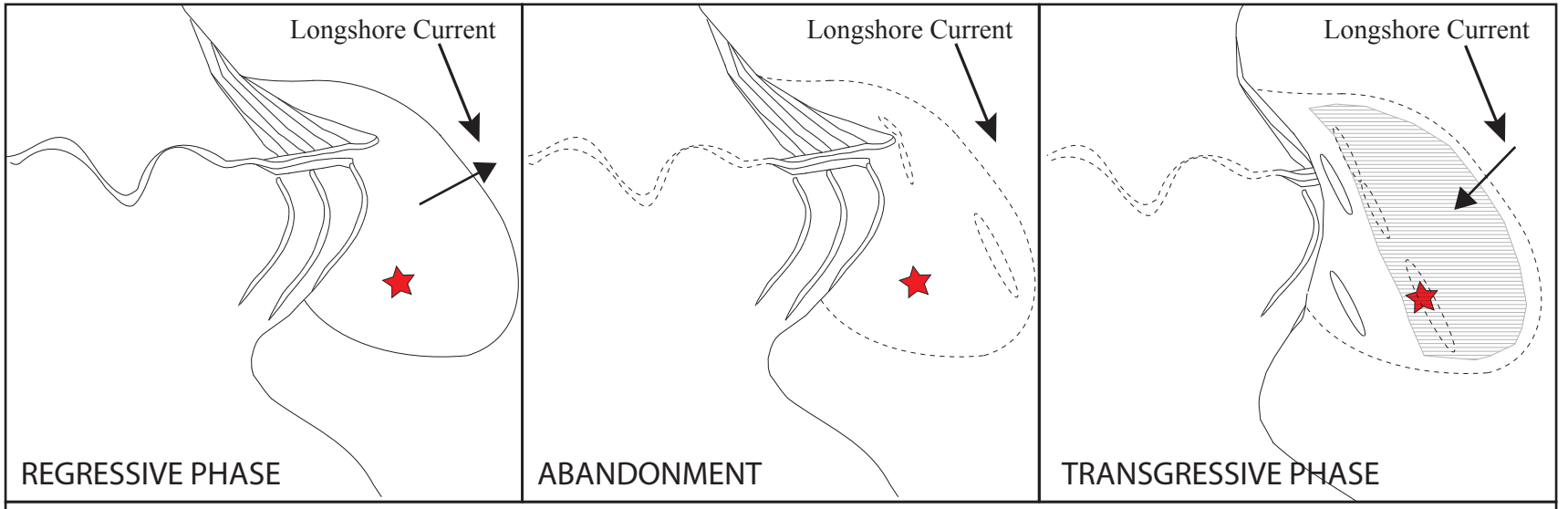

Figure 19: Depositional evolution of the lower member of the Eagle Formation. Deltaic deposition within the lower member of the Eagle Formation occurred during two phases of evolution; a regressive phase and a transgressive phase. REGRESSIVE PHASE: Basinward delta progradation resulted in deposition of pro-delta and delta front deposits of facies 1 and 2; ABANDONMENT: A reduction in fluvial input leads to the "abandonment" of the regressive delta lobe which results in delta top subsidence and an increase in the affects of wave and storm processes allowing for wave-reworking of deltaic headlands and delta front sediments. Shore proximal deposits are re-worked into barrier islands and delta front finer grained sediments are carried down drift and deposited as sandy shoals (Penland and Boyd, 1986). The Type 3 surface (a maximum regressive surface) separates underlying regressive deposits from overlying wave-reworked deposits. TRANSGRESSIVE PHASE: The decrease in fluvial input, allows for the develompent of a wave scour generated trangressive ravinement surface (Type 4 surface) on the basinward side of shoal deposits. Transgression of the abandoned delta lobe results in the landward progradation and migration of shoals that developed after abandonment. As transgression continues, the Type 4 surface also propogates landward and truncates the basinward side of shoal deposits. ★ represents Billings, MT, and ▤ represents the Type 4 surface generated by wave-scour.

Facies Name	Lithology	Bed Thickness (cm)	Composition (QFL - Normalized)	Grain Size	Sedimentary Structures	Bioturbation Index	Ichnofauna	Depositional Process	Depositional Environment
Facies F5	Graded, Massive, Planar Laminated, and Planar Cross Laminated Sandstone	60 to 110	Q66, F19, L15	fL to fU, silt 2% to <1%	Planar lamination, planar cross beds, and silt drapes.	0 to 2	*Ophiomorpha, Skolithos, Monocraterion, Planolites, Palaeophycus tubularis*	Sustained flow generated turbidites - upper flow regime dominant	Proximal Shoal
Facies F4	Planar and Ripple Laminated Sandstone	20 to 80	Q61, F20, L19	vfU to fL, silt 2% to 4%	Planar lamination, asymmetric ripples, asymmetric dunes, combined flow ripples, oscillatory ripples, loading structures, and scours.	0 to 3	*Planolites, Palaeophycus tubularis, Ophiomorpha, Skolithos*	Sustained flow generated turbidites - upper and lower flow regime, wave-reworking	Mid Shoal
Facies F3	Laminated Mudstone and Planar to Ripple Laminated Siltstone	<10 to 40	N/A	Clay to Silt	Planar laminations and ripples, infrequent carbonate laminae	0 to 4	*Palaeophcus tubularis*	Sediment settle-out, waning stages of turbidity currents	Distal Shoal & Suspension Settleout
Facies F2	Bioturbated Massive Sandstone	N/A	Q54, F23, L23	vfL to fL, silt ~5%	None observed.	5 to 6	*Ophiomorpha , Terebellina , Skolithos, Cylindrichnus concentricus*	Sediment gravity flows	Delta front, Pro-delta
Facies F1	Bioturbated Interbedded Mudstone, Siltstone, and Sandstone	<1 to 10	N/A	Fine grained sand, silt, clay	Planar lamination, hummocky cross stratification in sandstone beds	1 to 6	*Ophiomorpha, Terebellina, Palaeophycus tubularis, Planolites*	Sediment graviy flows, storm events, & suspension settleout	Pro-delta

Table 1: Facies descriptions and definitions. Characteristics of the 5 facies identified within the lower member of the Eagle Formation.

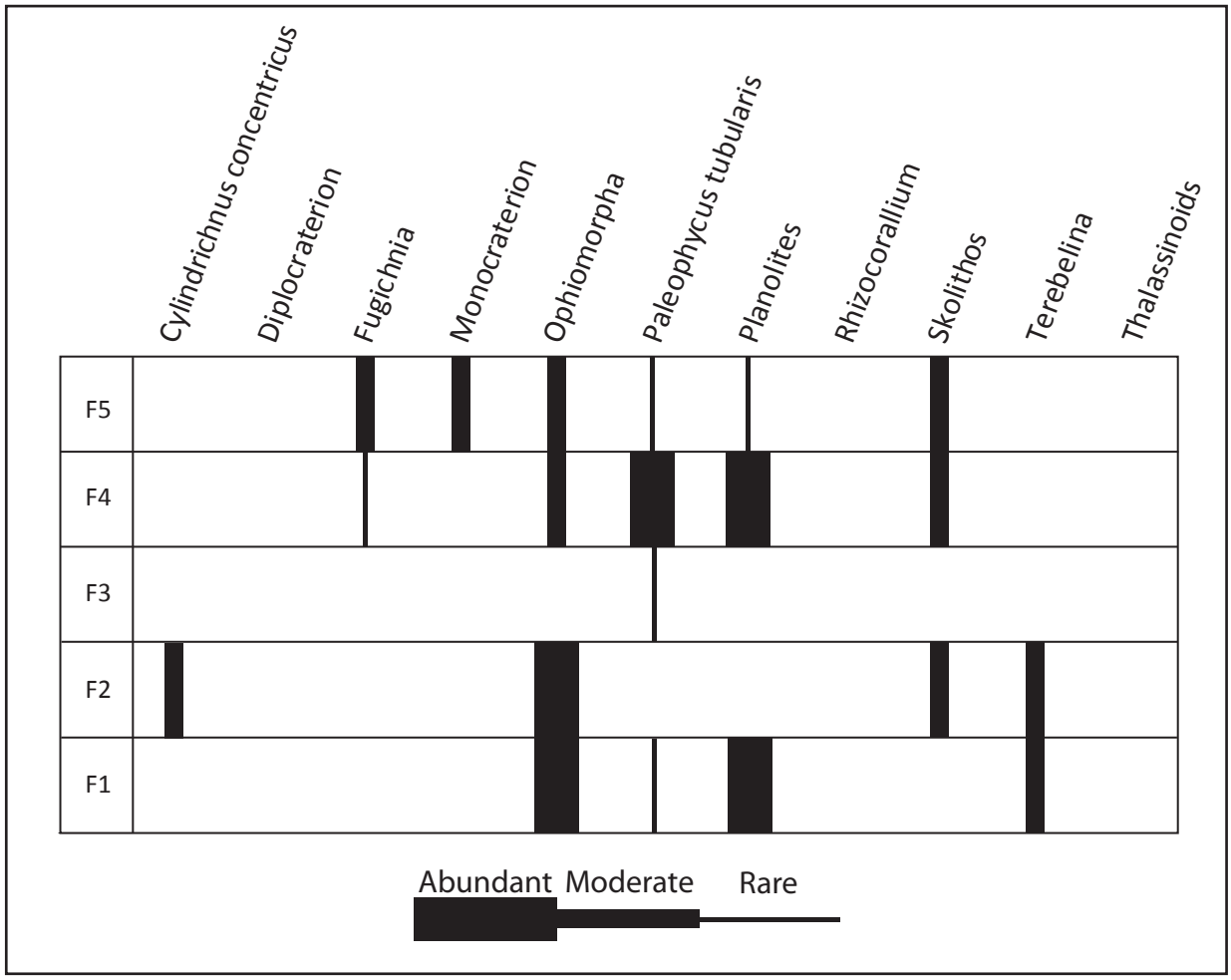

Table 2: Trace fossil abundance for facies 1 through 5.

Bounding Surfaces	Underlying Facies	Overlying Facies	Associated Ichnofauna	Cementation	Geometry/Truncation	Regional Extent	Significance	Interpretation
Type 1 Surfaces S1	Facies 3, 4, & 5	Facies 4 & 5	*Planolites, Paleophycus tubularis* , BI 3	Calcite cementation, varies between 20 cm thick in proximal locations and 45 cm thick in distal locations	Paleolandward dipping, clinoformal shape, bedding parallel, truncates up-dip against the type 4 surface	Traceable for 100s of meters, areal extent between 1.1 km² and 3.3 km²	Highest order surfaces, separates small scale depositional packages	Accretion surfaces
Type 2 Surfaces S2	Facies 3, 4, & 5	F3 <10 cm thick in east, up to 40 cm thick in west	*Planolites, Paleophycus tubularis* , BI 4	Calciate cementation, approximately 25 cm thick	Paleolandward dipping, clinoformal shape, bedding parallel, truncates up-dip against the type 4 surface	Traceable for 1000s of meters, areal extent between 1.2 km² and 6.62 km²	Intermediate order surfaces, separates large-scale depositional packages	Accretion surfaces
Type 3 Surface S3	Facies 2	Facies 3, 4, & 5	*Planolites, paleophycus tubularis, Ophiomoropha* , BI 5-6	Calcite Cementation present, not in significant amounts	Paleoseaward dipping, non-erosional	Traceable for 10000s of meters, areal extent 60 km²	First of 2 lowest order surfaces	Surface of non-deposition or reduced-sedimentation
Type 4 Surface S4	Facies 4 & Facies 5	Middle Eagle Formation	*Diplocraterion, Thalassinoides, Rhizocorallium* , BI 6	Calciate cementation, between 25 and 35 cm thick	Paleoseaward dipping, truncates oldest strata in the northeast and progressively younger strata to the west and south	Traceable for 10000s of meters, areal extent 60 km²	Second of 2 lowest order surfaces, truncates all depositional packages	Surface of marine erosion, *Glossifungites* ichnofaices immediately beneath

Table 3: Descriptions of stratigraphic surfaces. Characteristics of the 4 surface types identified within the lower member of the Eagle Formation.

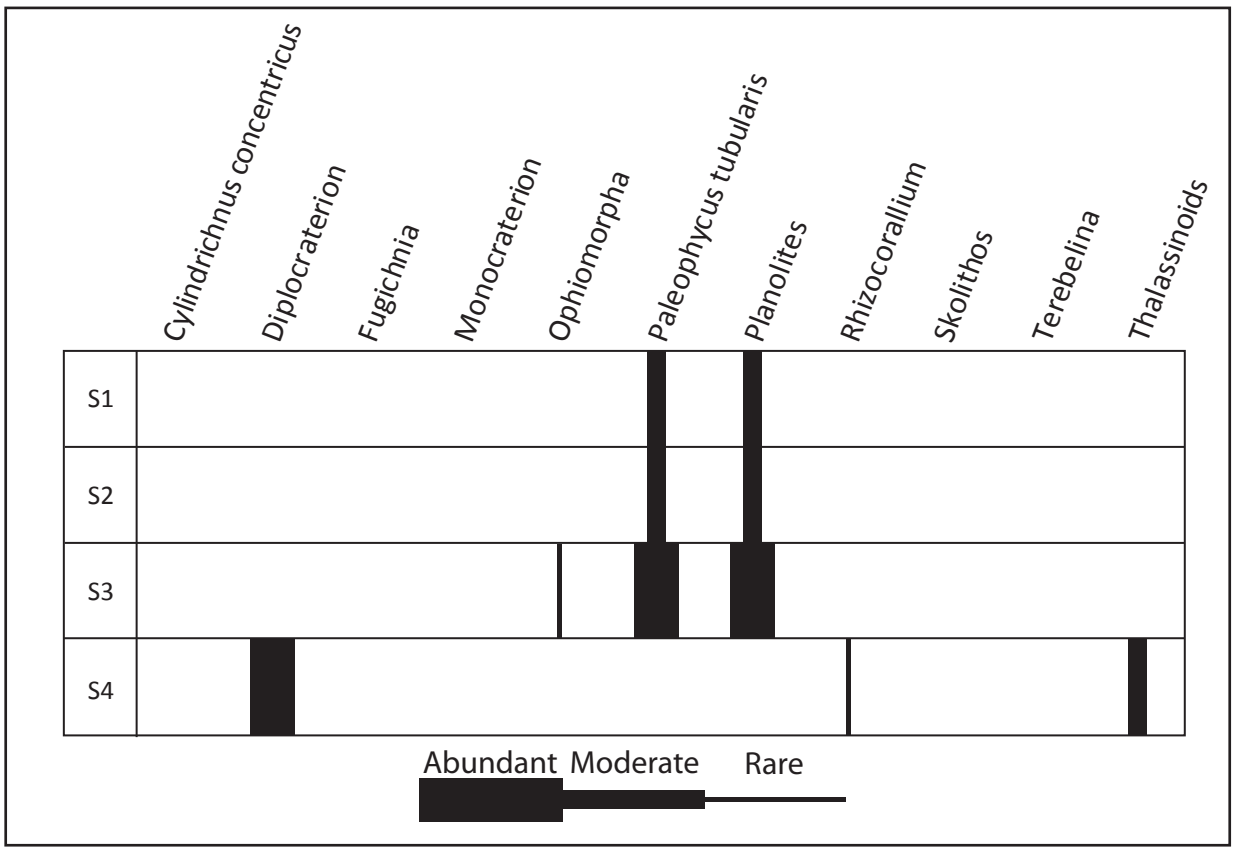

Table 4: Trace fossil abundance for sediments immediately underlying surface types 1-4.

Appendix A: Stratigraphic Sections

In this study, 15 stratigraphic sections were measured along 11 km of outcrop (Figures A1-A16). Because most of the sandstone interval outcrops as steep cliff faces, section locations were limited to accessible ravines. Centimeter scale resolution was used to describe facies variation and bedding geometries. Also recorded were grain size, sedimentary structures, and the type of trace fossils present. The bioturbation intensity within each facies was recorded following the guidelines of Bann (2004) and MacEachern (2005) which uses a numerical ranking from 0 (no bioturbation) to 6 (complete bioturbation). Because of the gradational basal contact with the Telegraph Creek Formation, the base of each measured section started with the first appearance of cliff forming Eagle sandstone.

Along vertical cliff exposures where a lack of ravines prevented the measurement of stratigraphic sections, bedding geometries were documented by measuring bedding thickness variations. Measurements were made at 50 locations made by dropping a rope with markings at quarter meter intervals down the side of a vertical cliff and counting the number of quarter meter intervals between beds. Only 12 of the 50 bedding geometry measurments were used in the correlation diagrams, and therefore are the only locations depicted on the figure below.

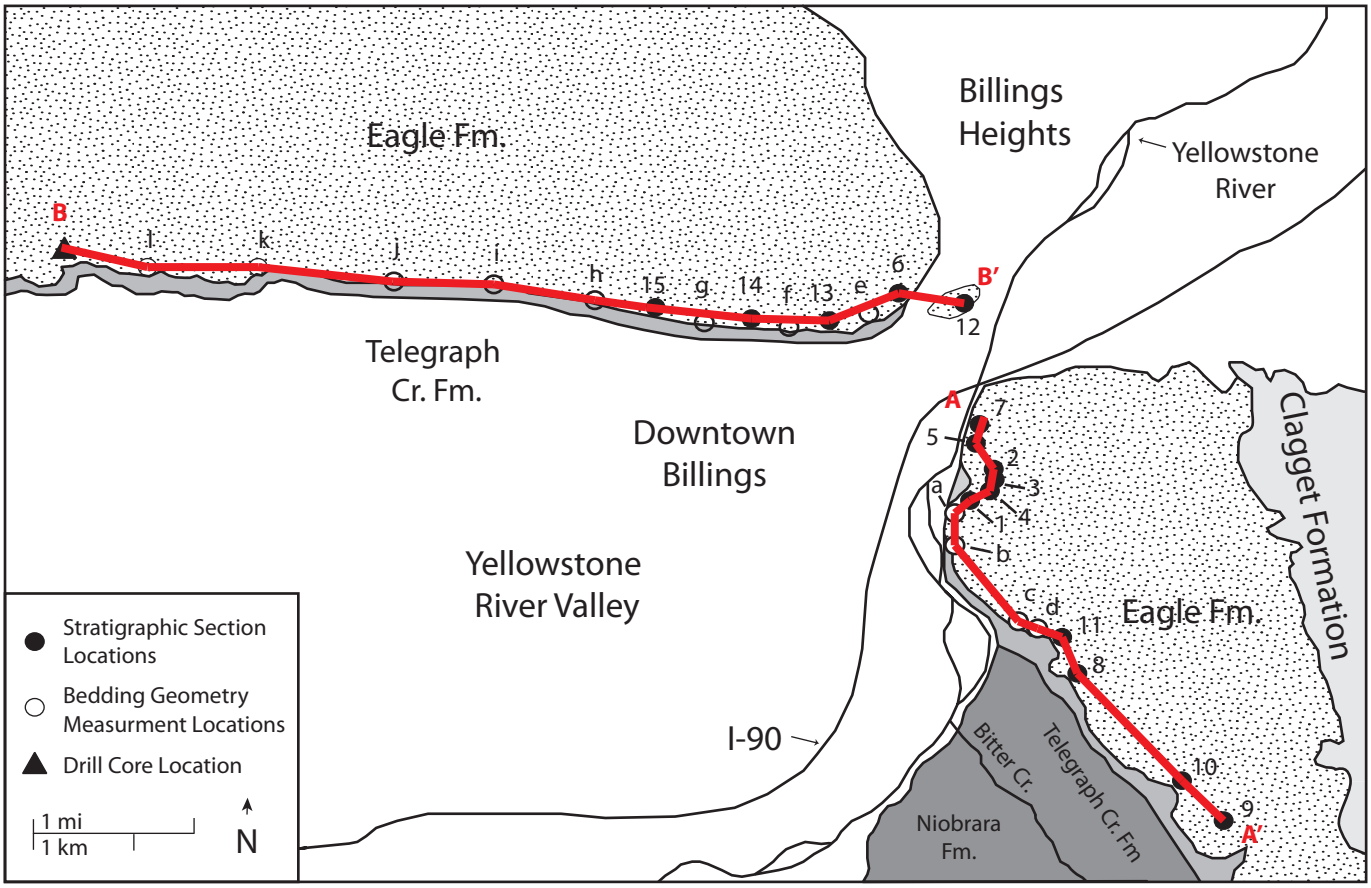

Figure A1. Map showing the locations of the 15 stratigraphic sections measured in this study, the drill core location, and the 12 bedding geometry measurment locations that were utiliized in generating the two correlation diagrams. Red lines indicate the two correlation diagram lines (A-A' and B-B').

Key for the 15 measured stratigraphic sections in the study area (Figures A2-A16) and the 2 correlation diagrams (Figures A18 and A19).

Sedimentary Structures and Lithology

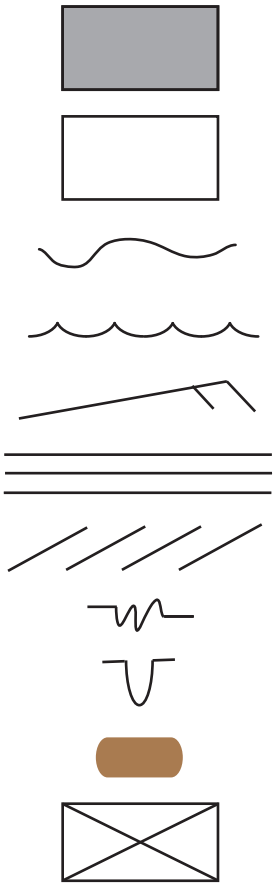

Silty Sandstone drapes

Sandstone

Troughs and Basal Scours

Wave Ripples

Combined Flow Ripples

Planar Lamination

Cross Bedding

Soft Sediment Deformation

Pervasive Bioturbation

Cementation

Vegetative Cover

Surfaces

Type 4 Surface

Type 3 Surface

Type 2 Surface

Type 1 Surface

Ichnofauna

C- Cylindrichnus concentricus

D- Diplocraterion

M- Monocraterion

Oph- Ophiomorpha (Undifferentiated)

OF- Organic Fragments

Pl- Planolites

Pt- Palaeophycus tubularis

R- Rhizocorallium

Sk- Skolithos

Te- Terebellina

Th- Thasalassinoides

UB - Unidentified Burrow

UEB - Unidentified Escape Burrow

Depositional Packages

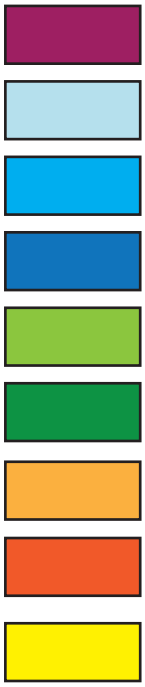

Package A

Package Ba

Package Bb

Package Bc

Package C

Package D

Package E

Package F

Package G

Figure A2. Stratigraphic section #1.

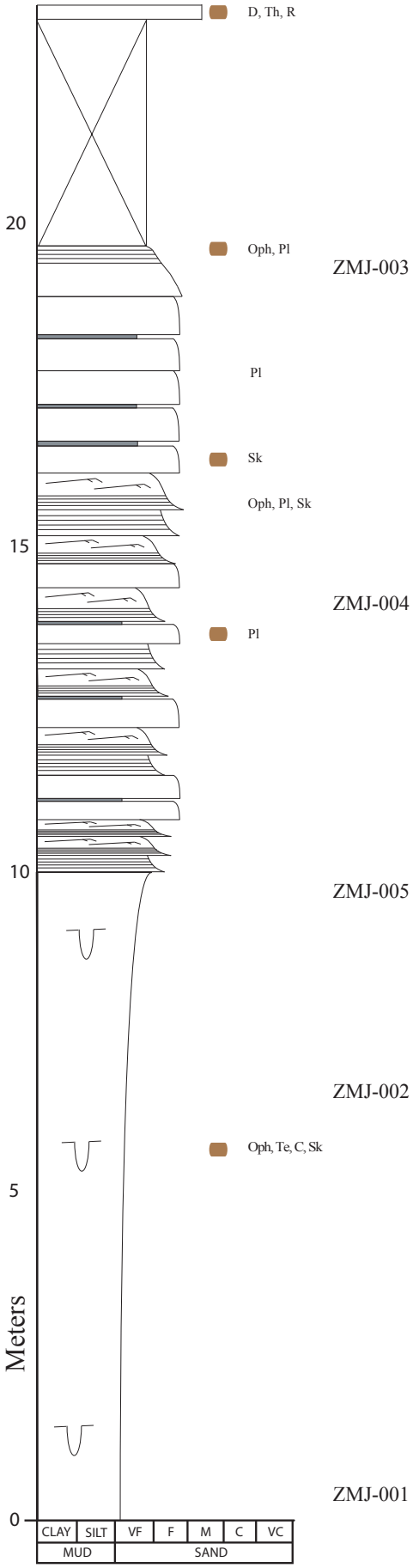

Figure A3. Stratigraphic section #2.

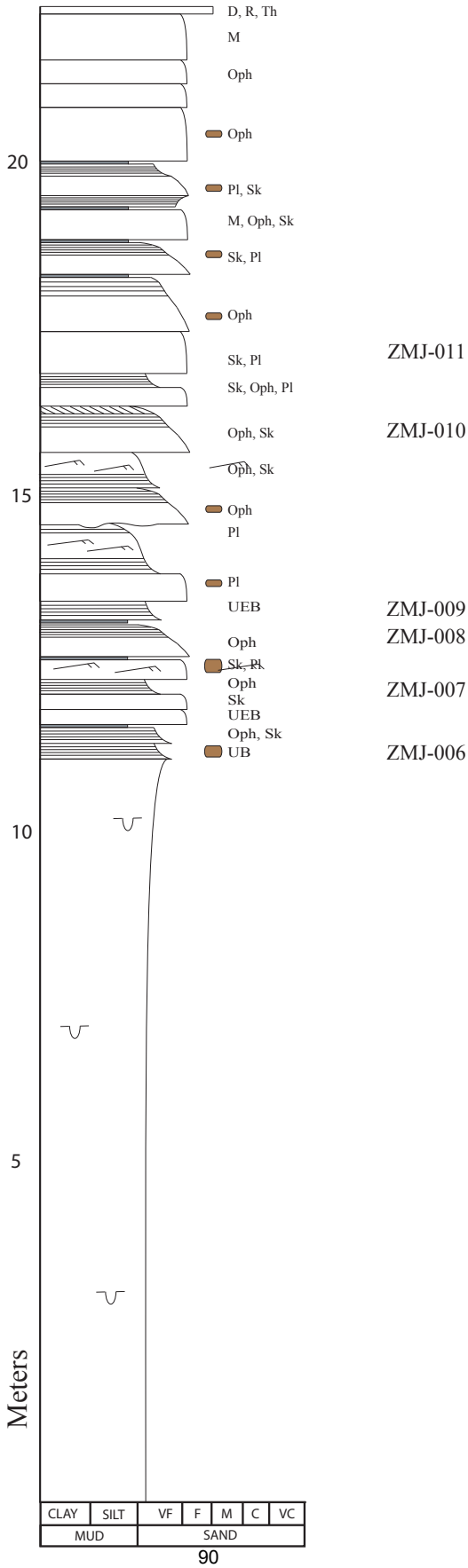

Figure A4. Stratigraphic section #3.

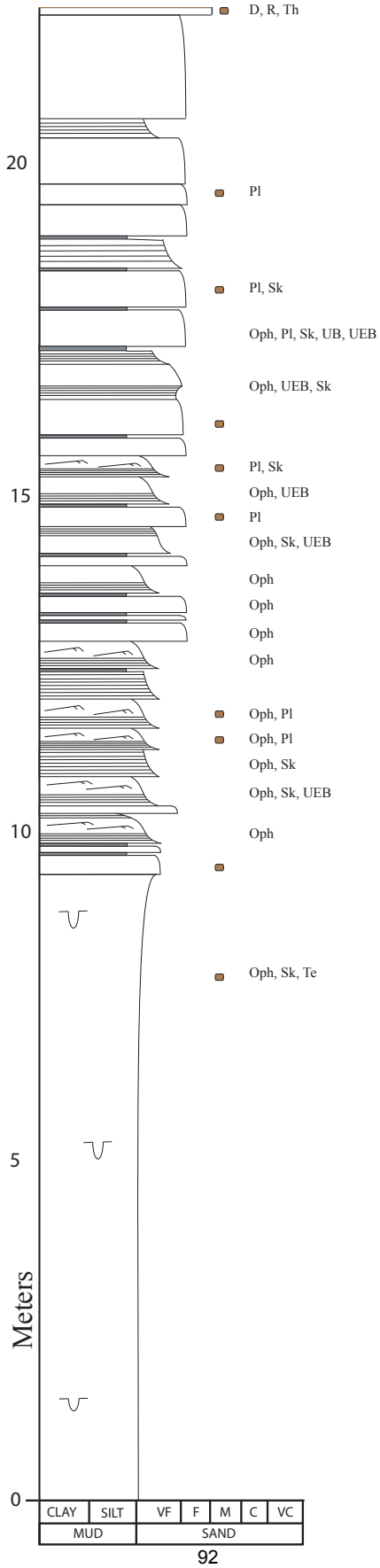

Figure A5. Stratigraphic section #4.

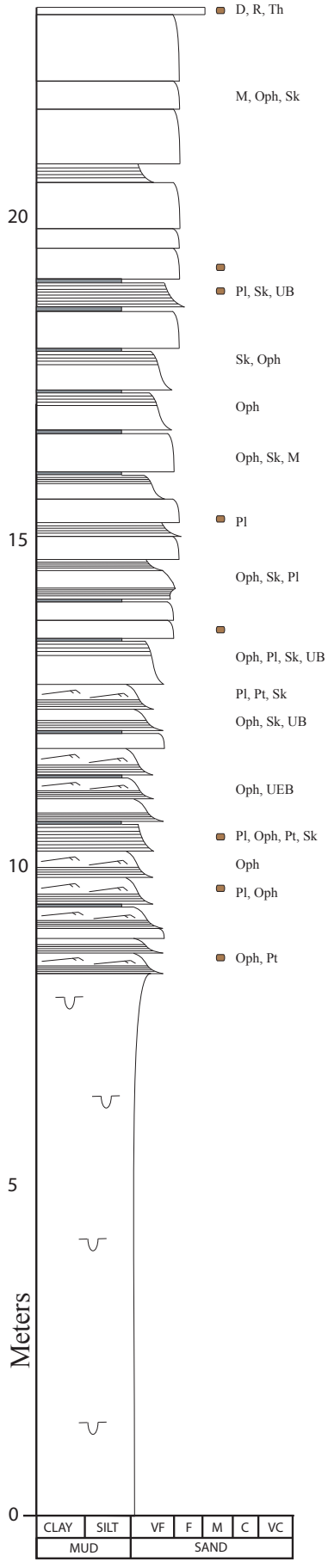

Figure A6. Stratigraphic section #5.

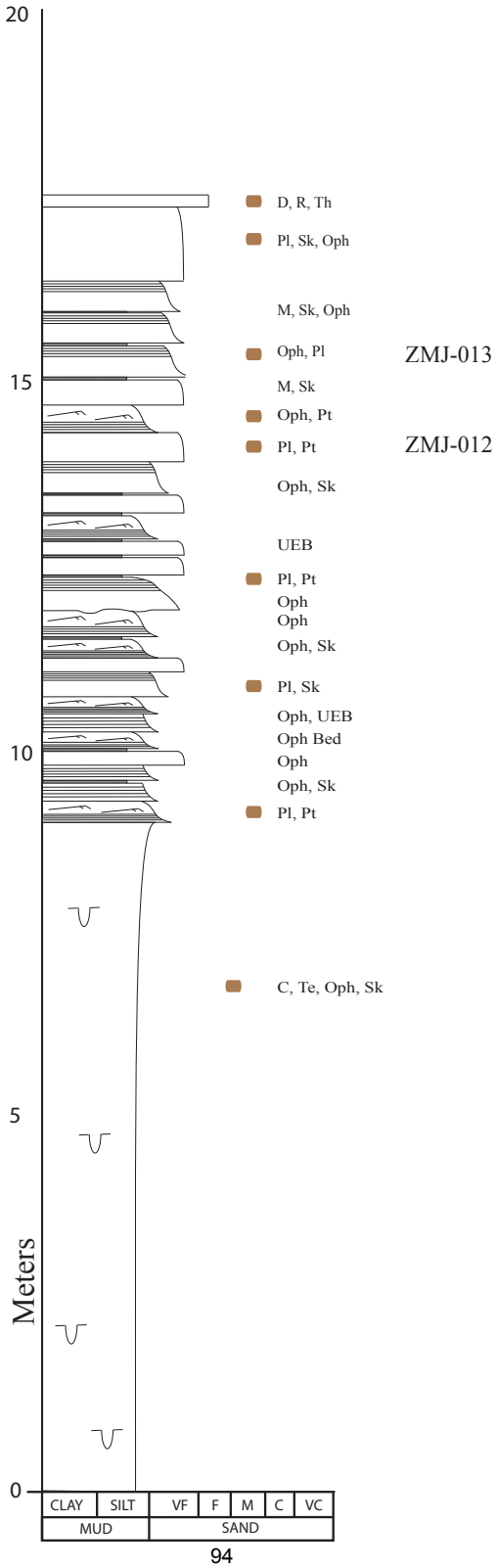

Figure A7. Stratigraphic section #6.

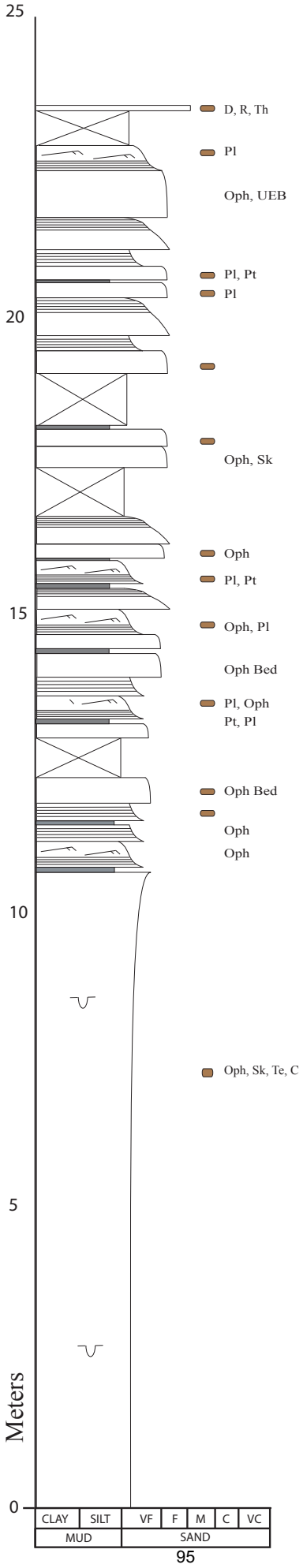

Figure A8. Stratigraphic section #7.

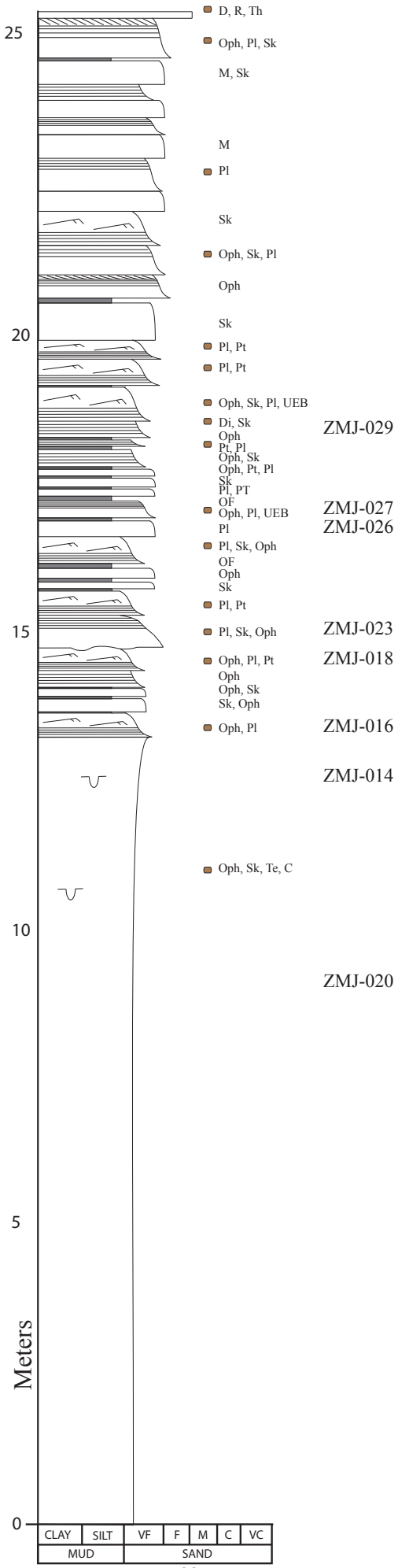

Figure A9. Stratigraphic section #8.

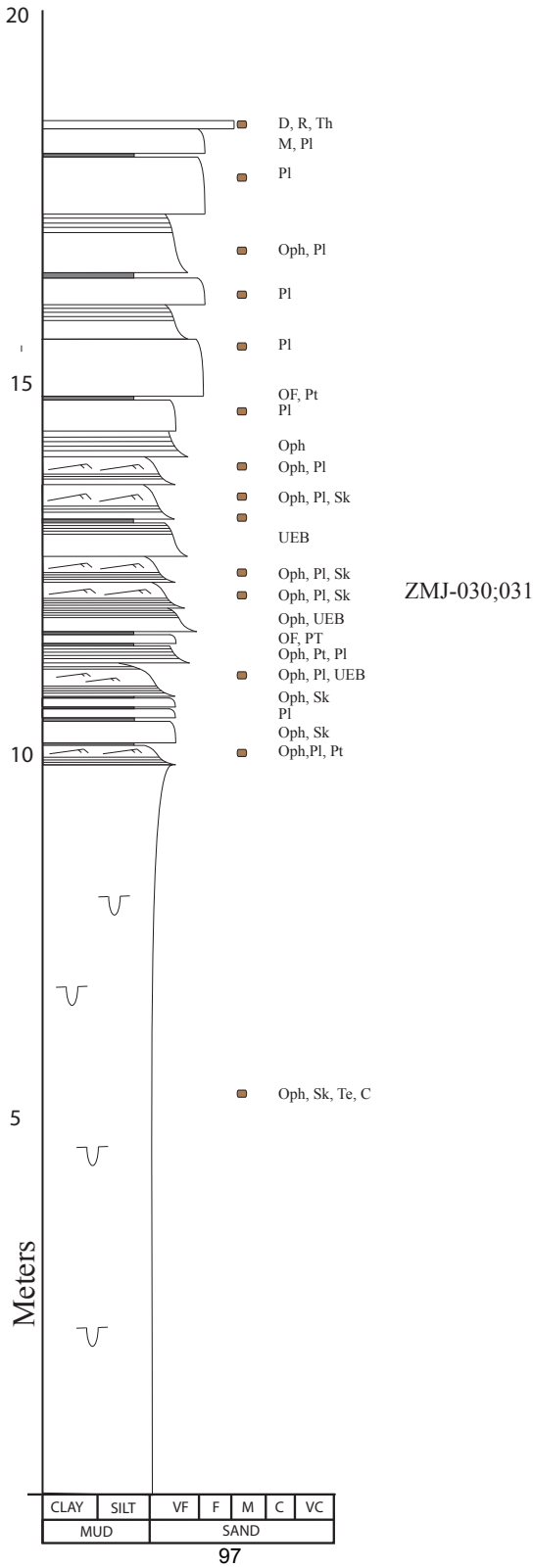

Figure A10. Stratigraphic section #9.

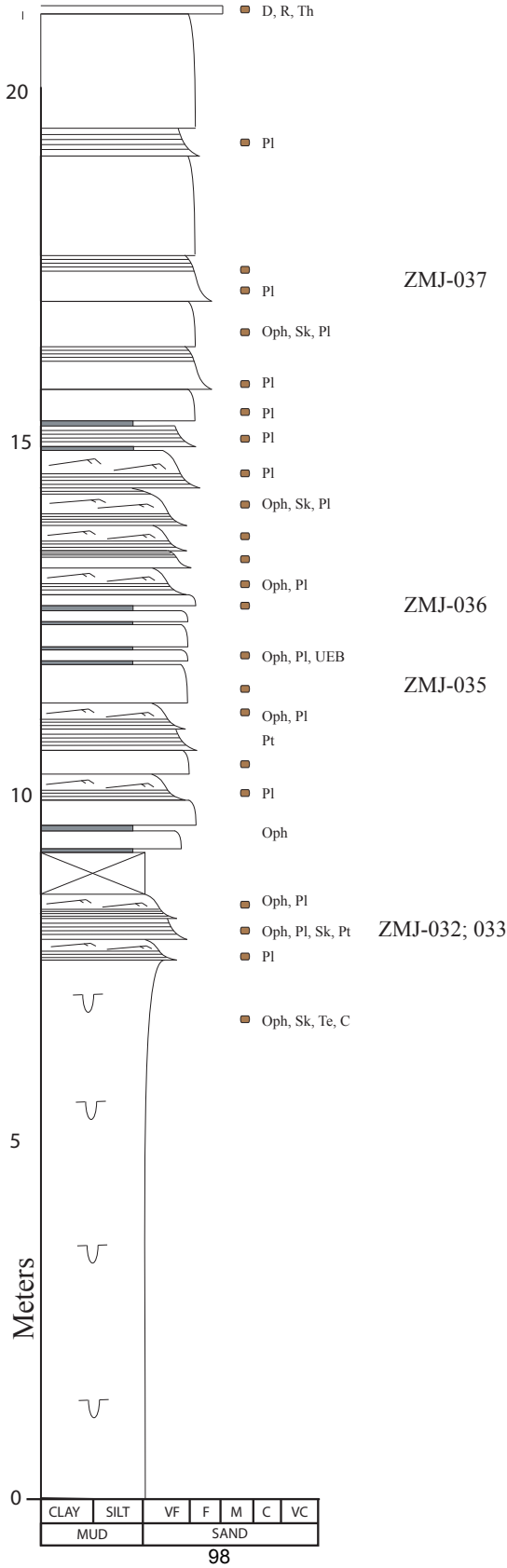

Figure A11. Stratigraphic section #10.

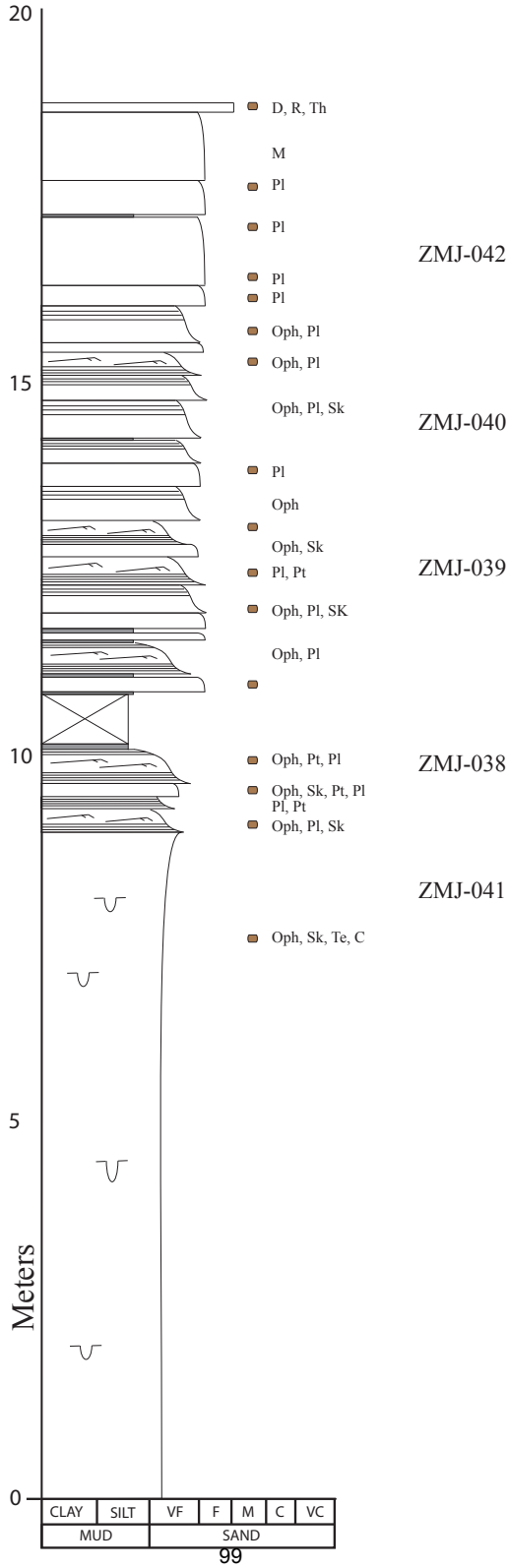

Figure A12. Stratigraphic section #11.

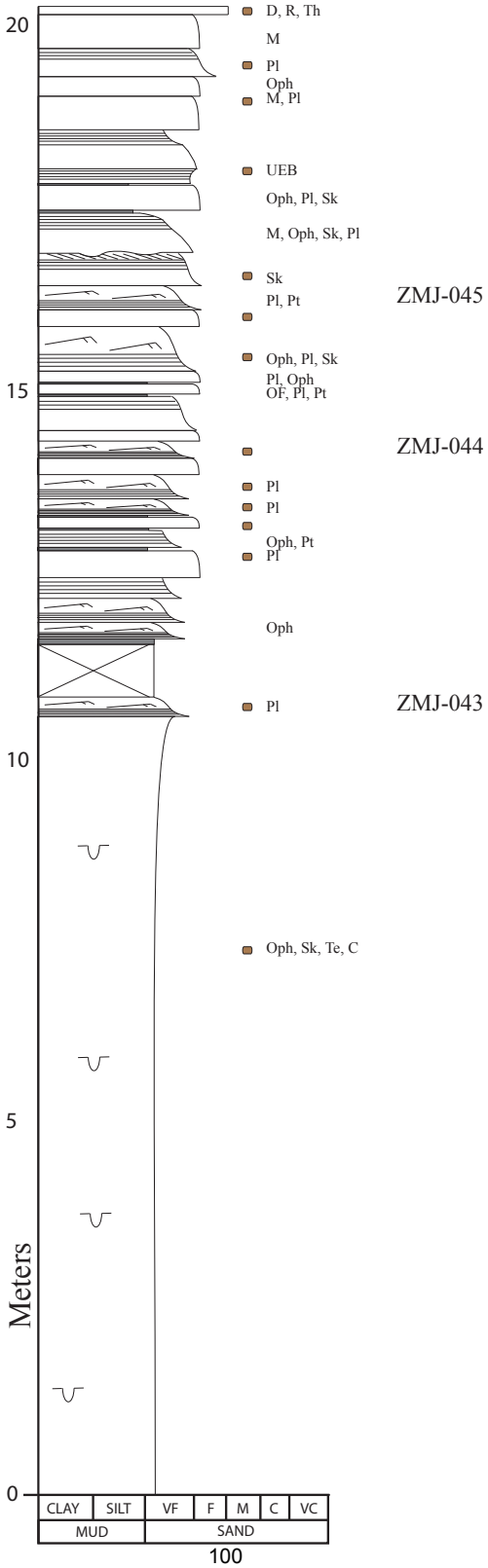

Figure A13. Stratigraphic section #12.

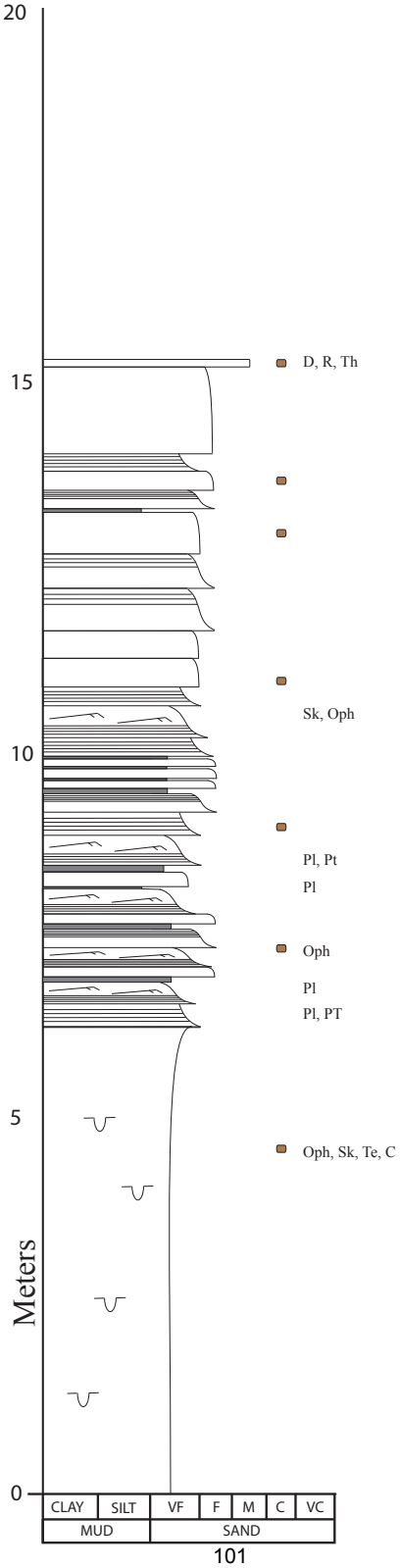

Figure A14. Stratigraphic section #13.

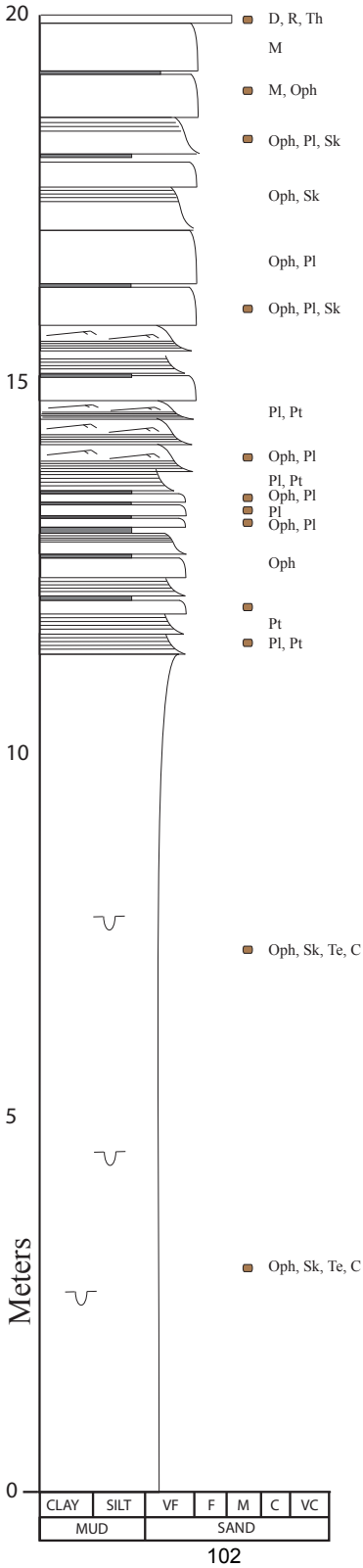

Figure A15. Stratigraphic section #14.
This stratigraphic section only reflects estimated grain size (based on observations at other section locations and weathering profiles) and bedding thicknesses, due to vertical cliff exposures preventing access. Bedding thickness was section was measured by dropping a rope with meter and 1/2 meter intervals marked over a vertical cliff, and documenting bed thickness relative to the markings.

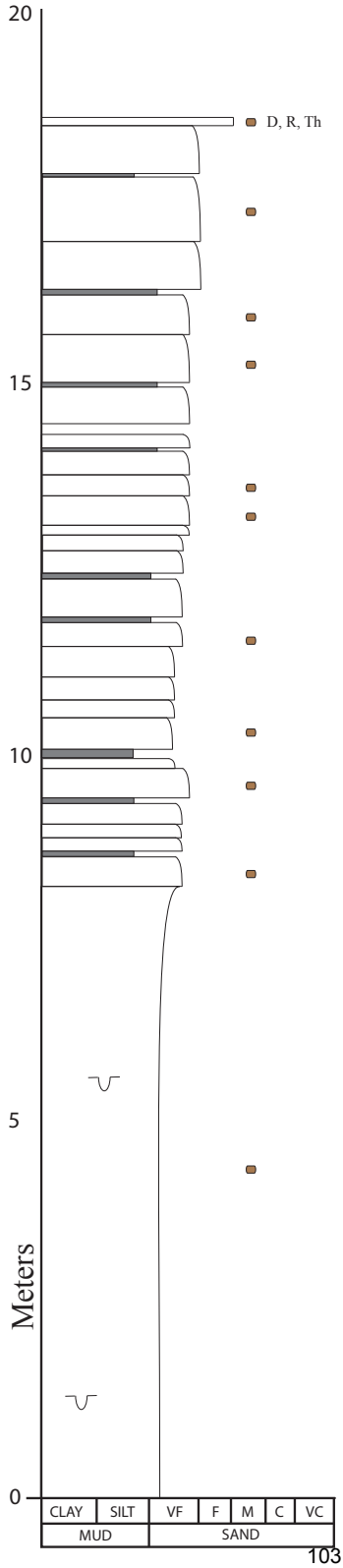

Figure A16. Stratigraphic section #15.
This stratigraphic section only reflects estimated grain size (based on observations at other section locations and weathering profiles) and bedding thicknesses, due to vertical cliff exposures preventing access. Bedding thickness was section was measured by dropping a rope with meter and 1/2 meter intervals marked over a vertical cliff, and documenting bed thickness relative to the markings.

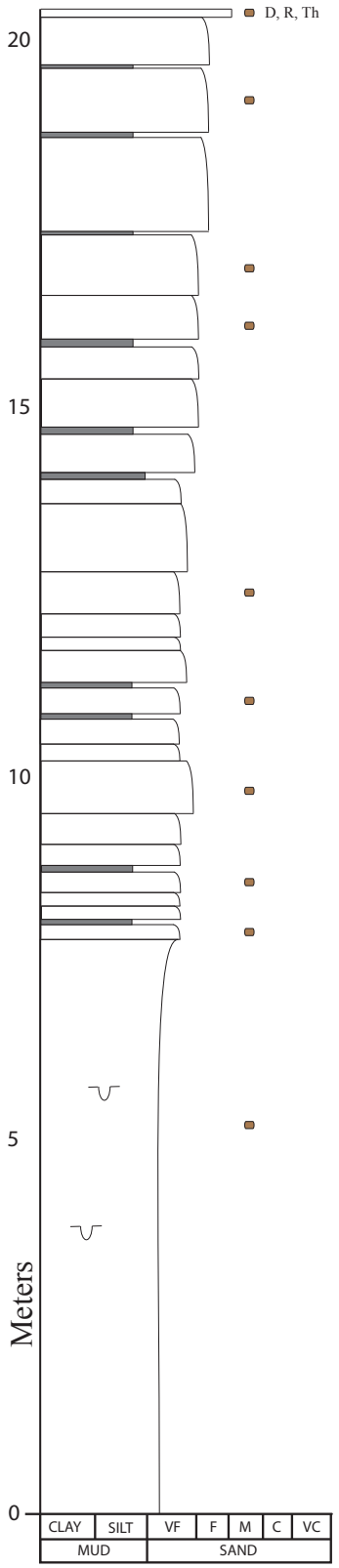

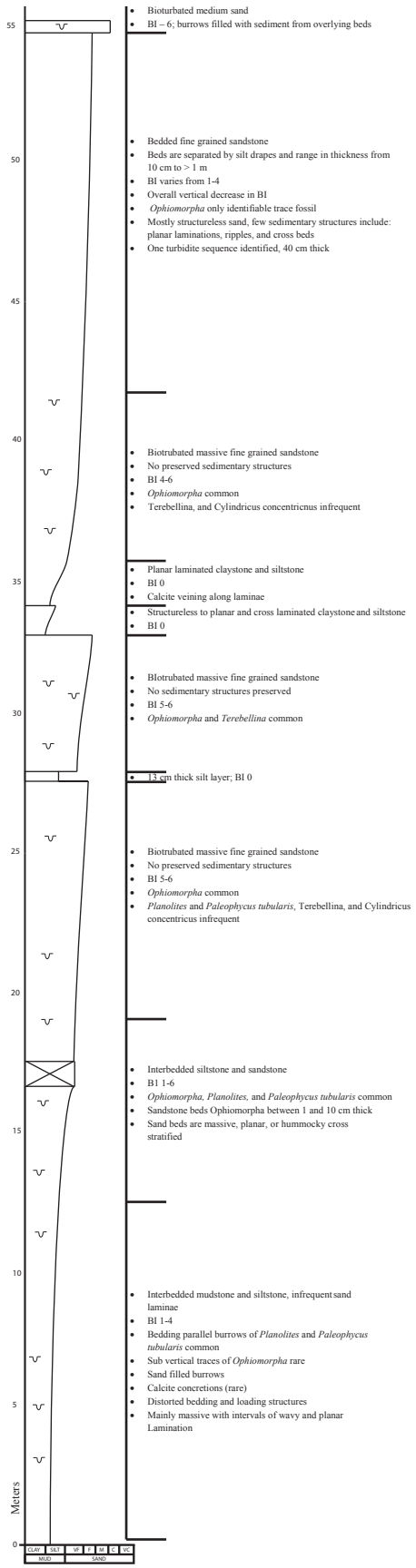

Figure A17. Stratigraphic section from core

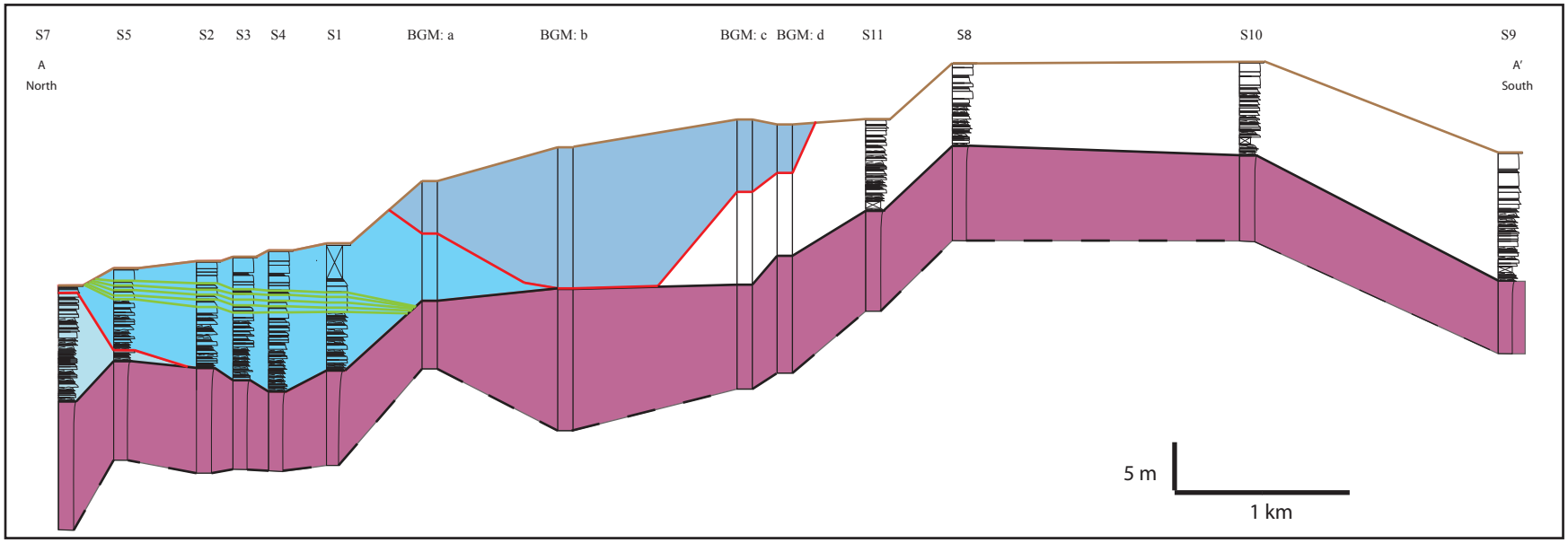

Figure A18. Correlation of stratigraphic sections #7, 5, 2, 3, 4, 1, 11, 8, 10, and 9, and bedding geometry measurments (BGM) a, b, c, and d along the N-S trending cliffs in Billings, MT. Note that regional dip is approximately 4 degrees to the NE; elevation of stratigraphic sections and BGM locations ins in meters; the black dashed line represents the approximate contact between the lower member of the Eagle Formation and underlying Telegraph Creek Formation (as marked by the first appearance of cliff forming sandstone above the Telegraph Creek Formation); the solid black line represents the Type 3 surface; red lines represent Type 1 surfaces; the brown line represent the Type 4 surface; and green lines represent correlations of individual beds between stratigraphic sections. The vertical scale only applies to measured sections and BGM's and not the elevation difference between the measurment locations. The elevation change between the sections has been reduced to 1/4 the original scale

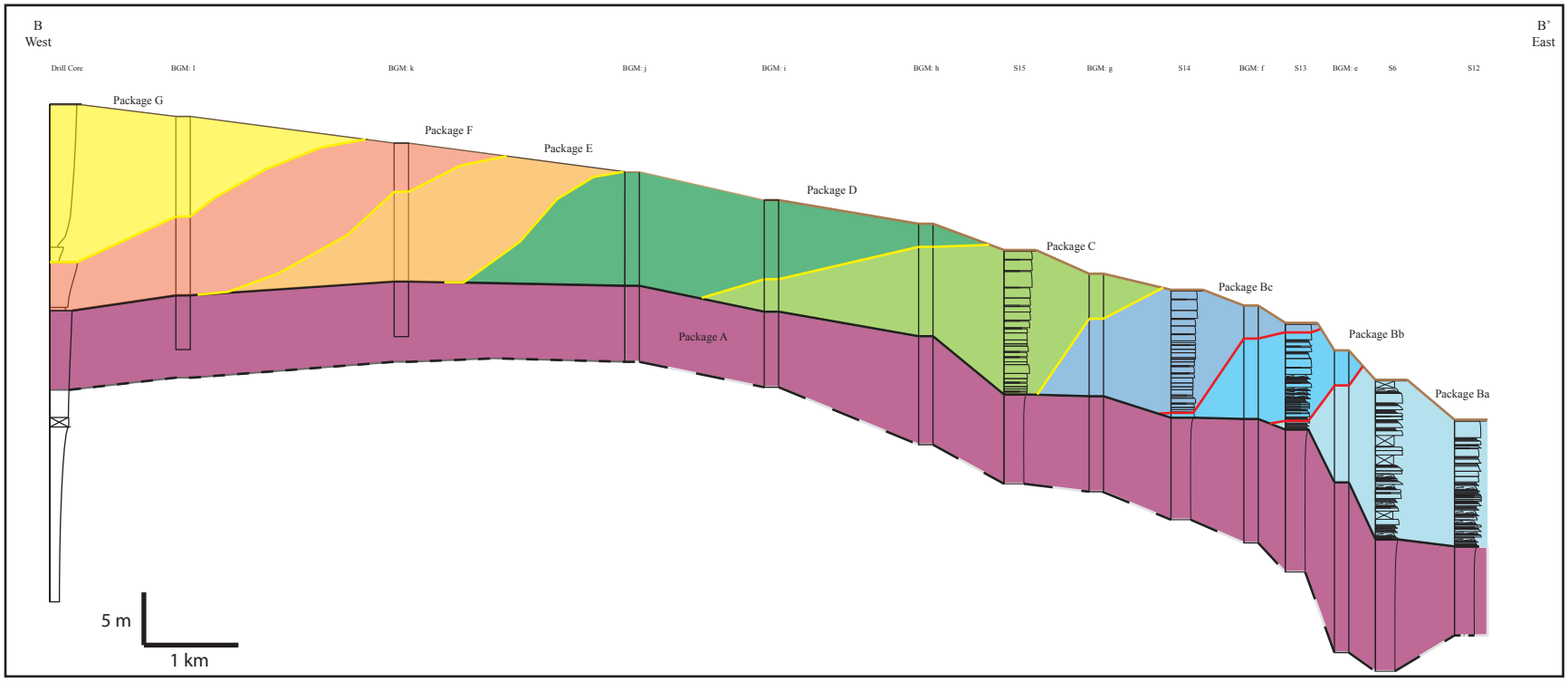

Figure A17. Correlation of stratigraphic sections (#15, 14, 13, 6, 12), the drill core section, and bedding geometry measurments (BGM: e, f, g, h, i, j, k, and l) along the E-W trending cliffs in Billings, MT. Note regional dip is approximately 4˚to the NE; elevation of sections and BGM locations is in meters; the black dashed line represents the approximate contact between Package A and F1 (as marked by the first appearance of cliff forming sandstone above the Telegraph Creek Formation); the solid black line represents the Type 3 surface; red lines represent Type 1 surfaces; yellow lines represent Type 2 surfaces; and the brown line represents the Type 4 surface. The vertical scale only applies to measured sections and BGM's and not to the elevation difference between the measurment locations. The elevation change between the sections has been reduced to 1/4 the original scale.

Appendix B – 3-Dimensional Data

Total Station Data

A Leica TC-307 robotic total station was used in this study to survey laterally continuous surfaces at 5 locations (Figure 1b), and enabled 3 dimensional data collection. The Leica TC-307 is capable of measuring x, y, z coordinates from a distance of 500 m with an accuracy of < 5mm (Lavine et al., 2003). A total of 282 x, y, z, coordinates were collected within an area of 60 km^2. The 5 tables below contain the x, y, z coordinates for the 5 surveys.

Survey #1 - Reference Point: 695302.383 5074456.277 949.456

Object ID	X	Y	Z
RRN001	694808.561	5074598.004	1022.514
RRN002	694818.884	5074597.94	1022.081
RRN003	694827.949	5074597.498	1021.764
RRN004	694827.858	5074597.234	1021.768
RRN005	694838.258	5074596.669	1021.288
RRN006	694843.418	5074596.557	1021.108
RRN007	694857.908	5074595.67	1020.521
RRN008	694862.631	5074595.487	1020.299
RRN009	694880.047	5074594.434	1019.743
RRN010	694888.46	5074595.567	1019.277
RRN011	694902.132	5074596.169	1018.858
RRN012	694917.676	5074597.568	1018.195
RRN013	694924.233	5074595.955	1017.945
RRN014	694933.609	5074595.566	1017.535
RRN015	694946.975	5074595.059	1017.051
RRN016	694962.711	5074594.308	1016.589
RRN017	694972.795	5074594.091	1016.191
RRN018	694984.867	5074593.399	1015.709
RRN019	694987.664	5074593.882	1015.62
RRN020	694992.482	5074590.901	1015.434
RRN021	695001.103	5074590.37	1015.178
RRN022	695011.812	5074588.18	1014.73
RRN023	695016.17	5074587.116	1014.5
RRN024	695022.39	5074588.552	1014.183
RRN025	695028.203	5074590.881	1013.897
RRN026	695044.981	5074592.682	1013.028
RRN027	695062.927	5074591.426	1012.28
RRN028	695079.414	5074592.202	1011.82
RRN029	695092.787	5074592.345	1011.31
RRN030	695099.504	5074594.078	1011.078
RRN031	695103.868	5074592.406	1010.92

RRN032	695116.065	5074594.665	1010.42
RRN033	695149.041	5074597.974	1009.189
RRN034	695153.503	5074599.705	1009.134
RRN035	695157.005	5074597.521	1008.879
RRN036	695176.363	5074592.17	1008.321
RRN037	695182.04	5074590.461	1008.044
RRN038	695185.041	5074590.54	1007.941
RRN039	695216.96	5074596.375	1006.524
RRN040	695226.709	5074596.942	1006.109
RRN041	695227.812	5074598.185	1006.089
RRN042	695234.019	5074602.481	1005.828
RRN043	695241.847	5074601.299	1005.295
RRN044	695252.713	5074603.518	1004.84
RRN045	695264.772	5074610.225	1004.363
RRN046	695268.64	5074612.211	1004.206
RRN047	695278.318	5074613.721	1003.704
RRN048	695283.457	5074615.849	1003.41
RRN049	695306.944	5074630.342	1002.129
RRN050	695321.153	5074633.323	1001.451
RRN051	695330.865	5074638.747	1001.07
RRN052	695337.452	5074639.039	1000.79
RRN053	695343.663	5074644.069	1000.475
RRN054	695349.252	5074645.129	1000.007
RRN055	695362.261	5074653.446	999.564
RRN056	695369.517	5074652.719	999.107
RRN057	695377.678	5074655.849	998.818
RRN058	695383.893	5074661.063	998.476
RRN059	695389.644	5074661.087	998.187
RRN060	695394.305	5074665.294	997.957
RRN061	695403.588	5074667.165	997.478
RRN062	695414.019	5074671.123	996.9
RRN063	695418.85	5074675.49	996.794
RRN064	695424.66	5074676.855	996.551
RRN065	695429.149	5074673.917	996.318
RRN066	695438.236	5074677.586	995.789
RRN067	695455.874	5074689.016	995.102
RRN068	695443.173	5074679.034	995.623
RRN069	695466.429	5074694.45	994.552
RRN070	695479.438	5074704.249	993.722
RRN071	695483.008	5074708.677	993.575
RRN072	695489.933	5074713.297	993.221
RRN073	695499.121	5074718.733	992.738
RRN074	695518.246	5074727.941	991.609
RRN075	695521.813	5074732.422	991.267

RRN076	695525.788	5074734.445	990.904
RRN077	695553.674	5074758.714	989.458
RRN078	695564.062	5074759.527	988.735
RRN079	695570.258	5074762.528	988.734
RRN080	695580.784	5074766.91	988.06
RRN081	695601.082	5074782.658	986.926
RRN082	695606.041	5074782.278	986.452
RRN083	695607.16	5074787.234	986.759
RRN084	695614.866	5074790.272	986.291
RRN085	695620.907	5074795.239	986
RRN086	695624.547	5074797.143	985.781
RRN087	695633.496	5074805.058	985.32
RRN088	695637.587	5074808.209	985.083

Survey #2 - Reference Point: 696477.817 5073659.645 993.872

Object ID	X	Y	Z
SS2001	696441.187	5073235.349	1011.448
SS2002	696442.479	5073233.422	1011.328
SS2003	696449.418	5073238.7	1011
SS2004	696464.147	5073239.012	1010.386
SS2005	696478.078	5073240.332	1009.741
SS2006	696500.549	5073234.13	1009.354
SS2007	696520.766	5073231.165	1008.662
SS2008	696529.14	5073227.471	1008.672
SS2009	696535.047	5073229.772	1009.339
SS2010	696550.983	5073222.079	1007.883
SS2011	696566.221	5073215.918	1007.659
SS2012	696577.416	5073216.355	1007.262
SS2013	696601.903	5073205.9	1006.429
SS2014	696606.583	5073203.342	1006.422
SS2015	696614.726	5073201.293	1006.191
SS2016	696615.61	5073201.15	1006.189
SS2017	696620.6	5073201.635	1006.329
SS2018	696622.241	5073198.496	1006.033
SS2019	696623.61	5073189.53	1006.128
SS2020	696633.277	5073191.406	1006.012
SS2021	696631.928	5073177.177	1006.941
SS2022	696615.983	5073180.922	1007.263
SS2023	696619.907	5073167.307	1007.736
SS2024	696608.267	5073165.181	1008.244
SS2025	696611.426	5073153.181	1008.586
SS2026	696620.43	5073147.271	1008.504
SS2027	696614.807	5073138.432	1008.987
SS2028	696617.63	5073133.314	1009.085
SS2029	696614.244	5073130.024	1009.35
SS2030	696616.269	5073120.24	1009.546
SS2031	696613.352	5073111.333	1009.995
SS2032	696614.687	5073100.994	1010.484
SS2033	696612.359	5073089.859	1010.944
SS2034	696615.821	5073080.14	1011.266
SS2035	696612.347	5073074.857	1011.575
SS2036	696619.289	5073066.572	1011.75
SS2037	696610.188	5073060.806	1012.202

SS2038	696627.753	5073051.086	1012.162
SS2039	696628.375	5073041.038	1012.513
SS2040	696637.957	5073022.327	1013.063
SS2041	696645.413	5073014.202	1012.912
SS2042	696649.101	5073009.299	1012.943
SS2043	696651.48	5072999.44	1013.003
SS2044	696669.136	5072985.881	1013.325
SS2045	696673.742	5072976.19	1013.558
SS2046	696685.377	5072967.694	1013.398
SS2048	696502.451	5073022.22	1017.069
SS2049	696508.084	5073031.05	1006.254
SS2start	696441.386	5073234.728	1011.29

Survey #3 - Reference Point: 697463.322 5071263.892 1071.653

Object ID	X	Y	Z
YYR001	697281.381	5071506.61	1065.511
YYR002	697286.251	5071508.005	1065.272
YYR003	697288.799	5071506.636	1065.224
YYR004	697294.145	5071508.435	1065.009
YYR005	697297.804	5071505.003	1064.938
YYR006	697301.41	5071506.867	1064.751
YYR007	697311.778	5071504.795	1064.622
YYR008	697319.723	5071508.822	1064.283
YYR009	697326.132	5071506.638	1064.246
YYR010	697341.143	5071505.073	1063.907
YYR011	697358.136	5071503.095	1063.393
YYR012	697367.209	5071503.829	1062.949
YYR013	697370.034	5071506.318	1062.776
YYR014	697377.592	5071509.093	1062.347
YYR015	697383.669	5071512.142	1061.92
YYR016	697364.924	5071503.069	1063.019
YYR017	697417.287	5071434.172	1064.851
YYR018	697418.988	5071429.311	1065.116
YYR019	697427.585	5071410.561	1065.941
YYR020	697427.315	5071407.246	1065.971
YYR021	697431.229	5071402.262	1066.247
YYR022	697433.019	5071397.241	1066.389
YYR023	697434.095	5071394.979	1066.392
YYR024	697451.718	5071378.895	1066.866
YYR025	697453.626	5071370.814	1067.011
YYR026	697458.027	5071370.42	1066.972
YYR027	697457.873	5071365.003	1066.967
YYR028	697483.432	5071369.313	1066.375
YYR029	697483.511	5071369.247	1066.385
YYR030	697476.313	5071346.257	1067.426
YYR031	697478.27	5071347.076	1067.478
YYR032	697471.473	5071312.694	1069.393
YYR033	697471.665	5071310.363	1069.566
YYR034	697470.109	5071299.816	1070.088
YYR035	697478.503	5071293.653	1070.207
YYR036	697475.013	5071285.927	1070.706
YYR037	697469.58	5071278.018	1071.096
YYR038	697482.411	5071275.093	1071.106
YYR039	697480	5071269.671	1071.433
YYR040	697474.524	5071265.007	1071.748
YYR041	697469.695	5071261.263	1072.003
YYR042	697477.456	5071256.732	1072.14
YYR043	697487.34	5071255.96	1072.012
YYR044	697487.511	5071249.425	1072.3

YYR045	697499.057	5071241.19	1072.453
YYR046	697495.924	5071216.162	1073.615
YYR047	697469.498	5071226.945	1073.693
YYR048	697444.887	5071225.334	1074.557
YYR049	697416.994	5071218.665	1075.917
YYRstart	697463.322	5071263.892	1071.653

Survey #4 - Reference Point: 699459.680 5069048.743 1053.378

Object ID	X	Y	Z
TICK001	699522.291	5068959.284	1056.42
TICK002	699509.722	5068972.316	1056.512
TICK003	699504.165	5068973.58	1056.668
TICK004	699500.212	5068975.802	1056.589
TICK005	699503.39	5068985.861	1056.036
TICK006	699495.08	5068998.075	1055.649
TICK007	699495.055	5068988.749	1056.173
TICK008	699504.502	5068998.727	1055.271
TICK009	699508.843	5069003.11	1054.839
TICK010	699509.723	5069009.357	1054.478
TICK011	699504.467	5069012.249	1054.511
TICK012	699500.125	5069016.433	1054.524
TICK013	699495.798	5069023.221	1054.235
TICK014	699500.223	5069031.969	1053.648
TICK015	699496.854	5069034.476	1053.671
TICK016	699497.538	5069049.902	1052.955
TICK017	699496.169	5069034.197	1053.697
TICK018	699495.808	5069059.817	1052.209
TICK019	699493.229	5069070.075	1051.719
TICK020	699483.116	5069083.51	1051.568
TICK021	699458.093	5069089.666	1052.854
TICK022	699437.05	5069113.446	1053.202
TICK023	699429.523	5069122.934	1053.074
TICK024	699422.015	5069131.903	1053.367
TICK025	699377.869	5069175.308	1054.068
TICK026	699367.648	5069182.803	1054.744
TICK027	699366.655	5069180.946	1054.742
TICK028	699356.038	5069189.502	1055.173
TICK029	699352.904	5069187.476	1055.301
TICK030	699349.595	5069192.832	1055.402
Tick Start	699459.68	5069048.743	1053.378

Survey #5 - Reference Point: 698492.013 5070006.822 1094.35

Object ID	X	Y	Z
BCR001	698468.983	5070006.49	1095.734
BCR002	698470.235	5070002.545	1095.845
BCR003	698475.527	5070005.716	1095.42
BCR004	698477.481	5070000.319	1095.489
BCR005	698483.116	5070002.672	1095.156
BCR006	698484.473	5069998.123	1095.263
BCR007	698489.978	5070008.844	1094.542
BCR008	698494.513	5070004.132	1094.491
BCR009	698498.696	5070003.844	1094.339
BCR010	698500.274	5070010.821	1093.969
BCR011	698507.349	5070010.303	1093.639
BCR012	698516.252	5070008.048	1093.389
BCR013	698517.398	5070013.414	1093.204
BCR014	698526.333	5070012.544	1092.796
BCR015	698526.157	5070017.452	1092.688
BCR016	698540.561	5070021.867	1091.787
BCR017	698550.727	5070023.398	1091.291
BCR018	698580.374	5070030.299	1089.77
BCR019	698589.468	5070030.532	1089.34
BCR020	698597.437	5070030.126	1089.012
BCR021	698607.767	5070029.905	1088.477
BCR022	698618.45	5070028.946	1088.155
BCR023	698626.384	5070029.077	1087.753
BCR024	698631.27	5070029.777	1087.541
BCR025	698638.627	5070030.935	1087.065
BCR026	698646.869	5070028.878	1086.62
BCR027	698663.127	5070031.311	1085.833
BCR028	698662.368	5070021.516	1086.252
BCR029	698663.672	5070015.93	1086.594
BCR030	698659.952	5070013.627	1086.622
BCR031	698659.377	5070002.024	1086.859
BCR032	698664.962	5069998.133	1087.139
BCR033	698664.641	5069991.652	1087.057
BCR034	698671.654	5069988.027	1087.276
BCR035	698674.966	5069978.212	1086.95
BCR036	698680.452	5069974.963	1087.343
BCR037	698679.929	5069968.041	1087.301
BCR038	698687.95	5069961.132	1087.565
BCR039	698691.824	5069952.984	1087.634
BCR040	698697.531	5069943.829	1087.74
BCR041	698701.398	5069931.789	1087.799

BCR042	698705.564	5069925.856	1087.952
BCR043	698706.744	5069916.739	1088.137
BCR044	698712.021	5069906.434	1088.305
BCR045	698717.349	5069892.234	1088.462
BCR046	698720.676	5069881.893	1088.738
BCR047	698730.308	5069866.507	1088.825
BCR048	698735.844	5069850.425	1089.084
BCR049	698733.219	5069831	1090.058
BCR050	698722.068	5069815.898	1091.275
BCR051	698726.193	5069809.527	1091.194
BCR052	698715.851	5069804.926	1092.005
BCR053	698724.907	5069801.169	1091.587
BCR054	698728.556	5069787.753	1091.832
BCR055	698718.179	5069771.905	1092.797
BCR056	698721.974	5069764.222	1093.016
BCR057	698706.561	5069746.589	1094.416
BCR058	698714.049	5069732.439	1094.293
BCR059	698717.068	5069728.899	1094.451
BCR060	698712.286	5069725.753	1094.684
BCR061	698721.76	5069711.159	1095.054
BCR062	698709.074	5069709.234	1095.197
BCR063	698673.824	5069672.364	1095.834
BCR064	698677.197	5069649.795	1097.182
BCRstart	698492.013	5070006.822	1094.35

Stratigraphic Sections GPS Points:

GPS points were recorded at the top of each stratigraphic with a Trimble TSC1 Asset Surveyor. The top of each stratigraphic section was marked by the Type 3 surface. The numbered locations of each stratigraphic section on Figure A1 in Appendix A, correspond to the stratigraphic section number in the following table.

Stratigraphic Section	X	Y	Z
1	696509.213	5073042.32	957.14
2	696614.726	5073201.293	1006.191
3	696616.269	5073120.24	1009.546
4	696612.359	5073089.859	1010.944
5	696420.482	5073469.312	1002.79
6	695666.762	5074908.619	981.171
7	696477.817	5073659.645	993.872
8	697609	5071060	1085.6976
9	699308.668	5069543.239	1048.251
10	698659.952	5070013.627	1086.622
11	698663.672	5070015.93	1086.594
12	696165.1	5074874.26	959
13	695466.429	5074694.45	994.552
14	695185.041	5074590.54	1007.941
15	694843.418	5074596.557	1021.108

Appendix C: Dip Correction for Bedding and Surface Dip Measurments

Outcrops of the Eagle Formation in south-central Montana wrap around the Pryor Mountains and in the study area exhibit an approximate 4° dip to the northeast awa from the Pryor Mountains (GIll and Cobban, 1973; Olson and Smith, 2007). In the study area, the MRS (Type 3 surface) is interpreted to have formed on a slope with a dip near horizonal, and its current dip is interpreted to reflect the structural dip in the study area. Thus, the MRS is here used to reconstruct structural dip. The azimuth and dip for the MRS, bedding planes, and laterally continuous surface were imported into Stereonet7 and projected as planes. The calculation "Angle Between Selected Planes" was performed to determine the angle (in degrees) between the structural dip plane (MRS: 345, 004) and each bedding plane and laterally continuous surface. The calculated angle indicates the degree to which each bedding and surface plane needs to be modified by to correct for structural dip.

Measurment Type	Regional Azimuth	Regional Dip (degrees)	Measured Azimuth	Measured Dip (degrees)	Calculated Angle Between Regional Dip Plane and Measured Dip Plane (degrees)	Dip of Plane After Correction (degrees)
Type 3 Surface (Average of 15 Measurments)	345	4	345	4	0	0
Bedding Plane	345	4	130	1	4.9	5.9
Bedding Plane	345	4	131	0.5	4.4	4.9
Type 1 Surface	345	4	120	1	4.8	5.8
Bedding Plane	345	4	128	1	4.8	5.8
Bedding Plane	345	4	125	1	4.8	5.8
Bedding Plane	345	4	143	1	4.9	5.9
Bedding Plane	345	4	170	0.5	4.5	5
Bedding Plane	345	4	160	1	5	6
Bedding Plane	345	4	143	1	4.9	5.9
Bedding Plane	345	4	122	1	4.8	5.8
Type 1 Surface	345	4	121	0.5	4.4	4.9
Bedding Plane	345	4	100	0.5	4.2	4.7
Bedding Plane	345	4	110	1	4.6	5.6
Bedding Plane	345	4	111	1	4.7	5.7
Type 2 Surface	345	4	110	1	4.6	5.6
Bedding Plane	345	4	130	1	4.9	5.9
Bedding Plane	345	4	113	0.5	4.3	4.8
Bedding Plane	345	4	165	1	5	6
Bedding Plane	345	4	140	1	4.9	5.9
Bedding Plane	345	4	141	1	4.9	5.9
Type 1 Surface	345	4	145	0.5	4.5	5
Bedding Plane	345	4	123	1	4.8	5.8
Bedding Plane	345	4	122	1	4.8	5.8
Bedding Plane	345	4	150	0.5	4.5	5

Bedding Plane	345	4	140	1	4.9	5.9
Bedding Plane	345	4	144	1	4.9	5.9
Bedding Plane	345	4	112	1	4.7	5.7
Bedding Plane	345	4	150	1	5	6
Type 1 Surface	345	4	132	0.5	4.4	4.9
Bedding Plane	345	4	131	1	4.9	5.9
Bedding Plane	345	4	128	1	4.8	5.8
Bedding Plane	345	4	136	0.5	4.4	4.9
Type 2 Surface	345	4	131	1	4.9	5.9
Bedding Plane	345	4	135	1	4.9	5.9
Bedding Plane	345	4	155	1	5	6
Bedding Plane	345	4	111	1	4.7	5.7
Bedding Plane	345	4	110	0.5	4.3	4.8
Bedding Plane	345	4	125	0.5	4.4	4.9
Bedding Plane	345	4	140	0.5	4.5	5
Type 1 Surface	345	4	139	1	4.9	5.9
Bedding Plane	345	4	138	1	4.9	5.9
Bedding Plane	345	4	110	1	4.6	5.6
Bedding Plane	345	4	122	1	4.8	5.8
Bedding Plane	345	4	133	1	4.9	5.9
Bedding Plane	345	4	136	1	4.9	5.9
Bedding Plane	345	4	126	1	4.8	5.8
Bedding Plane	345	4	138	1	4.9	5.9
Bedding Plane	345	4	115	0.5	4.3	4.8
Bedding Plane	345	4	125	1	4.8	5.8
Bedding Plane	345	4	126	1	4.8	5.8
Bedding Plane	345	4	131	0.5	4.4	4.9
Ophiomorpha Bed	345	4	349	4	0.3	0.3
Ophiomorpha Bed	345	4	340	4	0.3	0.3
Ophiomorpha Bed	345	4	348	4	0.2	0.2
Ophiomorpha Bed	345	4	341	4	0.3	0.3
Ophiomorpha Bed	345	4	340	4	0.3	0.3
Ophiomorpha Bed	345	4	338	4	0.5	0.5
Ophiomorpha Bed	345	4	347	4	0.1	0.1
Ophiomorpha Bed	345	4	335	4	0.3	0.3
Ophiomorpha Bed	345	4	339	4	0.4	0.4

Ophiomorpha Bed	345	4	338	4	0.5	0.5
Type 4 Surface (Average of 25 Measurments)	345	4	340	4	0.3	0.3

Appendix D - Petrographic Data

Thin Sections were processed from hand samples collected at stratigraphic sections within the study area. Samples were pre-processed into billets before sending to Spectrum Petrographics Inc. for processing.

D1 - Point count data for 35 samples from facies 2, 4, & 5 in the lower member of the Eagle Formation. A minimum of 500 grains were counted on each slide and all samples were point-counted using the Gazzi (1966)-Dickinson (1970) method. Represented in table B are the calculated QFL modal percentages for each point count by facies type and the mean and standard deviations (2σ) from the normalized components within each facies. Figure C is a ternary diagram plot of the QFL compositional data for each sample by facies type (where ○ represents F2, ● F4, and ● F5), and average QFL composition (black circles) and standard deviations for each facies type (polygons).

(A)

Thin Section #	Strat Section #	Qm	Qp	cht	plag	k-spar	Clay	bt	ms	glauc	lv	ls	lm	lu	Organic	Calcite	Other	Silt	Pores	Cement	Total Grains	Total Counts
Facies 2																						
Zmj-001	1	201	5	0	85	21	20	4	5	5	0	37	64	0	0	40	16	69	101	0	523	693
Zmj-002	1	192	16	6	90	24	18	12	4	6	0	28	66	0	0	30	36	54	114	6	510	702
zmj-005	1	254	15	1	56	46	18	3	1	2	1	6	102	0	0	17	0	7	124	0	504	635
zmj-014	7	230	6	0	69	14	17	11	0	1	0	0	155	0	1	15	0	11	18	15	501	545
zmj-020	7	242	3	0	77	10	1	2	0	0	0	0	148	0	0	18	0	5	37	6	500	548
zmj-041	10	251	19	2	60	58	20	2	1	1	0	2	100	0	0	11	3	9	165	0	510	684
Facies 4																						
Zmj-004	1	224	5	4	70	12	0	4	0	11	0	21	40	0	0	12	12	17	54	25	511	607
zmj-006	2	245	26	0	58	60	12	4	2	0	0	2	98	1	0	4	0	8	141	16	500	665
zmj-007	2	279	9	1	55	43	23	6	3	2	1	6	88	0	0	12	0	27	104	0	505	636
zmj-009	2	293	21	1	34	49	6	2	1	2	0	8	89	0	0	0	0	9	17	174	500	700
zmj-016	7	225	3	0	57	17	6	8	0	2	0	0	172	0	0	18	0	14	45	18	500	577
zmj-018	7	289	3	0	43	10	2	3	0	0	0	0	150	0	0	1	1	1	6	200	500	707
zmj-029	7	258	2	0	83	10	6	3	0	1	0	0	132	0	0	11	0	14	50	1	500	565
zmj-030	8	285	28	3	70	26	17	5	0	1	1	6	85	4	0	0	0	6	125	0	514	645
zmj-031	8	271	26	0	65	28	27	8	3	2	0	5	102	0	0	2	0	9	106	25	512	652
zmj-032	9	249	29	4	54	34	30	17	1	4	0	9	87	0	0	12	0	13	137	7	500	657
zmj-033	9	246	64	8	19	34	15	6	4	5	1	6	102	0	0	5	0	26	16	151	500	693
zmj-038	10	257	30	5	55	39	3	8	1	1	0	10	86	0	0	8	0	16	176	3	500	695
zmj-039	10	258	15	4	63	56	7	8	1	2	0	5	82	0	0	16	0	4	9	20	510	543
zmj-043	11	299	22	0	41	34	21	4	1	1	1	4	92	0	0	0	1	13	31	180	500	724
zmj-044	11	276	26	9	48	36	6	4	1	1	0	9	89	1	0	0	0	6	29	114	500	649
zmj-045	11	289	15	0	51	42	11	1	2	1	0	3	98	0	0	1	0	8	94	118	503	723
Facies 5																						
Zmj-003	1	279	18	5	86	18	0	5	0	10	0	22	49	0	0	14	27	22	45	81	533	681
zmj-008	2	304	24	2	46	35	25	5	1	2	0	14	70	0	0	0	1	11	23	144	504	682
zmj-010	2	302	20	1	51	43	20	6	1	2	0	6	68	0	0	0	0	2	47	170	500	719
zmj-011	2	282	22	4	53	43	13	2	1	1	0	10	73	0	0	9	0	11	129	6	500	646
zmj-012	5	298	16	4	48	43	3	10	6	8	0	12	45	0	0	9	1	11	49	142	500	702
zmj-013	5	309	20	5	53	34	5	8	2	3	1	10	53	0	0	1	1	10	34	114	500	658
zmj-023	7	282	2	0	58	12	0	1	0	2	0	0	143	0	0	1	1	5	1	166	500	672
zmj-026	7	224	1	0	61	10	5	5	0	1	0	0	185	0	0	13	1	8	39	3	500	550
zmj-027	7	287	25	7	51	50	8	10	3	5	1	8	49	0	0	4	0	5	110	20	500	635
zmj-035	9	290	40	6	48	35	14	11	3	4	0	3	58	0	0	2	0	14	72	167	500	753
zmj-036	9	326	32	1	47	22	7	2	1	0	0	3	65	0	0	1	0	8	73	119	500	700
zmj-037	9	282	48	3	45	28	10	4	0	4	0	6	79	0	0	1	0	3	26	192	500	721
zmj-040	10	272	21	6	37	54	11	3	1	4	0	6	76	1	0	21	1	4	115	8	503	630
zmj-042	10	302	13	0	56	47	15	6	1	2	1	3	69	0	0	0	0	15	53	147	500	715

(B)

Thin Section #	Q (norm)	F (norm)	L (norm)
Facies 2			
Zmj-001	49.88	25.67	24.45
zmj-002	52.51	24.50	22.99
zmj-005	56.13	21.21	22.66
zmj-014	54.30	23.60	22.10
zmj-020	51.04	18.13	30.83
zmj-041	55.29	23.98	20.73
Average %	53.19	22.85	23.96
STD - DEV	4.93	5.48	7.15

Thin Section #	Q (norm)	F (norm)	L (norm)
Facies 4			
Zmj-004	62.00	21.81	16.18
zmj-006	55.88	24.33	19.79
zmj-007	59.96	20.33	19.71
zmj-009	63.21	21.66	15.13
zmj-016	56.00	19.50	24.50
zmj-018	60.20	19.30	20.50
zmj-029	61.00	21.00	18.00
zmj-030	62.20	18.90	18.90
zmj-031	59.76	18.71	21.53
zmj-032	64.00	22.00	14.00
zmj-033	66.25	11.04	22.71
zmj-038	60.58	19.50	19.92
zmj-039	57.35	24.64	18.01
zmj-043	65.11	15.21	19.68
zmj-044	63.08	17.04	19.88
zmj-045	61.04	18.67	20.28
Average %	61.10	19.60	19.29
STD - DEV	5.96	6.66	5.32

Thin Section #	Q (norm)	F (norm)	L (norm)
Facies 5			
Zmj-003	63.35	21.79	14.86
zmj-008	66.67	16.36	16.97
zmj-010	65.78	19.14	15.07
zmj-011	64.19	20.34	15.47
zmj-012	68.87	17.94	13.20
zmj-013	68.24	19.53	12.23
zmj-023	64.50	19.00	16.50
zmj-026	63.00	21.00	16.00
zmj-027	66.42	21.27	12.31
zmj-035	70.59	17.44	11.97
zmj-036	72.38	13.91	13.71
zmj-037	68.10	14.93	16.97
zmj-040	63.35	19.28	17.37
zmj-042	64.15	20.98	14.87
Average %	66.40	18.78	14.82
STD - DEV	5.81	4.81	3.74

(C)

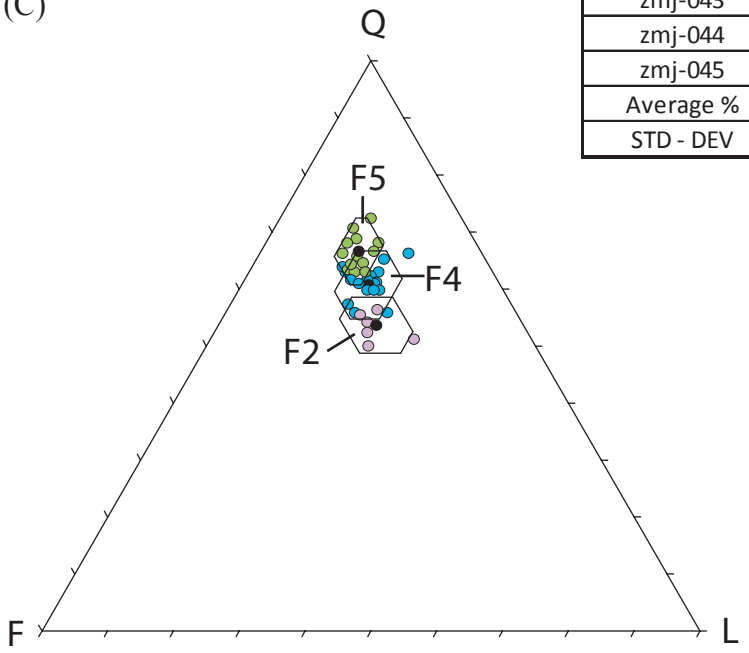

D2 - Table showing the average shape, degree of roundness, grain size, and sorting observed in the 35 thin section samples. Grain size and rounding measurments were taken from 100 grains per sample. Grain size was recorded in mm to the nearest 0.05 mm. Grain size classification was done according to Wentworth (1922) and grain roundness and grain shape was reported based on the the classification schemes discussed in Powers (1953). Grain shape catagories are: prolate (1), bladed (2), oblate (3), equant (4). Rounding: very angular (5), angular (4), sub-angular (3), sub-rounded (2), rounded (1), and well-rounded (0). Sorting was determined by calculating the standard deviation of grain size measurments within individual samples and classified following the guidelines of Folk (1974).

Thin Section #	Average Shape	Average Roundness	Average Grain Size (mm)	Average Grain Size (ϕ)	Grain Size Classification	Grain Size Standard Deviation	Sorting
Facies 2							
Zmj-001	2	3	0.1387	2.8503	FL	0.51	Mod. Well
Zmj-002	1	2	NA	NA	NA	0.48	Well
zmj-005	1	2	0.1629	2.6694	FL	0.38	Well
zmj-014	2	4	0.1539	2.6997	FL	0.44	Well
zmj-020	2	3	0.1554	2.6862	FL	0.38	Well
zmj-041	2	2	0.1582	2.6602	FL	0.45	Well
Facies 4							
Zmj-004	2	3	0.1907	2.3909	FU	0.47	Well
zmj-006	4	2	0.1541	2.775	FL	0.47	Well
zmj-007	3	2	0.1382	2.8547	FL	0.36	Well
zmj-009	4	3	0.1497	2.7400	FL	0.42	Well
zmj-016	2	3	0.1480	2.7568	FL	0.56	Mod. Well
zmj-018	2	4	0.1765	2.5024	FU	0.45	Well
zmj-029	2	3	0.1861	2.4260	FU	0.43	Well
zmj-030	4	2	0.1682	2.5718	FU	0.48	Well
zmj-031	4	2	0.1490	2.7466	FL	0.44	Well
zmj-032	1	2	0.1576	2.6657	FL	0.44	Well
zmj-033	2	2	0.1618	2.6277	FL	0.53	Mod. Well
zmj-038	4	2	0.1365	2.8730	FL	0.43	Well
zmj-039	2	2	0.1615	2.6304	FL	0.45	Well
zmj-043	2	3	0.1457	2.7785	FL	0.44	Well
zmj-044	2	2	0.1742	2.5214	FU	0.44	Well
zmj-045	1	2	0.1517	2.7210	FL	0.40	Well
Facies 5							
Zmj-003	2	4	0.1775	2.4943	FU	0.41	Well
zmj-008	2	2	0.1600	2.6437	FL	0.39	Well
zmj-010	2	3	0.1621	2.6254	FL	0.48	Well
zmj-011	4	2	0.1614	2.6311	FL	0.44	Well
zmj-012	4	3	0.1318	2.9236	FL	0.41	Well
zmj-013	1	2	0.1400	2.8365	FL	0.41	Well
zmj-023	2	3	0.1596	2.6478	FL	0.44	Well
zmj-026	2	3	0.1754	2.5115	FU	0.43	Well
zmj-027							
zmj-035	4	3	0.1624	2.692	FL	0.45	Well
zmj-036	4	3	0.1514	2.776	FL	0.40	Well
zmj-037	4	3	0.1365	2.925	FL	0.40	Well
zmj-040	3	2	0.1363	2.9163	FL	0.34	Well
zmj-042	1	3	0.1572	2.7245	FL	0.40	Well

D3 - Operator error analysis and point count data for sample zmj-013. Sample zmj-013 was point counted 10 times (A) in order to calculate operator counting error. for each normalized component (B). Operator error was determined by first calculating the QFL modal percentage for each count, followed by calculating the mean and standard deviation (2σ) from the normalized components. The standard deviation and operator error for each normalized component is Q - 4.4%, F - 2.7%, L - 3.5%. Figure (C) below is a ternary diagram showing the QFL modal compositions for each of the 10 zmj-013 point counts (open circles), the mean QFL modal composition calculated from the 10 point counts (closed circle), and the standard deviations for each modal percent (polygon).

(A)

Sample #	qm	qp	cht	plag	k	clay	bt	ms	glauc	lv	ls	lm	lu	lplu	Org	Ca	u	silt	pores	cement	Total Grains	Total Counts
zmj-013	307	24	11	77	21	0	2	1	4	4	32	21	0	0	0	0	3	10	9	110	504	636
zmj-013	291	17	9	76	32	0	2	1	3	5	35	34	0	0	0	0	2	10	6	124	505	647
zmj-013	309	20	5	53	34	5	8	2	3	1	10	53	0	0	0	1	1	10	12	114	500	663
zmj-013	306	25	8	68	20	0	3	1	7	5	14	46	1	0	0	0	0	8	5	132	504	649
zmj-013	313	19	7	70	15	0	2	1	1	6	25	42	0	0	0	1	0	11	14	88	501	614
zmj-013	292	25	5	72	17	0	2	0	4	6	30	47	0	0	1	0	0	13	11	129	500	653
zmj-013	295	39	7	75	16	0	2	2	5	6	20	43	0	0	0	1	1	7	6	136	510	659
zmj-013	294	18	7	75	17	0	3	1	2	5	18	60	0	0	0	0	2	5	3	116	500	624
zmj-013	303	9	6	77	19	0	1	0	3	8	28	46	0	0	0	1	1	6	5	128	500	639
zmj-013	301	20	8	71	20	0	2	1	3	5	25	44	0	0	0	0	0	9	7	108	500	624

(B)

Sample #	Q	F	L
zmj-013	68.11	20.16	11.73
zmj-013	62.86	22.04	15.10
zmj-013	68.87	17.94	13.20
zmj-013	68.25	18.14	13.61
zmj-013	67.76	17.35	14.90
zmj-013	64.83	18.20	16.97
zmj-013	67.61	18.42	13.97
zmj-013	64.07	18.89	17.04
zmj-013	63.67	19.59	16.73
zmj-013	66.05	18.72	15.23
zmj-013 Mean	66.21	18.95	14.85
zjm-013 St. Dev.	4.39	2.71	3.52

(C)